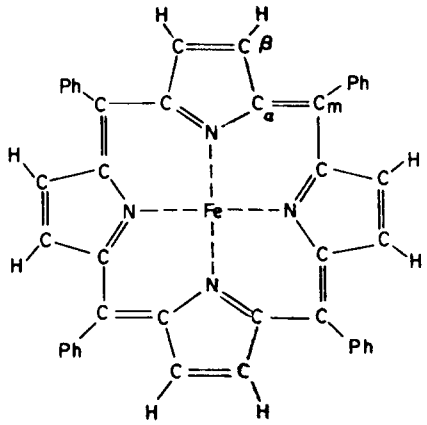

Fig. 45. Structure of iron tetraphenylporphine (Ph = phenyl). (From ref. [173].)

The original work on cytochrome C and hemoglobin has stimulated much work on other proteins and model systems. Only a few representative studies can be cited here. This work has led to detailed discussions of vibronic effects which have not been previously observed. Some of the resonance Raman spectra have been reviewed by Spiro [171] and Carey [172].

Fig. 45 shows the structure of the synthetic porphyrin, iron tetraphenyl porphine (Fe TPP). This compound is known to form a dimer with a bridging oxygen atom $(Fe(TPP))_2O$. Fig. 46 shows the spectra of this compound in CS_2 solution, excited by both 457.9 nm and 571.6 nm radiation [173]. Clearly the relative enhancement of various modes depends on the exciting frequencies. Polarization data allow modes to be separated into three different symmetry classifications. Those with $\rho < 0.75$ belong to A_{1g}, $\rho > 0.75$ are A_{2g}, and $\rho = 0.75$ are B_{1g} or B_{2g} modes.

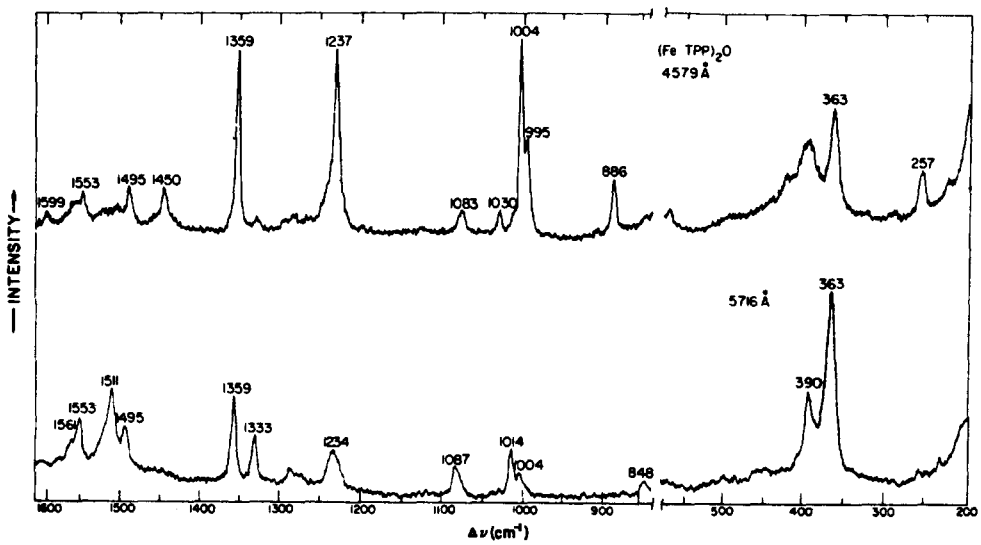

Fig. 46. Resonance Raman spectra of $[Fe(TPP)]_2O$ in CS_2, concentration 1 mg/ml. (From ref. [173].)

This work provides a good illustration of the analysis of excitation profiles from resonance Raman spectra. These are obtained by tuning a dye laser over the range of the visible spectrum while measuring the intensity of several Raman bands relative to an internal standard. Results are shown in fig. 47. Strekas et al. [174] have discussed some of the cautions to be observed in measuring such profiles. One sees a variety of Franck–Condon factors at work here, as well as other vibronic mechanisms. Particularly striking is the enhancement observable for the Fe–O–Fe stretch at 363 cm^{-1} (assignment confirmed by isotopic substitution). Spiro et al. have discussed how this may occur through interactions with a C–N ring mode at 1359 cm^{-1}.

Spiro, Burke et al. [175] have studied the so-called picket fence porphyrin. This is the only synthetic iron porphyrin currently known to form an isolable O_2 complex. The Fe–O_2 stretching vibration for this molecule is proven to occur at 568 cm^{-1} (confirmed by removal of O_2 and $^{18}O_2$ substitution). Its frequency is virtually identical with the 567 cm^{-1} observed for oxyhemoglobin. This is a significant finding, since X-ray work has established that the Fe–O–O linkage is bent for picket fence porphyrin. In that case, the identity of the frequencies for Fe–O stretching (and O–O stretching as established from

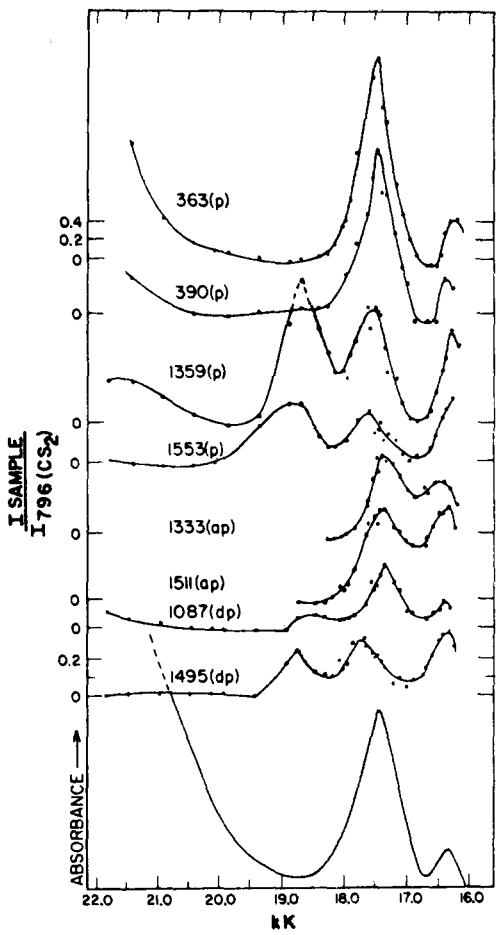

Fig. 47. Resonance Raman excitation profiles of $[Fe(TTP)]_2O$. The visible absorption spectrum is shown at bottom of figure. Raman intensity is corrected for self-absorption. (From ref. [173].)

Table 15
Structure-sensitive bands of iron TPP and $T_{piv}PP$ complexes[a]

	A	B	C
Fe(III)h.s.[b]	1555	1366	390
Fe(III)l.s.[c]	1568	1370	390
Fe(III)O_2[d]	1563	1366	384
Fe(II)i.s.[e]	1565	1370	392
Fe(II)l.s.[f]	1557	1354	382
Fe(II)h.s.[g]	1537	1342	372

[a]Frequencies in cm^{-1}; all three bands are polarized.
[b]High-spin Fe(III): Fe(TPP)Cl, Fe($T_{piv}PP$)Br, and the μ-oxo dimers.
[c]Low-spin Fe(III): bisimidazole adducts.
[d]Fe($T_{piv}PP$) (1-MeIm)O_2.
[e]Intermediate spin: four-coordinate FeTPP and Fe$T_{piv}PP$.
[f]Low-spin Fe(II): bisimidazole adducts.
[g]High-spin Fe(II): 2-methylimidazole adducts.

infrared spectroscopy) gives excellent assurance that the linkage is bent in hemoglobin as well, confirming Pauling's proposal [176].

Spiro et al. have determined the sensitivity of several bands in TPP and picket fence porphyrin to both oxidation state and spin state of the iron. A summary is shown in table 15. This sensitivity is somewhat different from that found for the naturally occurring hemes. Of particular note is the low value of 1537 cm^{-1} which occurs in the one five coordinate iron case. This may be diagnostic for five coordination.

Ferris et al. [177] have examined resonance Raman spectra of copper–sulfur complexes. The biological significance here is the potential of these complexes as models for a series of proteins known as blue copper proteins. Another question is just which sulfur ligand is coordinated to copper in these proteins. Four possibilities are shown in fig. 48. By analysis of Cu–S stretching frequencies, excitation profiles, and other aspects of the electronic spectrum, the authors have concluded that proposal 2 (fig. 48), a methionine ligand, is responsible in all of the blue copper proteins which contain methionine.

A rather different use of resonance enhancement was made by Brown et al. [178]. The protein lysozyme was among the first studied by laser excited Raman spectroscopy. Brown et al. have excited this spectrum in the ultraviolet region (363 nm) to selectively enhance the bands due to tryptophan residues. They have then used this selective enhancement to elucidate the role of tryptophan residues in the binding of lysozyme to glucose. Relative intensity changes are observed in the lysozyme spectrum as a result of this interaction. Again, reference is made to vibronic interactions as they affect the polarizability tensor in order to explain the observed changes.

Carey and co-workers [172] have utilized the resonance Raman effect in biological systems in yet another way. They use small chromophoric molecules as labels of non absorbing biologically active molecules.

The resonance label can be a carefully designed molecule so that its vibrational spectrum can yield

1. Deprotonated cysteine (mercaptide) coordination:

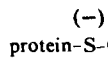

2. Methionine (thiaether) coordination:

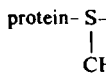

3. Protonated cysteine (thiol) coordination:

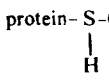

4. Cystine (disulfide) coordination:

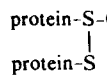

Fig. 48. Four possible modes of coordination of sulfur ligands to copper in a Cu–S protein. (From ref. [177].)

the maximum information about the biochemically active site. Essentially, as with naturally occurring chromophores (porphyrin in hemoglobin), only the label spectrum is seen.

A number of general classes of this approach have been studied, including drug–enzyme interactions in which the drug is the resonance Raman chromophore, antibody–antigen interaction, and enzyme–substrate reactions. In the enzyme reactions, time dependence or unstable intermediates can sometimes be detected.

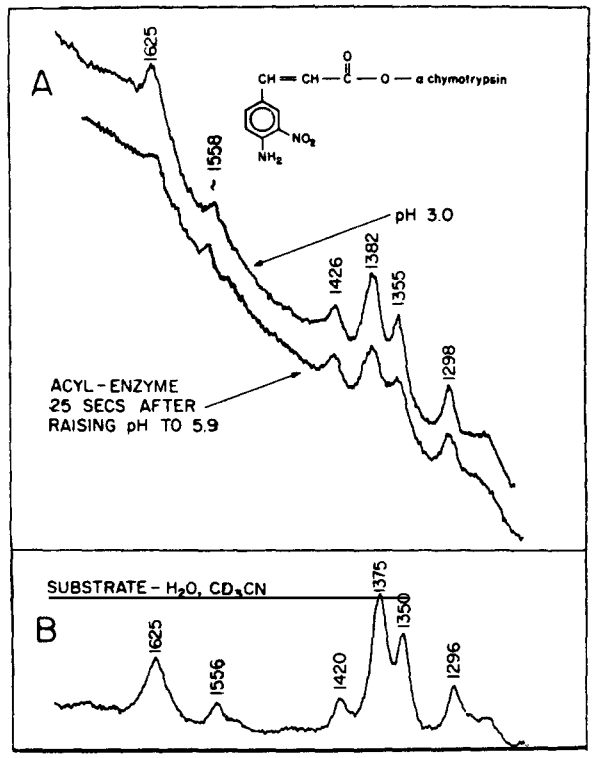

Fig. 49. Resonance Raman spectra of: (A) 4-amino-3-nitro-trans-cinnamoyl-α-chymotrypsin at *p*H 3.0 (top) and *p*H 5.9 (bottom); (B) methyl 4-amino-3-nitro-trans-cinnamate. The spectrum of the unstable intermediate at *p*H 5.9 was obtained in a flow system. Essentially identical spectra were recorded in the range *p*H 5.9 to 7.0. (From ref. [172].)

An example of the technique is shown in fig. 49. The acyl label is attached to the enzyme chymotrypsin, as shown in the figure. This labeled enzyme is actually an intermediate in the enzyme substrate reaction. The spectrum at *p*H 3 shown in fig. 49A is identical to that of the substrate shown in fig. 49B. This enzyme substrate system is stable at *p*H 3, but when the *p*H is raised, reaction occurs. Using a flow system, Carey and Schneider obtained the lower spectrum in fig. 49A. The major change is a decrease in the intensity of the 1625 cm^{-1} mode, primarily C=C stretching. The authors explain this decrease in terms of a twisting of the

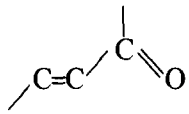

unit out of the plane. Such distortion has often been postulated for substrate reactions but never observed experimentally.

From the very first work of Spiro and Strekas, it has been clear that resonance Raman spectra of biomolecules requires a detailed knowledge of the basic physics involved in the transitions. As work in this area has progressed, this aspect has not changed. Resonance Raman spectroscopy is not a routine tool for the biologist. Rather it requires a careful spectroscopic analysis. These analyses are solving biological problems while extending our knowledge of vibronic effects.

8.4. Lipids and membranes

Infrared spectroscopy has been used for some years to study soaps and related lipids. More recently the Raman work has shown great promise for revealing details about membrane structure.

Fig. 50 shows a schematic portion of a cell membrane in cross section. Lipid molecules, consisting of polar heads and hydrophobic tails (usually long chain hydrocarbons), assemble in a bilayer in which proteins are immersed. Nutrients must pass through this bilayer into the cell, waste products out.

It is known that lipid-water gels undergo phase transitions as the ratio of lipid to water is changed or as the temperature is increased. It is also known that the principal endothermic phase transition observed on heating is a melting of the hydrocarbon chains. Below this transition the chains are primarily in an all trans, extended format; above the transition a significant number of gauche conformers exists. The melting of the hydrocarbon chains greatly affects the fluidity of the membrane, hence the transport properties. Raman spectroscopy has been a good probe of this transition. Indeed,

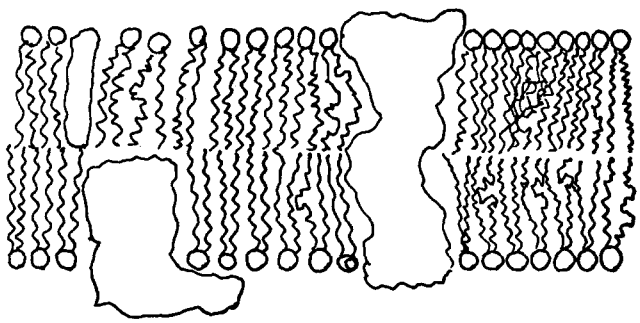

Fig. 50. Schematic cross section of a biological membrane, showing lipid bilayer with immersed proteins.

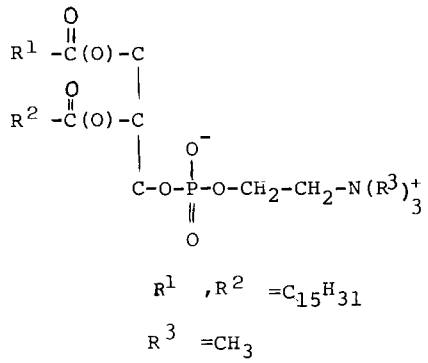

Fig. 51. Structure of lecithin or phosphatidyl choline. For dipalmitoyl phosphatidyl choline the alkyl groups are as indicated.

because these are phases of intermediate order and fluidity, Raman spectroscopy is one of the few techniques which can give information at the molecular level regarding the melting process.

The original Raman spectroscopic work on the phase transition was carried out by Bulkin and Krishnamachari [179] and by Lippert and Peticolas [180]. While the sensitivity of the spectrum in the C–H and C–C stretching regions to trans-gauche ratio in the hydrocarbon chains has been clear for some time, there has been considerable recent discussion over the assignments of the various modes observed and the reasons for their sensitivity to the chain conformation.

For dipalmitoyl phosphatidyl choline (dipalmitoyl lecithin), whose structure is shown in fig. 51, there are two thermal phase transitions observed for the gels containing 30% or more water. The main transition, already discussed above, occurs at 41°. At 35°, however, there is a much weaker endotherm. As shown in fig. 52, using data tabulated from spectra, this transition is also observable by Raman spectroscopy [181]. Indeed, the Raman measurements have been interpretable as showing that the transition is a rotation of apposed hydrocarbon chains with respect to one another. This type of phase transition and its thermodynamic properties has many analogues in other solids.

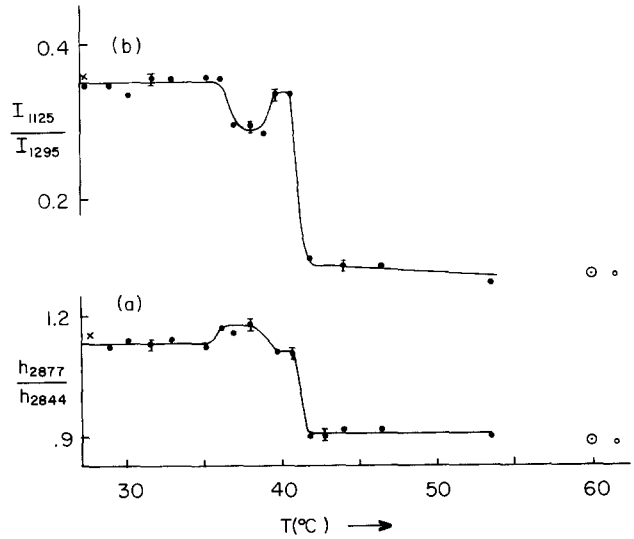

Fig. 52. The effect of temperature on the Raman spectrum of dipalmitoyl lecithin: 30% water gels; a, relative peak heights in CH stretching region; b, relative peak areas in C–C stretch and CH_2 twisting regions. (Unpublished data of Bulkin and Yellin.)

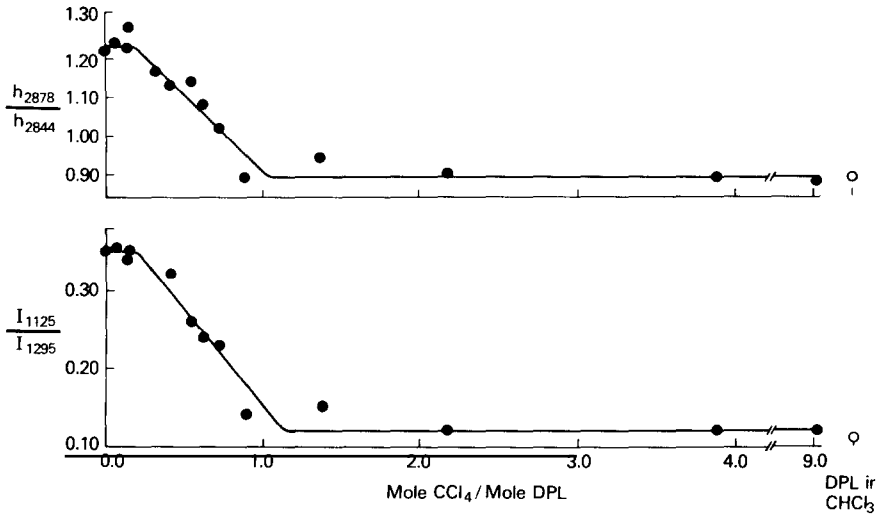

Fig. 53. Effect of addition of carbon tetrachloride on the Raman spectrum to a dipalmitoyl lecithin: 30% water gel; upper, relative peak heights in CH stretching region; lower, relative peak areas in C–C stretch and CH_2 twisting regions. (From ref. [185].)

Real biological systems contain mixtures of lipids as well as proteins. There have been a number of attempts to study such systems. Mendelsohn and Maisano [182] showed that if one of the lipids had its hydrocarbon chains deuterated in the mixture, one could easily observe the phase transitions of both species in the Raman spectrum. The conformation of each component can thus be monitored. They studied two very similar lipids, differing only in the chain lengths of the hydrocarbon chains. By contrast, work of Bulkin and Krishnamachari [183] on rather dissimilar lipids, in which polar head groups varied, indicated that the behavior of the mixed lipid system was more complicated, involving both eutectic and peritectic phases.

Lis et al. [184] investigated the interaction of amino acids, simple peptides, and proteins with lecithin. As expected, all the small molecules which they added to the lipid bilayers increased the concentration of gauche conformers. This problem, the effect of small molecules on crystallinity or fluidity, has also been studied by Bulkin and Yellin [185], who investigated the induction of the main phase transition in lecithin–water gels using carbon tetrachloride and chloroform. Fig. 53 shows that the fluidity increases over a broad concentration range. In this range there is a two phase region, as predicted thermodynamically for a first order phase transition. Results such as these may have some importance to elucidation of the mechanism of anesthesia.

Membranes and fragments of membranes have been investigated by several groups [186] following the first report of a spectrum of hemoglobin-free erythrocyte (red blood cell) ghosts by Bulkin [187] in 1972. Milanovich et al. [188] examined sarcoplasmic reticulum membranes, with a typical spectrum shown in fig. 54. They concluded that this membrane was probably more fluid than the erythrocyte membranes. An important complication in several of the reports is low levels of carotenoids which exhibit resonance enhanced spectra. In the systems we discussed in 8.3 under resonance Raman spectroscopy, the presence of the chromophoric group is well known. In biological systems, however, where there is a mixture of many different components, a chromophore may be present at a level of 10^{-3} below that of the species of primary interest, yet interfere strongly with the spectroscopic results.

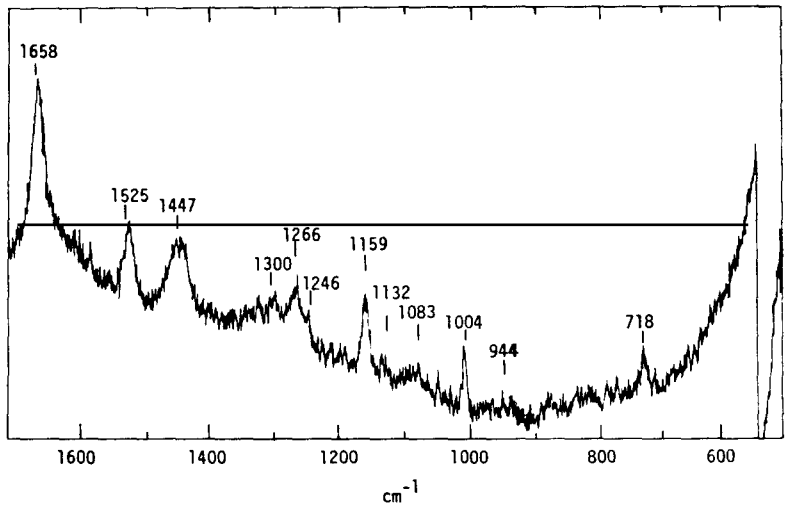

Fig. 54. Raman spectrum of sarcoplasmic reticulum membranes in H_2O. Maximum signal, 3×10^3 photons/s; wavelength, 488.0 nm; power, 200 mW; resolution, 4 cm^{-1}; time constant, 30 s; temperature, 10°C. (From ref. [188].)

9. Liquid crystals

Infrared and Raman spectroscopy have been used for many years to study strong intermolecular interactions such as hydrogen bonding. It is natural that many research groups should have thought to apply these techniques to the study of liquid crystals.

Although studies of the vibrational spectra of liquid crystals began many years ago, there has been a flurry of activity in the years since 1968. Work in this area has been the subject of several reviews [189].

The application of vibrational spectroscopy to mesophases has proceeded in stages. In the early work, and in some of the work still being published today, the main contribution has been the observation of phenomena in the spectra--intensity changes, frequency shifts, etc.--which occur at or near the various phase transitions. Also, as is characteristic of the application of spectroscopic studies to liquid crystals, a certain amount of attention has been focussed on measurement of order parameters.

There now seems to be sufficient background of this sort available, however, to begin to make some generalizations about the sort of expectations one has for the vibrational spectra of liquid crystals. Further, we can begin to make some quantitative assignment of the phenomena observed to changes at the molecular level.

Liquid crystals are ordered, fluid phases which occur for several thousand organic compounds and polymers between the crystalline and isotropic liquid phase. Such phases are also present in mixtures of compounds. For certain of the latter cases, the individual compounds may not in themselves form liquid crystals, while the mixture, at certain concentrations and temperatures, does. These are known as lyotropic liquid crystals, while materials which, when pure, show liquid crystalline behavior, are known as thermotropic liquid crystals. Metastable liquid crystalline phases also exist, i.e. a material may show a simple phase transition form crystal (c) to isotropic liquid (l) on heating, but exhibit a liquid crystalline phase on cooling. These are known as monotropic liquid crystals.

Liquid crystals can be divided into several classes, according to the type of long range order which is present. In general, crystalline phases are characterized by three dimensional order, whereas liquid

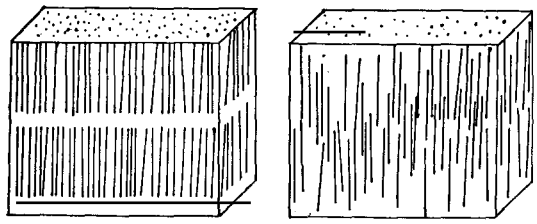

Fig. 55. Schematic view of molecular arrangements in the (a) smectic and (b) nematic liquid crystalline states. There are other smectic phases as well; for example, those in which the molecules tilt in the layers.

crystalline phases possess at most two dimensional order. Fig. 55a shows a schematic diagram of the order of molecules in a smectic liquid crystal. Here the molecules are arranged in layers with their long axes parallel within the layers. No other order exists within the layers, however. The figure also introduces the idea that the molecules must be anisotropic in shape for liquid crystalline behavior to be found.

Fig. 55b shows a different type of liquid crystal, the nematic phase. In this phase the long axes of the molecules are parallel, but no other order exists. It is perhaps not surprising that some molecules on heating show first a smectic and then a nematic phase before being converted to the isotropic liquid. A third general class of liquid crystals are cholesteric liquid crystals, in which the molecules are arranged in two dimensional layers which look like a cut through a nematic phase; but successive layers are twisted with respect to one another, so that if one were to follow the direction of the long axes of the molecules through successive layers it would describe a helix. While some work has been done on the vibrational spectra of cholesteric phases [190], it will not be discussed in this article.

The question of chain fluidity in nematic and smectic phases has been the subject of several Raman investigations [191]. Schnur [192] has studied the alkoxy azoxy benzenes (fig. 56) in all spectral regions;

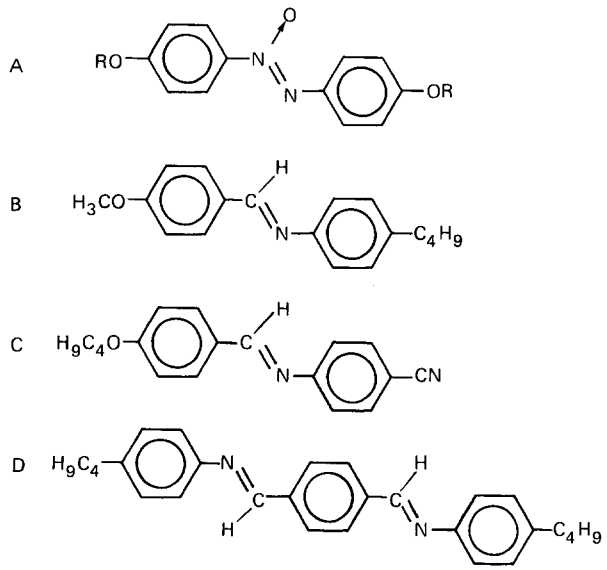

Fig. 56. Structures of some molecules which form liquid crystals: (A) The alkoxyazoxybenzene series; (B) 4,methoxybenzylidene, 4'n-butylaniline (MBBA); (C) 4,methoxybenzylidene, 4'cyanoaniline (BBCA); (D) 4,4'bisterephthal, bis, butylaniline (TBBA).

but with particular emphasis on the region from 200 to 400 cm^{-1}, where it is asserted that an accordion-like vibration of a short (3–8 carbon) all trans hydrocarbon chain attached to a benzene ring should occur. An approximate calculation [191] was carried out to confirm the assignment, although again one must assume that there is some mixing with ring modes and other modes of the chain.

The result of these studies indicate that near the crystal–nematic (c–n) transition and, to some extent, in the nematic phase as well there are conformational changes taking place in the end chains. An illustration of the changes observed for the C_6 homolog is shown in fig. 57. Of course, these compounds also show other spectral changes as discussed above, but the changes observed by Schnur seem to have a distinct phase and temperature dependence. In some of the compounds, solid phase polymorphism exists and this seems to drastically affect the intensity of the accordion mode. An example is shown for the C_4 homolog in fig. 58. Note that this might be interpreted as a pretransition effect in the crystal rather than a distinct solid phase.

Additional evidence regarding chain fluidity comes from a paper by Bulkin et al. [193], who showed that in the nematic phase of MBBA the CH stretching vibrations show an increase in bandwidth, so that the entire contour of the CH stretching modes appears to lose resolution. As temperature is increased until just below the nematic–isotropic phase transition, the bands sharpen with a slight shift in the position of the frequency maxima. This behavior was interpreted as arising from a reorganization of butyl chain conformations on the time scale of the infrared measurement. Since the two time scales

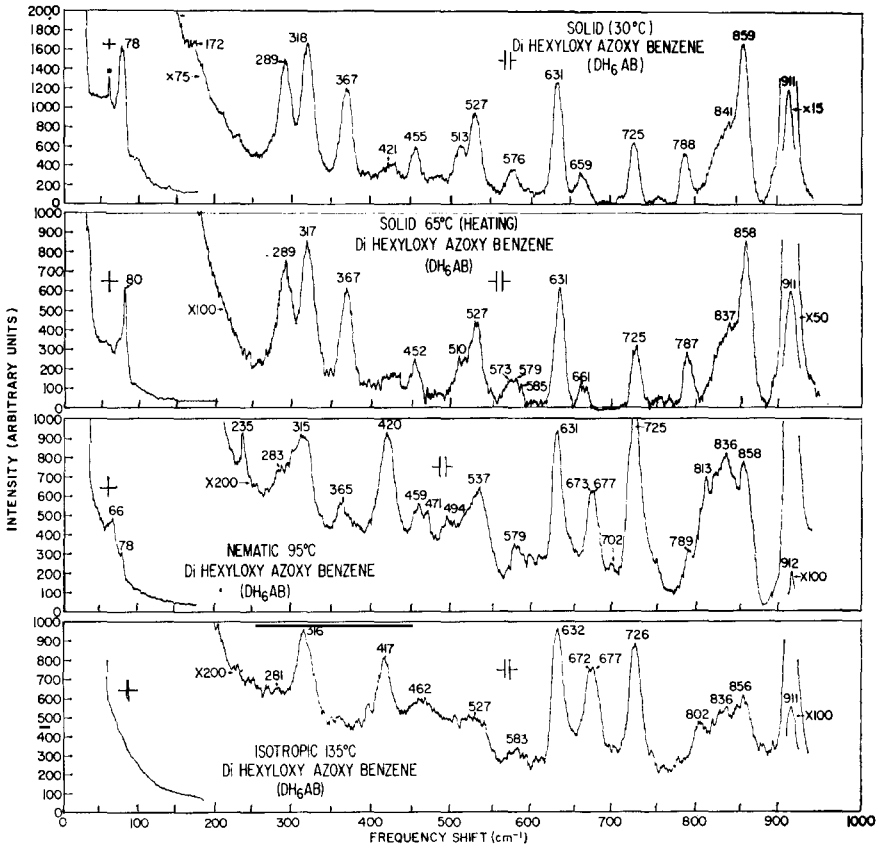

Fig. 57. Tracing of observed Raman spectra of dihexyloxyazoxybenzene (C_6). (From ref. [192].)

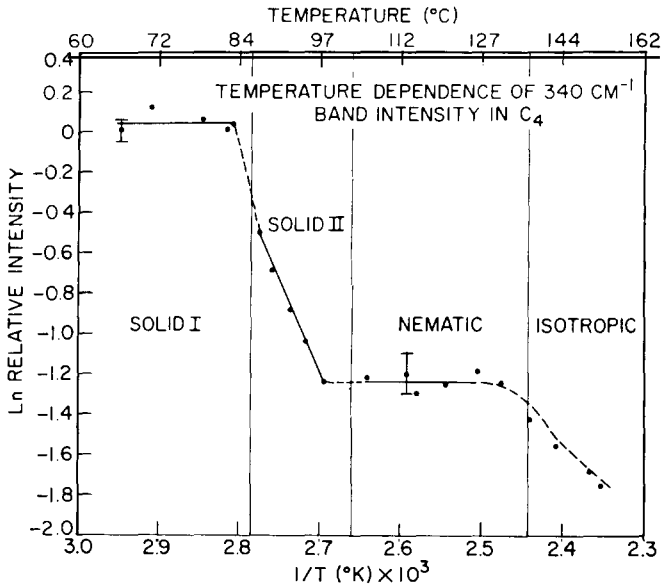

Fig. 58. The relative integrated intensity in logarithmic units of the accordion band in C_4 versus reciprocal temperature. The integrated intensity of the 340 cm^{-1} band was calculated relative to the adjacent 320 cm^{-1} band which appeared to remain reasonably constant. (From ref. [192].)

(internal rotation and CH stretching) overlap for a short temperature range, broadening is observed. Such phenomena are common in nuclear magnetic resonance. Similar reorganization of conformers in MBBA was deduced from ultrasonic measurement of Jahnig [194] and is consistent with these data.

Lugomer and Lavrencic [195] have reexamined the Raman intensity data for a wide variety of nematic materials with different length carbon end chains in an attempt to interpret these data in terms of the elastic constants. They have presented evidence that the Raman intensities follow the so-called universal curve of Gruler [196] for the bend/splay elastic constant ratio K_{33}/K_{11}, which shows a very strange temperature dependence in the nematic phase.

At the nematic to isotropic (n–l) transition, there are few, if any, real changes observed in the spectra. One likely candidate is the change in intensity of the accordion mode observed by Schnur [191]. There has been confusion on this transition from Raman spectroscopic observations in the past.

This confusion arises as follows: In the Raman spectrum of a low symmetry, nematogenic molecule, the Raman bands are all polarized but may have widely varying depolarization ratios. In an unaligned or imperfectly aligned sample, the Raman exciting radiation and the scattered light have their electric vectors rotated due to refractive index discontinuities. Such an effect is well known in the Raman spectrum of powders [197]. When the n–l transition occurs, this scrambling of polarization disappears and the result is a different set of relative intensities. This has been documented in a more quantitative fashion by Bulkin et al. [198]. Thus, any changes in relative intensity of bands (and changes in apparent frequency maxima which may occur from overlapping bands changing in relative intensity) must be carefully checked to correct for the band polarization. The effects can also be checked by study of the infrared spectra in most cases.

The question of measuring polarization in the Raman spectrum of liquid crystals has been a difficult one. Some initial attempts were unsuccessful, with authors observing a depolarization ratio of 1.0 in the nematic phase. This is indicative of complete scrambling of the radiation. If changes from a ratio of 1.0 are observed at the n–l transition, as has been reported [199], then this is not surprising.

The most thorough treatment of oriented nematics in the Raman has been done by Pershan and co-workers [200–201]. They have shown that it is, in principle, possible to measure both the first ($\cos^2\theta$) and second ($\cos^4\theta$) terms in the order parameter or distribution function from the Raman spectrum. Experimentally, they have used samples of MBBA in which a probe molecule that also forms a nematic phase N-p-butoxybenzyliden-p-cyanoaniline (BBCA) is dissolved. (See fig. 56 for structures of these molecules.) The sample is aligned by rubbing two plates and 180° Raman scattering is observed. The BBCA molecule shows a strong CN stretching vibration, which is approximately along the long axis and is isolated from other intramolecular vibrations. From these measurements, the terms in the order parameter can be deduced. Comparison with existing mean field theories of the nematic order parameter has been made from these measurements. It is asserted that the fit is better with the Humphries–James–Luckhurst [202] approach than with the Maier–Saupe [203] theory for the P_2 term, but that neither does particularly well with the P_4 observations. The authors have discussed possible reasons for the strange P_4 results, including those which may arise from the measurement technique itself.

Boyd and Wang [204] have applied the Raman technique to the study of the effect of pressure on nematic materials. In this case, the Raman spectrum simply becomes the analytical probe by which the phase transition is detected. It was shown that the c–n and n–l transitions are effectively first order (follow the Clausius–Clapeyron equation) when measured in this way for one case. This technique is useful in that it also allows one to determine the change in volume at the phase transition; in both cases (c–n and n–l) the higher temperature phase had the lower density.

One of the areas in which vibrational spectroscopy yields quite unique information is the study of intermolecular or lattice vibrations. These are seen close to the exciting line in the Raman spectrum, hence a good rejection of stray light and a relatively low Rayleigh scattering level are needed for their observation. In the infrared spectrum, the lattice modes occur in the far infrared region, generally below $150\,cm^{-1}$ for organic crystals. They tend to absorb very strongly, particularly in molecules such as nematogenic crystals, which usually have dipolar groups present. Whereas in the Raman, spectrum measurements with single crystals are readily made and yield definitive assignment of the lattice modes to a particular symmetry species, in the far infrared single crystal measurements are difficult. This further complicates the observations, because the crystallite size may be comparable to the wavelengths of the radiation, leading to spectral distortions.

In the nematic phase we have the possibility of observing "pseudo-lattice" vibrations, i.e., intermolecular motions characteristic of the long range order in this phase. It should be noted that the intermolecular potential in such a phase with organic crystals probably is proportional to an intermolecular separation term of $1/r^3$ or higher power of $1/r^n$, so the force constants, which depend on the second derivative of $1/r^n$, fall off rather rapidly with distance. However, in cases where there is long range order, it may be possible to propagate phonons even in liquid crystals. As we shall see, there is not much evidence for this in the spectra of nematics, but there is some in the case of the more highly ordered smectic phases.

Although a substantial number of papers on nematics have appeared, almost all the attention has been concentrated on two materials, p-azoxyanisole (PAA) and N-(p-methoxybenzylidene)-p-butylaniline (MBBA) (fig. 56). We will discuss these two cases in some detail, referring relatively briefly to other work that has been carried out.

The Raman spectrum of PAA in the lattice vibration region was first published by Bulkin and Grunbaum [205]. Bulkin and Prochaska [206] examined the Raman spectrum of a single crystal of PAA at −90°C and were thus able to assign the lattice vibrations to particular symmetry species. Their spectrum, taken in two views to show the Ag and Bg modes clearly, is shown in fig. 59.

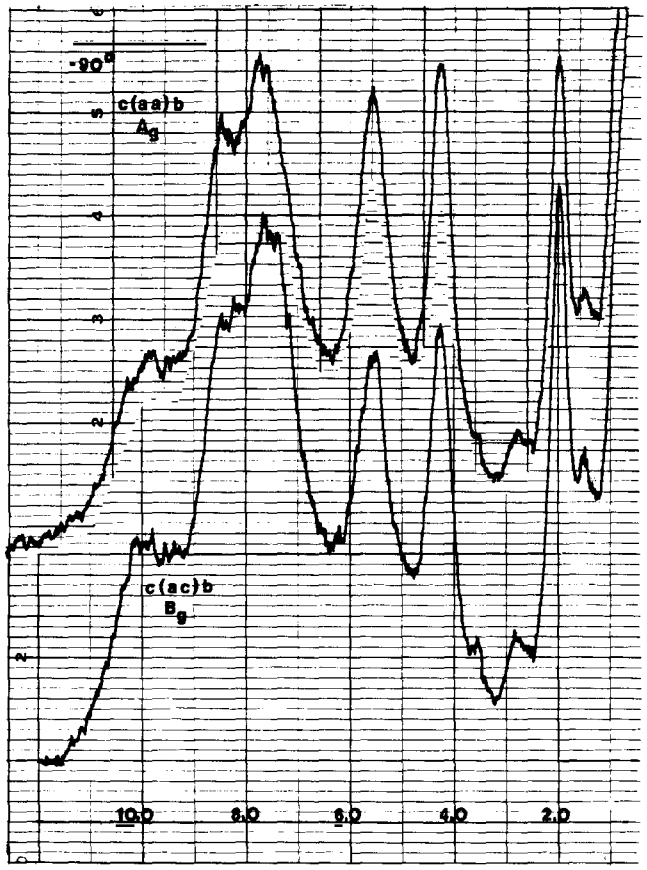

Fig. 59. Raman spectra of PAA at −90°C showing the A_g and B_g modes.

As the c–n transition is approached, Bulkin and Prochaska [206] observed pretransition effects which they interpreted as being indicative of a soft mode, such as is commonly observed near ferroelectric phase transitions. They asserted that this soft modelike behavior occurs with a mode or modes which initially (i.e., 5° below the phase transition) are in the vicinity of 70 cm^{-1}. It appears to shift rapidly toward zero frequency in the 2°–3° below the phase transition. Amer and Shen [207] did not find evidence for such pretransition effects and attributed this observation to problems with temperature control in the experiments of Bulkin and Prochaska. Sakamoto et al. [208] also failed to observe this effect, but in their case the lattice vibration spectrum even 8° below the phase transition shows only two broad bands, instead of six distinct maxima observed by other workers.

There is other evidence for the pretransition effects described above. First, it should be pointed out that to a certain extent there is a matter of definition of a pretransition effect. Some workers have seen the transition occurring over a 2°–3° range and stated that it was abrupt, yet this is the range over which it was asserted that the soft mode behavior occurred. Secondly, Riste and Pinn [209], using neutron scattering techniques, have observed identical pretransitional behavior at the PAA phase transition. As we shall see below, there are pretransition effects observed in the Raman spectra of other liquid crystalline materials at the c–n phase transition. The soft mode behavior was predicted in theoretical treatments of Kobayashi [210] and Ford [211].

Bulkin and Grunbaum [212] have carried out a calculation of the lattice vibrations of PAA. In table 16 the results of their calculation are shown, compared with experimental data from Bulkin and

Table 16
Observed[a] and calculated lattice vibration frequencies of p-azoxyanisole

Symmetry species	Translatory[b]			Rotatory[b]		
Ag						
Obsd	30	52	70	16	74	91
Calcd	28	55	62	20	69	94
Bg						
Obsd	30, 37	52	70	16	74, 90	95
Calcd	37	60	69	25	82	101
Au						
Obsd	50	70	—	135, 150	84	50?
Calcd	51	69	0[c]	130	89	55
Bu						
Obsd	—	—	70?	115	84?	50?
Calcd	0[c]	0[c]	67	119	78	52

[a]Raman data (Ag, Bg) from ref. [206], single crystal frequencies at −90°. Far-infrared (Au, Bu) data from ref. [213], polycrystalline sample at 25°.

[b]Modes are primarily rotatory or translatory in nature; however, the translation–rotation interaction force constants are not negligible.

[c]Acoustical modes.

Prochaska [206] and Bulkin and Lok [213]. The calculation is based on a model potential function for the unit cell, which uses atom–atom interactions of the form

$$V_n = -a/r^6 + b\,\mathrm{e}^{-cr}$$

where r is the nth atom–atom distance and a, b and c are parameters. In the calculation the parameters are transferred from the literature without any refinement on the experimental data. The potential is differentiated twice with respect to all motional coordinates to give the force constants, from which the frequencies are then calculated.

The results in table 16 are grouped according to motions about the same type of coordinate. Thus, when the frequencies in a particular column are close to one another, this is indicative of weak coupling between the molecules in the unit cell with respect to motion along that coordinate. A large splitting reflects a strong coupling. As expected for anisotropic molecules, both cases occur. It is interesting to note that the lowest and highest frequency bands observed in the spectrum result from very strong coupling, giving rise to a large splitting. Likewise, the case of weak coupling lead to bands in the 70 cm^{-1} region, which is where the putative soft mode was seen. This is as expected for such a mode. This calculation seems possible now for all nematogenic or smectogenic crystals for which crystal structure data are available. Raman spectra of the higher homologs of PAA have been studied by several groups in the lattice vibration region. Interestingly, none shows as well-defined a spectrum as does PAA. Bulkin [214] had previously commented that it seemed, on the basis of infrared data, to be more difficult to obtain highly ordered crystals of these materials. Schnur [192] has pointed out that there is considerable solid polymorphism in these materials and in macroscopic samples one wonders whether this might be affecting the resolution in the lattice vibration spectrum.

What of the spectra in the nematic phase? In all papers, the authors seem to agree that there is Raman scattering in the region below 100 cm^{-1} which appears in the nematic phase. There are distinct frequency maxima on the Rayleigh wing which subsequently disappear in the isotropic phase. Not surprisingly, there are differences in the positions of the quoted frequency maxima. These are due to the difficulty of accurately measuring the positions of broad bands on an intense background. It would seem desirable to carry out some computer deconvolution of the Rayleigh background in an attempt to find these bands more accurately. This information will be valuable in any attempt to model the nematic intermolecular vibrations. Also of some controversy is the question of whether the observed intermolecular Raman bands in the nematic phase disappear continuously or discontinuously at the n–l phase transition.

The other major class of compounds that has been studied in the low frequency region is the Schiff base nematics. MBBA has been studied in the most detail. The Raman spectrum of MBBA in the lattice vibration region was first reported by Billard et al. [215] and subsequently by Borer et al. [216] and Vergoten et al. [217]. The spectrum of Billard et al. is shown in fig. 60 at two temperatures in the solid state. At low temperatures, even in the polycrystalline sample, MBBA shows a very well-defined vibration spectrum. Nine distinct frequency maxima are observed between 39 and 180 cm^{-1} at −173°; but the two highest modes, at 179 and 181, are explained as internal vibrations. It seems possible that the mode at 142 cm^{-1} may also have a contribution from internal vibrations; this could be checked by study of solution spectra. Borer et al. are in essential agreement with these results.

At temperatures close to the c–n phase transition, Billard et al. have noted that the spectrum becomes quite broad and most of the fine detail is lost. Thus, in the spectrum at 15°, about 5–7° below the c–n phase transition, the bands are already quite broad. A spectrum given by Borer et al. at 2° also shows considerable broadening. This seems to be indicative of similar pretransition effects to those described earlier, although no soft mode was observed.

Some Raman work has been done on the spectra of thermotropic smectic phases. Amer and Shen [218] studied the Raman spectrum of diethylazoxybenzoate, and diethylazoxycinnamate, which have

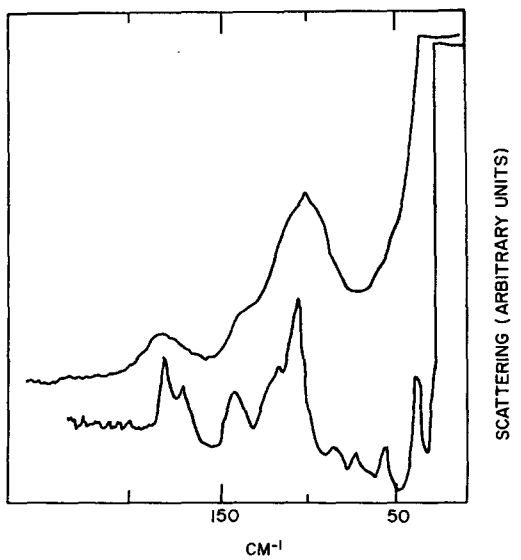

Fig. 60. Raman spectrum of solid MBBA in the lattice vibration region. Upper curve: 15°C; lower curve: 100°C. (From ref. [215].)

smectic A phases. These compounds show a single low frequency Raman mode in the crystalline phase at 22 and 26 cm^{-1}, respectively. In the smectic phase, this mode appears to shift with the maximum at about 14 cm^{-1}. It vanishes abruptly at the smA-1 transition. The mode is strongly overlapped by the Rayleigh line in the smectic phase, but it does seem to be of considerably lower intensity than that seen by neutron scattering discussed above. As usual, the modes are explained as being some sort of rotatory oscillations, but in this case one which is primarily associated with strongly interacting functional groups, such as C=O, within the molecule. This would account for the seemingly small mass dependence in the smectic phase. Probably such an explanation is not necessary, since a relatively small frequency shift in such a low frequency mode would be sufficient to account for the mass difference. The authors have also studied the internal vibrations of this compound, as have Zhdanova et al. [219]. No frequency shifts or relative intensity changes with temperature were observed such as have been with nematic materials.

The interesting compound terephthal-bis-butyl aniline (TBBA) (fig. 56) has been studied. This material has seven known fluid phases, viz., isotropic, nematic, three stable smectics (B or H, C, and A), and two monotropic liquid crystalline phases not yet characterized.

Schnur and Fontana [220] studied all of the stable phases in the low frequency and higher frequency Raman spectra. They have two important sets of observations. In the low frequency region, the lattice vibration spectrum, which contains a number of bands, appears in their spectra to be almost the same in the smectic B phase as it is in the crystal. At the smB–smC transition, most of this structure disappears and the spectra in the higher temperature phase all show only the broad scattering characteristic of these phases. Note that a band is observed by these workers in the 22 cm^{-1} region of the crystal, which shifts to 19 cm^{-1} in the smB phase and disappears in the higher temperature phases. If this were the same mode occurring in this region referred to earlier, we would expect to see it persist in the higher temperature phases.

A curious observation is seen in the 1550–1650 cm^{-1} region. In the solid and smB phases, one band is seen in this region at 1590 cm^{-1}. This is also true in the smB phase, but in the smC phase two new bands appear at about 1560 and 1620 cm^{-1}. This has not been observed in any other spectra of liquid crystals. The authors do not expound on the possible explanations of this phenomenon. Nonetheless, mechanisms can be enumerated by which new bands could appear in the spectrum. In particular, the most usual are the appearance of new conformations (in this case perhaps due to the multiple minimum potential which likely exists about the Schiff base linkages) or a breaking of symmetry, resulting in a lowering of selection rules. In this regard, it should be noted that the smB phase is expected to have a higher symmetry than the smC phase. In addition, TBBA is one of the few liquid crystalline molecules which has a fairly high molecular symmetry; it probably possesses an approximate or exact center of symmetry. The intersection of the molecular symmetry and smB symmetry could result in selection rules which would cause modes to be forbidden in smB but allowed in lower symmetry phases. This point should be explored further, as other molecular modes should show the same behavior if this is the case.

Dvorjetski et al. [221] have also investigated TBBA, concentrating their attention on the low frequency region Raman spectrum in the lower temperature phases (smB and the two monotropic phases called VI and VIII). In the solid phase their observations are in agreement with those of Schnur and Fontana, but this is not true in the smB phase. Here at 130°C (same temperature as Schnur and Fontana used), Dvorjetski et al. only observed broad, ill-defined scattering. In phase VI, at 80°C, they observed some additional structure, while in phase VII, at 67°C, the original crystalline spectrum is recovered intact. There is no apparent explanation of the difference in observations between these two groups and resolution must await further experimental work.

Dvorjetski et al. have studied the temperature dependence of the 19 cm^{-1} band in the solid state, approaching the c–smB transition. After correcting for background and Boltzmann factor, they find that this mode shows a small pretransition effect in its frequency, shifting toward zero frequency over a temperature range of about 4°C. They thus feel that this mode behaves as a soft mode and interpret their results in terms of the types of molecular motion possible in the various phases. They conclude that the data are consistent with free molecular rotation about the long axis in the smB phase. This rotation freezes out progressively as the molecules are cooled to phases VI and VII. Further work is needed to verify these conclusions in other regions of the spectrum.

10. Raman applications to inorganic and organometallic chemistry

The importance of Raman spectroscopy in the field of inorganic and organometallic chemistry is evident by the large number of books, review chapters and articles which are available [80, 222–228]. It is not only that Raman data are essential for the complete structural analysis of molecules, but is again the ease of obtaining Raman spectra on colored solids, in the molten state, or in solution that have contributed to the explosive recent growth in this field. The immense enhancement of intensity of Raman bands when resonance Raman conditions are met has generated an increase in activity in this area and excellent reviews by Clark, Stewart and Shorygin [229–230] summarize the field eloquently.

10.1. Structural studies: molecular species

The vibrational analysis of crystalline inorganics to assign internal modes of the ions, as well as crystal lattice modes, requires both infrared and Raman spectroscopy. Many examples of such structural studies are found in the texts and review articles, but some recent examples are worth noting.

Baran [231] measured the IR and Raman spectra of crystalline $MgTe_2O_5$ and assigned the internal vibrations of the $Te_2O_5^{2-}$ ion. He also did structural studies on crystalline magnesium orthovanadate [232]. IR and Raman spectra of $BaCl_2 \cdot 2H_2O$ powder were obtained and interpreted by Jain et al. [233]. Crystalline Na_2CrO_4 and $Na_2CrO_4 \cdot 4H_2O$ were compared by Carter et al. [234] and the effects of hydrogen bonding on the chromate frequencies noted. Carter subsequently studied $(NH_4)_2CrO_4$ and $(ND_4)_2CrO_4$ in a special rotating cell designed for liquids but modified for solid samples [29].

The utility of Raman spectroscopy in structural investigations of systems containing transition metal to transition metal bonds was shown by San Filippo and Sniadoch [235]. They found that the Raman spectra of simple homonuclear transition metal complexes showed an intense, sharp band in the low-frequency region due to the metal–metal stretching vibration. These metal–metal frequencies showed little variation with respect to the nature of the coordinated ligands but were considerably dependent on the order of the metal–metal bond.

Another example of Raman structural studies involves the polymorphs of cobalt molybdate [6]. The tetrahedral, purple, high temperature form (β) is metastable at room temperature and converts to the octahedral, green, low temperature form (α) with any pressure application. Therefore, it is impossible to prepare any of the α form for IR examination, but Raman can be used and Angell first obtained the spectra of both the α and β forms in 1972 [236].

Numerous other cobalt, molybdenum, tungsten and rare earth compounds have been examined by Raman. Py et al. [237] studied molybdenum trioxide, MoO_3, and found that results suggested that the

coordination of the O atoms around the Mo is tetrahedral rather than octahedral. Miller obtained the Raman spectrum of a single crystal of magnesium molybdate [238], but because of the complexity could not meaningfully assign bands to tetrahedral modes despite the fact that the oxygens were tetrahedrally coordinated about the molybdenum atoms.

A series of vibrational studies of molybdates, tungstates, and related compounds were done by Liegeois-Duyckaerts. He obtained the IR and Raman spectra of the three hexagonal perovskites $Ba_2B^{II}TeO_6$ (B^{II} = Ni, Co, Zn) [239] and compared them with those of the corresponding cubic perovskites [240]. Based on this comparison, he made a general assignment of the internal modes and discussed in detail two A_{1g} modes which he assigned to the symmetric stretch of two different types of TeO_6 octahedra.

Isotopic substitution and group analysis aided in the infrared and Raman structural studies of M_2TiO_5 compounds (M = rare earths: La to Dy). M. Paques-Ledent [241] found one interesting experimental feature occurring simultaneously in the IR and Raman spectra of these compounds -- a band in the frequency range 775–875 cm^{-1}, which is an exceptionally high value and signifies one short distance Ti–O in M_2TiO_5 compounds. This is particularly interesting because the fifth oxygen of a TiO_5 polyhedron is structurally different from the other four oxygen atoms which are strongly bonded to double groups M_IO_7–$M_{II}O_7$. Therefore, the comparison between the crystallographic study and the vibrational study allowed the detection of a local vibration in an inorganic crystal.

10.2. Structural studies: colored ionic species

The recently developed ability of Raman to examine highly colored samples has greatly increased its usefulness for structural determinations. Even though the compounds were colored, the Raman spectra of molecular metal halides, MX_4 (M = C, Si, Ge, Ti or Sn; X = F, Cl, Br or I) have been obtained [224]. All four fundamentals expected for molecules of T_d symmetry, $\nu_1(a_1)$, $\nu_2(e)$, $\nu_3(t_2)$ and $\nu_4(t_2)$ (only the t_2 fundamentals are IR active) were observed. Fig. 61 shows the spectrum of vanadium oxytribromide, which is dark red in color [242]. The appearance of six fundamentals (three of which are polarized) is consistent with C_{3v} symmetry.

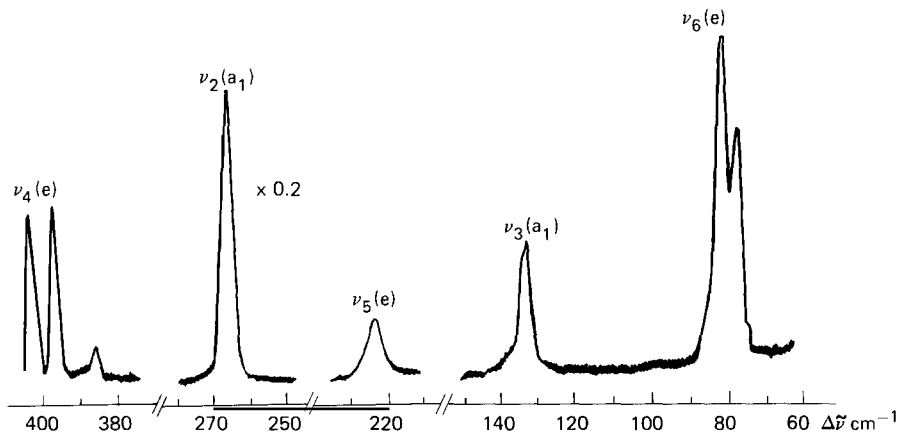

Fig. 61. Raman spectrum of crystalline vanadium oxytribromide, 647.1 nm excitation. Symmetry designations are given in C_{3v} nomenclature. (From R.J.H. Clark and P.D. Mitchell, J. Chem. Soc., Dalton (1972) 2429.)

10.3. Structural studies: colored coordination compounds

In the field of coordination chemistry, vast numbers of compounds are deeply colored. Work has been undertaken to obtain Raman values of fundamentals which, when combined with IR data, can be used for force constant calculations and bond strengths. Examples include studies of the square planar platinum or palladium complexes of the type $MX_2(SR_2)_2$ (X = Cl, Br or I; R = Me, Et, isopropyl, etc.) [242–243]. The biggest hindrance to the study of these colored compounds has been intense local heating caused by partial absorption of the laser beam, but sample rotation has done much to obviate these effects. (Also see section 4.4 on the rotating cell and ref. [41] on using low laser power and defocussing the laser beam.)

10.4. Structural studies: glasses and quartz

One of the major techniques used in the study of glasses and glassy solids, along with IR, NMR and EPR, has been Raman spectroscopy. A complete review of the application of spectroscopic approaches to borate, silicate, germanate, phosphate, arsenite, other oxides, chalcogenide glasses, and molten and glassy salts was published by Wong and Angell [244].

An example of the Raman spectra of glasses is shown in fig. 62 [2]. The spectrum 62a is of boric oxide glass and shows features characteristic of a borate ring structure. The spectrum 62j is sodium metaphosphate glass and represents the metaphosphate chain structure. The glasses of intermediate

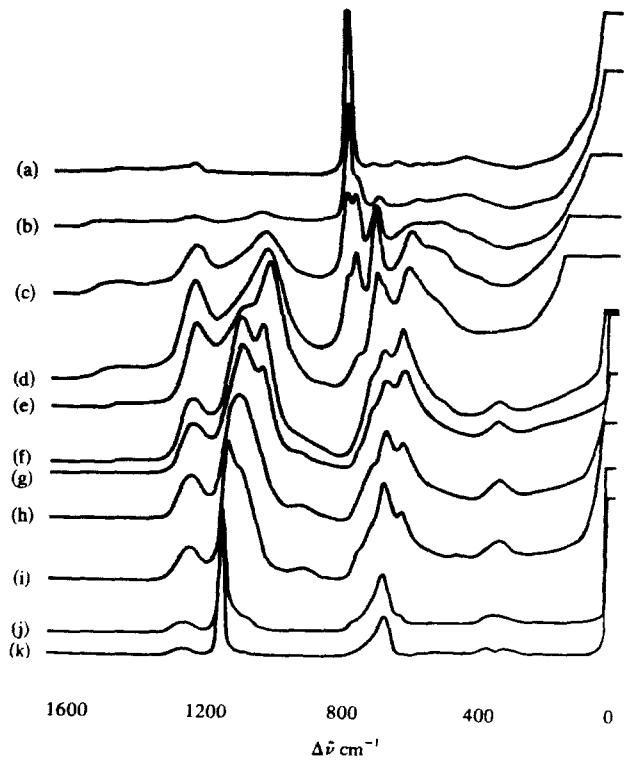

Fig. 62. Raman spectra of boric oxide/sodium metaphosphate glasses, 488.0 nm excitation. (From ref. [2].)

composition (figs. 62b thru 62k) show bands due to P–O–P, B–O–P and B–O–B links. Because of the increased disorder of the lattice, the bands are generally broad. Alkali phosphate glasses were also examined by Fawcett et al. [245] and Rouse et al. [246]. Raman and IR spectra for two crystalline phases of VPO_5 (A and B) were obtained, which greatly aided in the interpretation and band assignments of related VPO_5 glasses.

Structure of glasses in the systems calcium oxide–sodium oxide–diboron trioxide and magnesium oxide–sodium oxide–diboron trioxide were studied by Komjnendijk [247]. Verweij [248] studied the actual reactions in a potassium carbonate-silica glass-forming batch and was able to identify the various glassy and crystalline phases which occurred during the reactions. Other structure studies have involved lithium titanium silicate and lead silicate glasses [249], binary chalcogenide glasses [250], and lithium oxide–iron(III) oxide–silica glasses [251].

An unusual application of Raman involved the detection of OH^- and H_2O impurities in the crystal lattice of a quartz. This work was important because defects such as these lower the mechanical quality of quartz. Walrafen and Luongo [252] conducted investigations of hydrothermal α-quartz and obtained valuable information involving the geometrical distribution as well as interactions between the OH^- and H_2O impurities.

An unusual technique was used when the IRS (Internal Reflection Spectroscopy) method was successful in obtaining a spectrum of α-quartz. Raman-IRS spectra were first successfully recorded by Okeshoji et al. [253] for liquid carbon disulfide. Baptizmanskii applied the method to α-quartz, making it possible to compare the spectra of the surface layer and volume regions of the crystal [254]. Thus, the extension of the IRS method to Raman shows great promise in the study of the properties of thin surface layers of transparent crystals.

10.5. Structural studies: carbon compounds

The structural characterization of carbon compounds has been studied extensively by Vidano et al. [255–257]. The properties and behavior of carbon materials are strongly structure-dependent, and Raman spectroscopy can be used both to characterize virgin and treated-surface structures and textures of various kinds of carbon materials and to study their morphology and defects. An extensive survey of the Raman spectra of carbon materials has produced experimental evidence for at least five structure-sensitive bands [258]. In addition to the 1580 cm^{-1} graphite line and the 1360 cm^{-1} disordered C line which are always present, there is a disorder line at ~1620 cm^{-1} that is responsible for the apparent blue shift of the graphite line in very disordered C and there are lines at ~2700 and 2735 cm^{-1} that are strong in graphite and annealed C, but absent in disordered C. These additional lines increase the capability of Raman to characterize carbon materials. Further work is planned by Vidano on additional investigations of graphite-related compounds: the influence of various damaging treatments such as ion etching, mechanical polishing, nuclear irradiation, and studies on the polarization characteristics and temperature dependence of the carbon and graphite spectra.

10.6. Structural studies: sulfur compounds

Pure sulfur and sulfur compounds have also been examined by Raman. Gautier et al. [259] studied single crystals of monoclinic β-S at various temperatures above and below the transition temperature. Janz et al. [260] investigated the S_3^{2-} anion from 125 to 580°C using BaS_3 as the model system. He also studied potassium and sodium polysulfides in the polycrystalline, molten and glassy states [261–262].

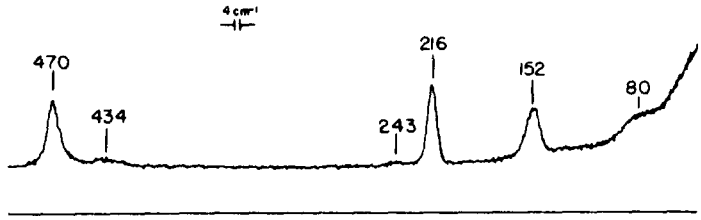

Fig. 63. Raman scattering from deposit in glass bubble, 514.5 nm excitation. (From ref. [266].)

Solutions of alkali metals and sulfur in liquid ammonia and amines have been the subject of numerous investigations by various techniques. The solutions are characterized by unusual colors and high conductivities, but the exact nature of the solvent or solute is not understood. The feasibility of using Raman spectroscopy to elucidate the nature of sulfur dissolved in amines was shown by Daly and Brown who obtained the Raman spectra of rhombic sulfur dissolved in various primary amines [263] and secondary amines [264].

A very practical application of Raman involved the study of sulfur in wood-bonding systems. The identification of CH_2–S bands indicated the S reacts with formaldehyde-urea copolymer present in the systems [265].

Another practical application involved the identification of sulfur deposits in bubbles in glass [266]. Fig. 63 shows the Raman spectrum obtained from a deposit on the surface of an inclusion from a clear soda-lime-silica glass plate. The lines clearly identify the deposit as elemental sulfur and the lack of structure indicates it is in its polymeric form $S_\infty + S_8$ [267]. Raman spectroscopy was also used to identify the gaseous contents of the same bubble and to observe a chemical reaction which changed the relative concentrations of the gases as the sample was heated.

10.7. Structural studies involving changes of state and phase transitions

Many studies of inorganic compounds involve changes of state or phase transformations, and Raman is particularly useful for following the structural changes during these processes. Fig. 64 shows the

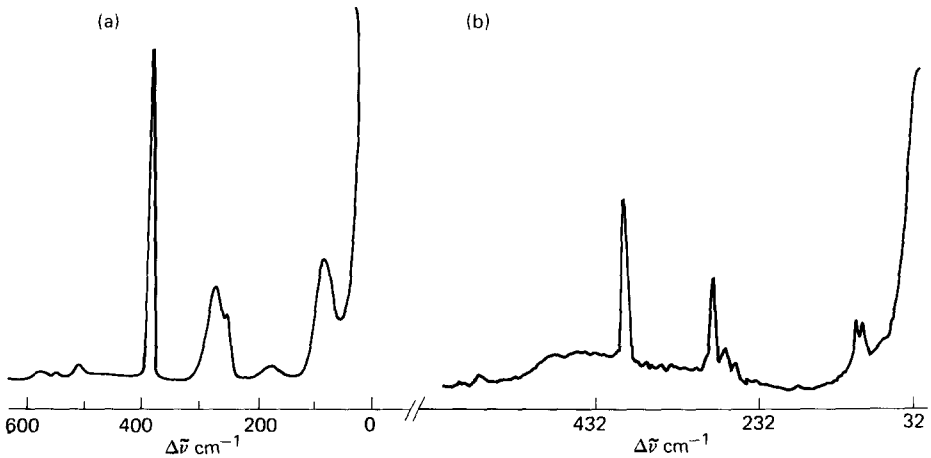

Fig. 64. The Raman spectrum of phosphorus(V) chloride. (a) In the vapor state at 430°K, 488.0 nm excitation, and (b) in the solid phase at 87°K, 632.8 nm excitation. (From ref. [2].)

Raman spectrum of phosphorus(V) chloride in the vapor state at 430°K and the solid state, formed by the rapid cooling of the vapor to liquid nitrogen temperature, at 87°K [268]. In the stable solid state, other spectroscopic studies have shown PCl_5 to have the ionic structure $PCl_4^+PCl_6^-$, but comparison of the spectra in fig. 64 of the vapor and this metastable state show they are the simple molecular form PCl_5 [269].

The study of Raman spectra of oriented crystals as a function of temperature and pressure can yield much valuable information about the structural changes which accompany phase transitions. Ammonium chloride [270], sodium nitrate [271] and potassium selenate [272] are among the inorganic crystals which have been studied. Phase transitions in dicesium lithium iron hexacyanide, $Cs_2LiFe(CN)_6$, were also studied and compared to those of related salts [273].

10.8. Molten state

Inorganic compounds have also been studied in the molten state. Studies of the wavenumbers, intensities, bandwidths and band shifts have given valuable information of the nature of interactions in this state. For example, such investigations show that for molten nitrates and sulphates, the position (wavenumber) of the symmetric stretching vibrations of the nitrate ion and the sulphate ion decrease approximately linearly with decrease of the ratio of Z, the cation charge, to r, the cation radius [274]. Fig. 65 shows the schematic representation of the Raman spectrum of molten gallium chloride ($GaCl_2$) [275] which proves that it is an ionic compound $[Ga^+][GaCl_4^-]$. This is in contrast to the halides of mercury(II), $HgCl_2$ and $HgBr_2$, which are consistent with the existence of the linear Cl–Hg–Cl and Br–Hg–Br molecules [276].

10.9. Equilibrium, dissociation and redistribution reactions

Raman spectroscopy is also particularly valuable for studying equilibrium, dissociation, or redistribution reactions, especially where products are difficult to isolate. Fig. 66 shows the Raman spectrum of a cyclohexane solution of a 2:1 mixture of $VOCl_3$ and $VOBr_3$ in the 260 to 420 cm^{-1} region where vanadium–halogen stretching bands occur [277]. Four bands can be seen and they are attributable to $VOCl_3$, $VOBr_3$, $VOCl_2Br$ and $VOClBr_2$. The redistribution reaction is almost instantaneous at room temperature and the resulting distribution of halogen atoms is approximately statistical.

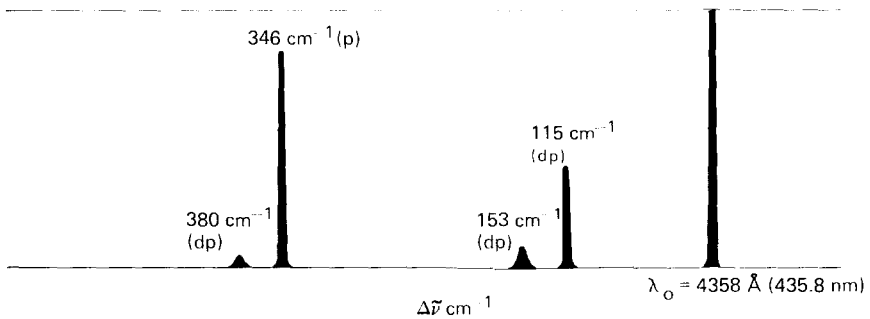

Fig. 65. Schematic representation of the Stokes Raman spectrum of molten $GaCl_2$, 435.8 nm excitation. (From ref. [2].)

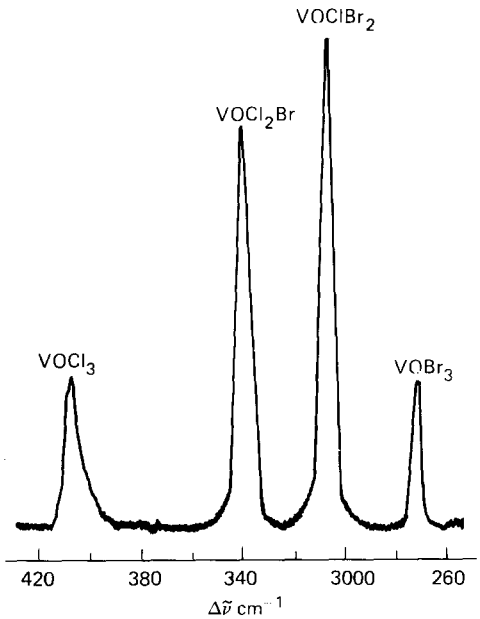

Fig. 66. Raman spectrum of a cyclohexane solution of a 2:1 mixture of vanadium oxytrichloride and vanadium oxytribromide in the region of the $\nu_2(a_1)$ fundamental of each molecule (676.4 nm, 647.1 nm and 568.2 nm excitation). The intensities of the a_1 bands of the bromine-containing species are greater than the abundance of such species (calculated statistically) would suggest, owing to the fact that metal–bromine bond polarizability derivatives are greater than metal–chlorine bond polarizability derivatives. (From R.J.H. Clark and P.D. Mitchell, J. Chem. Soc., Dalton (1972) 2429.)

10.10. Complex ions

Complex ions are another species which can be studied by Raman spectroscopy. Solvent extraction techniques to isolate a particular complex species have been particularly useful and have been applied to systems including the chloro- and bromo-complexes of mercury(II) [278], cadmium(II) [279], thallium [280], and arsenic [281]. Tytko and Schonfeld [282] investigated the relation between solid isopolymolybdates and their ions in solution and found that the octamolybdate ion $Mo_8O_{26}^{4-}$ is not present in appreciable quantities in solution at room temperature, contrary to previously published results.

Aqueous solutions of NaH_2PO_4 were investigated by Steger et al. [283]. A mathematical separation of IR bands between 700 and 1500 cm^{-1} and a study of the Raman spectra indicated the anions associated into chains which had a line group symmetry isomorphous with C_{2h}.

10.11. Resonance Raman of inorganic molecules

An area which is attracting an increasing amount of attention is that of the resonance Raman spectra of inorganic molecules, particularly those possessing allowed electronic transitions in the visible region. Comprehensive reviews have been written by Clark and Stewart [26, 230]. As indicated previously the resonance Raman effect (RRE) is always stronger when $(\nu_e - \nu_0) \approx 0$ (ν_0 = exciting frequency, ν_e = the frequency of the lowest allowed electronic transition of the molecule) and it is characterized by high-intensity overtone progressions in a totally symmetric fundamental. This is shown for the $Mo_2Cl_8^{4-}$ ion in fig. 67 [284]. The study of this ion is particularly interesting because it is known that the ca. 19 000 cm^{-1} transition involves excitation of the δ-electron of the so-called quadruple Mo–Mo bond

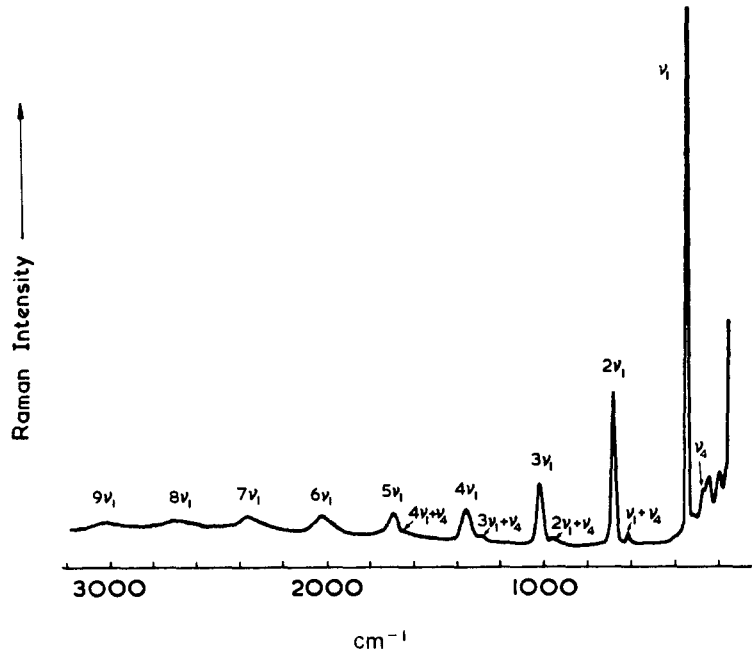

Fig. 67. Resonance Raman spectrum of $Cs_4Mo_2Cl_8$. (From ref. [284].)

[285–286]. By bringing the exciting frequency into coincidence with this band, then, it is the totally symmetric vibration ν(Mo–O–Mo) which is active in the resonance Raman, indicating a close relationship between absorption spectroscopy and RR.

Clark and Mitchell studied the resonance and preresonance spectra of titanium tetraiodide [287] and were able to determine the harmonic frequencies and anharmonicity constants for the $\nu_1(a_1)$ fundamental.

An unusual application of RRE is the identification of the sulfur species present in the deep blue mineral ultramarine, which is essentially a sodium aluminosilicate with the idealized formula $(Na_8Al_6Si_6O_{24}S_4)_n$ [288]. Resonance Raman has also been used as a probe of the annealing behavior of Cu_2O implanted with 180 keV Cd^{2+} ions [289]. As annealing progressed, large changes were observed in the resonance Raman spectra when compared to the spectra of unannealed samples. Analysis indicated a strong annealing stage at ~250°C which erases >99% of the damage caused by implantations. Other interesting applications can be found in Clark's review article [26] on resonance Raman spectra of inorganic ions and molecules.

10.12. Minerals

Raman spectroscopy can be used very effectively for diagnostic purposes on minerals. In general, the Raman spectra of minerals are simpler in appearance than the comparable IR spectra, the bands are sharper, and the interpretation simpler. The position of ν_1, the totally symmetric (MO_n) stretch and normally the strongest and sharpest band in the spectrum, is a useful preliminary guide to mineral identification. Griffith [226, 290] recorded the Raman spectra of a number of carbonate, phosphate, arsenate, vanadate, niobate, tantalate, sulphate, chromate, molybdate, and tungstate minerals. It appears from a study of these spectra that, for minerals containing MO_3 or MO_4 groups, a "fingerprint"

Table 17
Positions of strongest Raman bands (i.e. ν_1, totally symmetric stretch) in various (MO_3) and (MO_4) minerals (cm^{-1}) (From ref. [226].)

Carbonates	1100	Arsenates	830
Nitrates	1050	Chromates	880
Silicates	880–1000	Molybdates	870
Sulphates	990	Tungstates	910
Phosphates	960	Vanadates	830

approach is possible much the same as for IR mineral spectra. Table 17 lists the positions of the strongest Raman bands (i.e. ν_1, totally symmetric stretch) in various MO_3 and MO_4 minerals. But comparatively little is known about the Raman spectra of minerals thus far, leaving a vast field of potentially exciting investigations.

11. Adsorbed species and surfaces

The study of surfaces and surface phenomena is very important to the industrial chemical world in the fields of coatings, metals, corrosion chemistry, colloid chemistry, and catalysis. Chemistry at surfaces is different from chemistry of bulk materials. Analytical methods such as ESCA (electron spectroscopy for chemical analysis), Auger spectroscopy, electron microscopy and LEED (low energy electron diffraction) are all useful in characterizing various aspects of surface structure. Raman and infrared are included in this group of surface techniques because vibrational spectra reflect so well the chemical and physical changes in a molecule as affected by its environment. Thus, they are extremely valuable for studying adsorbed species to obtain information about the type and nature of the active sites of surfaces.

Infrared spectroscopy often achieves a higher signal-to-noise ratio and has been extensively used in studies of adsorbed species [291], but it is seriously hampered by the intense bands of common oxide substrates which interfere with much of the interesting spectral region. Raman spectroscopy offers a decided advantage in such cases, particularly for molecules that are good scatterers. In addition, its water transparency allows the study of solid–aqueous interfaces. Raman capabilities for surface studies have involved a considerable variety of systems and, especially since 1967, there have been a number of publications involving thorough studies of surface-adsorbent interactions, the chemical nature of surface films and layers, and even the study of electrodes beneath electrolyte in electrochemical cells.

There are several reviews available on Raman literature of solid–solid, solid–liquid and solid–gas interfaces, among which the most useful are ones by Paul and Hendra [292] and Cooney et al. [293]. Good examples of solid–solid interfaces were given by Buechler and Turkevich [294] who interpreted the spectra of molybdenum trioxide on porous Vycar, uranium oxide on porous glass, and platinum on silica.

Solid–gas interactions have been studied by Stencel and Bradley who exposed the surface of Ni(III) to CO, H_2 and O_2 in the 300°C temperature region [295]. The changes of a major Raman band at 80 cm^{-1} upon adsorption of the gases were shown and discussed in relation to possible adsorbed species. This work was extended [296] by the development of an ultrahigh vacuum chamber which enabled sample temperatures from −85° to 600°C to be obtained, along with surface-cleaning capabilities.

Another useful device for gas–solid reaction mechanism studies was developed by Kagel et al. [297] who constructed a high pressure cell capable of withstanding pressures in excess of 650 psig and evacuable to ~5 Torr. The entire cell is enclosed in a small furnace for elevated temperature studies.

Most of the substrates used for surface studies are of catalytic importance and can be divided into two main classifications. The first of these constitutes oxides and pure forms of the lighter elements, aluminum and silicon, and the important adsorbents derived from them – – the silica-alumina cracking catalysts and the zeolites, which are crystalline silica-aluminas with replaceable metal cations. B.A. Morrow [298] obtained the Raman spectrum of chemisorbed methanol on silica and compared it to the infrared spectrum. Yamamoto and Yamada [299] examined the spectral changes of the three diazines – pyrimidine, pyrazine and pyridazine-absorbed on SiO_2. A series of articles were published by Tam et al. [300–303] on the vibrational spectra of acetylene on A-type zeolites and pyrazine, acetylene dimethyl-acetylene, and cyclopropane on X-type zeolites. The dependency of the Raman line shift on the nature of the zeolitic cation is discussed in each case. Chemisorption and reactions on zeolite molecular sieves were studied by Trotter [304]. The Raman advantage of low frequency observation in the presence of the zeolite framework was critical because it allowed a kinetic comparison between silver complex formation with benzotriazole at 793 cm^{-1} and the surface formation of N–Ag–N bonds at 136 cm^{-1}.

In addition to the silicon and aluminum adsorbents, the second major type of support comprises the finely divided metals, usually stabilized in high surface area form by deposition on supports of the finely divided oxide types just described. Krasser et al. [305] observed the Raman scattering of hydrogen chemisorbed on silica-supported nickel. Enhanced intensity sometimes occurs when molecules are adsorbed on metals and this phenomenon is discussed by Meskovits [306], who proposes that the enhancement arises from preresonant or resonant excitations of conduction of electron resonances in adsorbate-covered metal protuberances on the surface. The theory that enhancement is a resonance Raman effect was also espoused by Hexter and Albrecht [307]. They included in their publications a thorough review of the theory of metal surface Raman spectroscopy with a discussion of the selection rules and relative intensities of the Raman spectra of adsorbed molecules.

The most extensive studies of surface interactions have involved the adsorption of pyridine on various adsorbates [308–311]. One of the reasons for the choice of pyridine is because its vibrational modes shift in very well-defined ways dependent upon the site to which it is attached. An excellent review and list of references can be found in the Paul and Hendra article [292]. Table 18 shows how sensitive these Raman bands of pyridine are to its different bonding environments since the pyridine can chemisorb on the surface by donation of the lone pair of electrons on the nitrogen atom to Lewis acid sites (a coordinate bond); it can hydrogen bond to surface OH groups; or it can form the pyridinium cation (Brönsted acid sites) by complete proton abstraction from surface OH groups.

Table 18
Variations in the frequencies (cm^{-1}) of the C–H stretch and ring-breathing vibrations of pyridine with the nature of the bonding

System	Bonding	Ring breathing vibrations		C–H stretch
Pyridine		991	1031	3060
10% pyridine in CH_3OH	H-bond	996	1030	3062
10% pyridine in H_2O	H-bond	1004	1036	3074
10% pyridine in HCl	Brönsted	1010	1029	3109
Zn (pyridine)$_2Cl_2$	Lewis	1023	1047	3075, 3085

In recent years there has been a very high interest in the nature of reactions which occur at electrode–electrolyte surfaces [312]. One of the reasons that an understanding of these reaction mechanisms is extremely important during the current energy crisis is because of the quest for new kinds of fuel cells and storage batteries. Because of its water transparency, Raman has been the major technique used to monitor changes at mercury [313], silver [308, 314–317], copper [318–319], and platinum [320] electrodes as a function of the applied potential.

Fleischmann et al. [319] selected pyridine as the molecule to probe the nature of the adsorption sites on the electrode surfaces. Fig. 68 shows the Raman spectra of pyridine in solution and at a silver electrode at various potentials in 0.05 pyridine/0.1 M aqueous potassium chloride. The bands at ~1008 and ~1036 cm^{-1} pass through an intensity maximum close to the zero of potential change. With increasing negative potential, there is a significant change in the frequency of the ring breathing mode and a new band is observed at 1025 cm^{-1}. This latter band had previously been interpreted [308] as being due to pyridine directly co-ordinated to silver, the other bands being due to pyridine adsorbed through a polarized layer of water molecules. However, some of the changes could also be due to the interaction of pyridine with adsorbed carboxylate groups on the surface of the electrode.

The development of resonance Raman has proved invaluable in the study of surfaces [321–323]. Yamamoto and Yamada [324] discussed the structures and formation mechanisms of carbonium ions on porous Vycor glass. Takenaka and Nakanaga [325] devised a new method of total reflection of the exciting line to record the resonance Raman spectra of monolayers adsorbed at the interface between carbon tetrachloride and an aqueous solution of a surfactant and a dye. Jeanmaire and Van Duyne [326] successfully interfaced electrochemical radical ion generation with resonance Raman to obtain spectra for the electrogenerated monoanion radical of tetracyanoquinodimethane upon excitation of its lowest $^2B_{1u}$ excited state [326–329]. Thus, resonance Raman has proven its utility as a molecularly specific monitor for electrochemical processes and an important tool for the characterization of charge-transfer solids.

We would be amiss if we did not allude to other applications of Raman surface spectroscopy so important to the industrial world – – for example, the study of thin films and coatings [330–331], insoluble

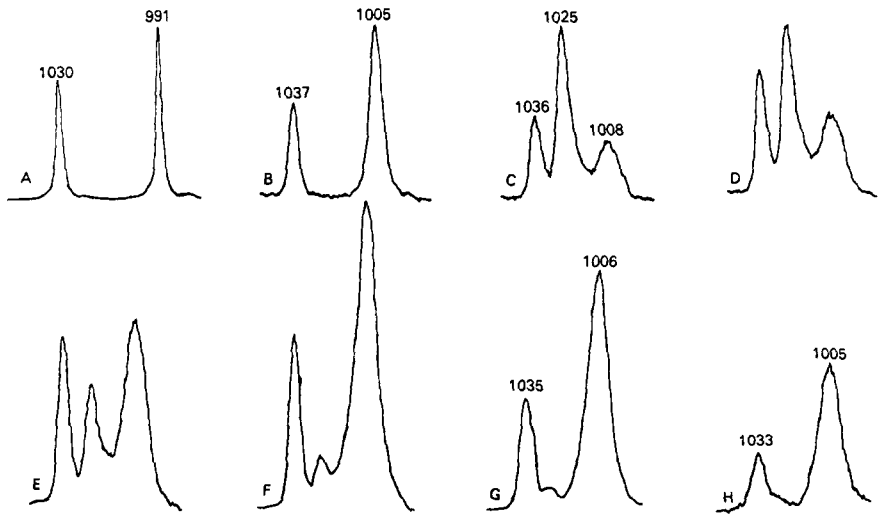

Fig. 68. Raman spectra of pyridine in solution and at the silver electrode. (A) liquid pyridine; (B) 0.05 M aqueous pyridine; (C) silver electrode in 0.1 M potassium chloride +0.05 m pyridine solution at 0V (SCE); (D) −0.2 V, (E) −0.4 V; (F) −0.6 V; (G) −0.8 V; (H) −1.0 V. (From ref. [292].)

monolayers spread on a water surface [332] or iron oxide films formed on metal surfaces (to facilitate the use of LRS for in-situ analysis of corrosion) [333]. It has also been used in the biological field, for example, to study molecular orientation at interfaces by polypeptide monolayers [334]. So, although Raman is a relatively new technique in surface science, it has already proven itself of immense value, especially in those areas of "real world" surfaces--dirty and heterogeneous, containing mixtures of corrosion products, grease, oxides, etc. This is in contrast to ESCA, LEED, and Auger spectroscopy which need chemically clean surfaces under high vacuum conditions and samples treated in specially prescribed manners.

12. Catalyst research

Raman spectroscopy has had an important impact on industrial catalyst research, especially in the selective oxidation of hydrocarbons by transition metal oxide catalysts. An impressive body of literature has developed over the last few years exploring the mechanisms of the reactions and delving into just how a heterogeneous catalyst works [335–336]. Most of today's modern spectroscopy tools have been focussed on the characterization of the surface and bulk structures of these complex oxide structures, and Raman spectroscopy has emerged as one of the most useful methods.

Molybdate catalysts have been used for the selective oxidation of methanol to formaldehyde and the selective ammoxidation of propylene to acrylonitrile, among others. In all cases, it has been recognized that the surface structure of the catalyst plays a vital role in the selectivity and activity of the catalyst [337–340]. The nature of the catalyst surface and the reaction mechanisms can be probed with studies of adsorbed species using both infrared and Raman spectroscopy. This topic was discussed in section 11. However, it is the catalyst structure itself which governs the reaction; therefore, the examples in this section will be concerned with the structural changes which occur.

12.1. Techniques

Most of the transition metal oxides are colored solids ranging from light yellow or green to brown or black. Therefore, in order to obtain good Raman spectra, it is necessary to carefully consider and control some of the instrumental parameters. Most investigators utilize a rotating cell in order to prevent decomposition or phase changes in the samples. It is also possible to obtain the Raman spectra of industrial catalysts and mixed transition metal oxides without a rotating cell by carefully controlling the microscope objective setting and laser power at the sample [41].

An interesting recent publication by Payen et al. [341] reports a Raman spectroscopic study of some cobalt molybdenum catalysts using the laser microprobe. As discussed in section 4.3, this instrument has a spatial resolution of the laser beam of approximately 1 micron. Only 3 mW of laser power at the sample was used. The authors observed segregation of phases on the alumina supports in agreement with ESCA data. The special design of this instrument's collection optics permits the use of such low power while still providing good spectral data.

In hydrodesulfurization, commercial catalysts are supported on alumina and several investigators have reported the interaction between the support and the cobalt molybdenum catalyst [341–345]. But very often the literature is not consistent on spectral data or structures of model compound metal oxides. In fig. 69, the spectra of ferric molybdate as obtained by Trifiro and co-workers [339] and

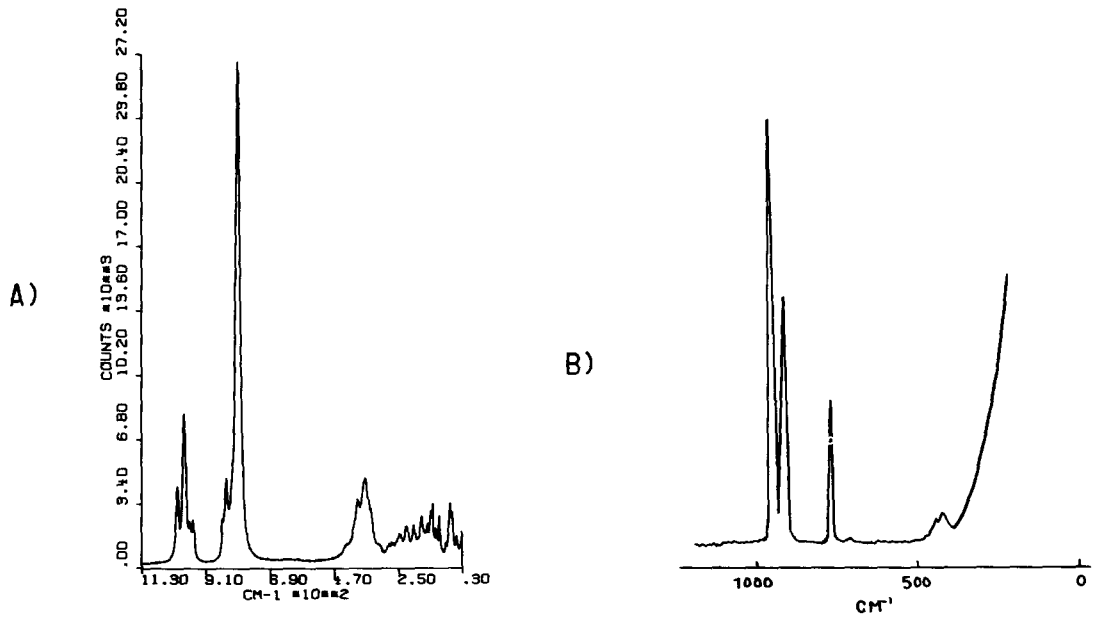

Fig. 69. Raman spectra of $Fe_2(MoO_4)_3$. (A) Sohio results (agree with Trifiro et al. [339]); (B) Medema et al. results, ref. [342].

Medema and co-workers [342] are compared. They differ markedly, primarily as a result of the method of preparation. Grasselli et al. report data [41] that agrees with that of Trifiro et al.

As previously mentioned, perhaps one of the most important aids in obtaining good Raman spectra is the use of a data processing system with the Raman spectrometer. The capability to signal average and smooth data in order to optimize the sensitivity, to mathematically minimize background interference, or to subtract spectra at will, along with accurate frequency and intensity output, make the computer an indispensable tool for Raman spectroscopy of catalysts. Fig. 70 shows a striking example of this capability reported by Grasselli et al. [41]. It is the spectrum of molybdenum dioxide, MoO_2, a black solid. Fig. 70a is a single scan, fig. 70b is 150 scans, and fig. 70c shows the final spectrum, 150 scans smoothed and baseline corrected. The spectrum was obtained without sample rotation.

12.2. Heated cell

In previous work, Grasselli et al. [6] described the application of a heated cell to follow phase transformations in molybdate catalysts. Since most industrial catalysts operate at elevated temperatures, it is very meaningful to examine the structures of the solids at these working temperatures. For example, bismuth molybdate is known to exist in three modifications, the alpha, beta and gamma phase. The γ phase of Bi_2MoO_6 is a metastable compound with an X-ray diagram similar to that of the mineral koechlinite [346]. Heating this compound to temperatures in excess of 660°C in air produces an irreversible transition to the γ' phase [336]. Fig. 71 shows the transition from γ to γ' for bismuth molybdate as followed in the heated cell. From these data it appears that the onset of the γ' modification actually begins around 600°C rather than the 650°C temperature reported in the literature. Such observations may be important when considering the relative activity of the various phases in catalysis, for example in the oxidative dehydrogenation of 1-butane to butadiene for which the γ phase is considered to be the active one.

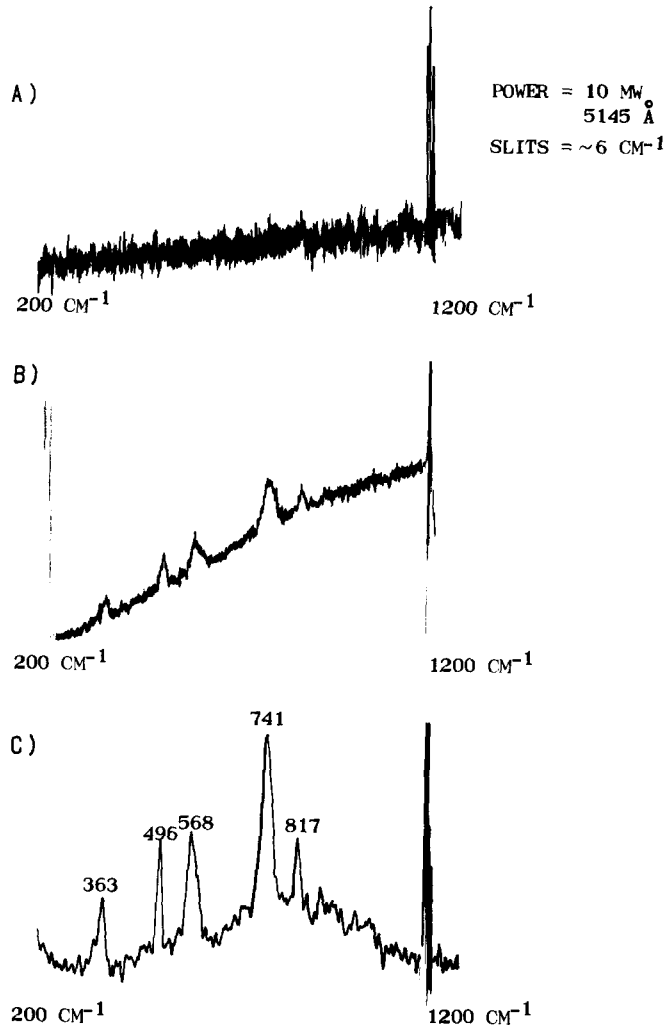

Fig. 70. Raman spectra of MoO_2, a black powder. (A) single scan, (B) 150 scans-raw data, (C) 150 scans-smoothed and baseline corrected.

12.3. Surface vs. bulk structures

The importance of the surface structure in oxide catalysts has already been mentioned, not only in terms of identification of active sites for hydrocarbon adsorption in mechanism studies, but also because the structure of the surface in relation to the bulk influences the redox capability of the catalyst. Boudeville and co-workers [347] have recently emphasized the importance of the surface structure relevant to the selectivity in olefin oxidation on antimony–tin–oxygen catalysts. Correlations between X-ray photoelectron spectroscopy data and the catalytic properties of these materials were reported. Segregated phases which exist at the surface of the catalyst were detected.

The reduction of ferric molybdate was studied in a Raman heated cell to gain some insight into surface versus bulk structures. A parallel study was conducted by ESCA [41]. The strongest band in the Raman spectrum of $Fe_2(MoO_4)_3$ is at 780 cm^{-1}, due to a Mo–O–Mo absorption (fig. 69). Fig. 72 shows successive scans of the 780 cm^{-1} band monitored at three-minute time intervals. In the Raman, it is clear that ferric molybdate initially undergoes a rapid reduction. This is followed by a slow, possibly

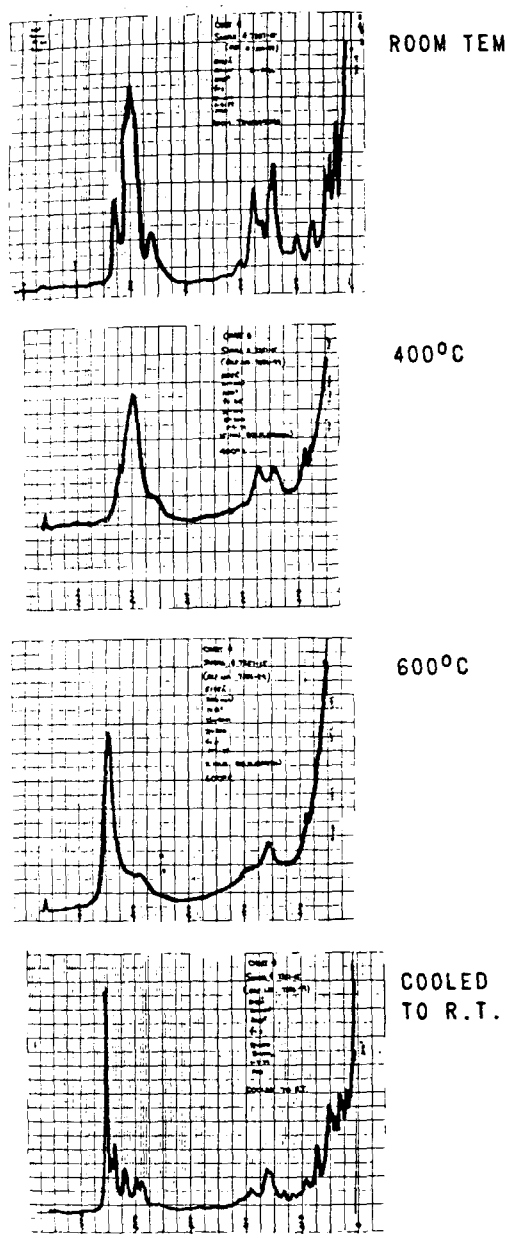

Fig. 71. Phase transition, γ–γ' Bi_2MoO_6.

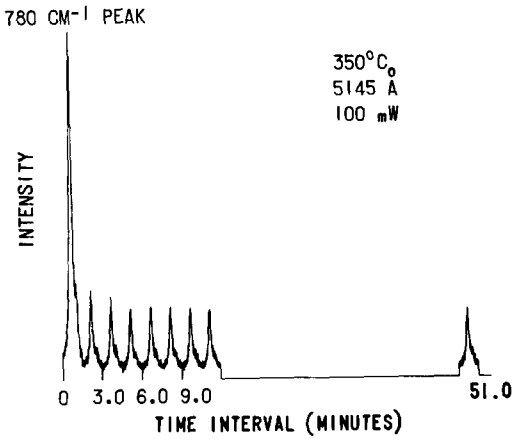

Fig. 72. Reduction of $Fe_2(MoO_4)_3$ with propylene.

first-order, reduction which is a function of the temperature. The sample reduces to ferrous molybdate at the end of the reduction. The ESCA data showed that only the molybdenum on the surface of the oxide is reduced. The combination of Raman and ESCA is a powerful tool for relating surface to bulk structure changes in catalysts.

13. Raman applications to the petroleum industry

Laser-excited Raman spectroscopy has not been utilized extensively in the petroleum field, mainly due to the sampling problems and fluorescence phenomena. There have been some applications,

however, and the number is rapidly growing. Spectra of various petroleum fractions have been reported. Low boiling products such as gasoline show many bands, mainly due to the presence of aromatic structures. Higher boiling fractions show broader, more poorly resolved bands [348].

Because of this complex and poorly resolved nature of the spectra, Raman has found greater application for the characterization of specific hydrocarbons than to the study of entire petroleum

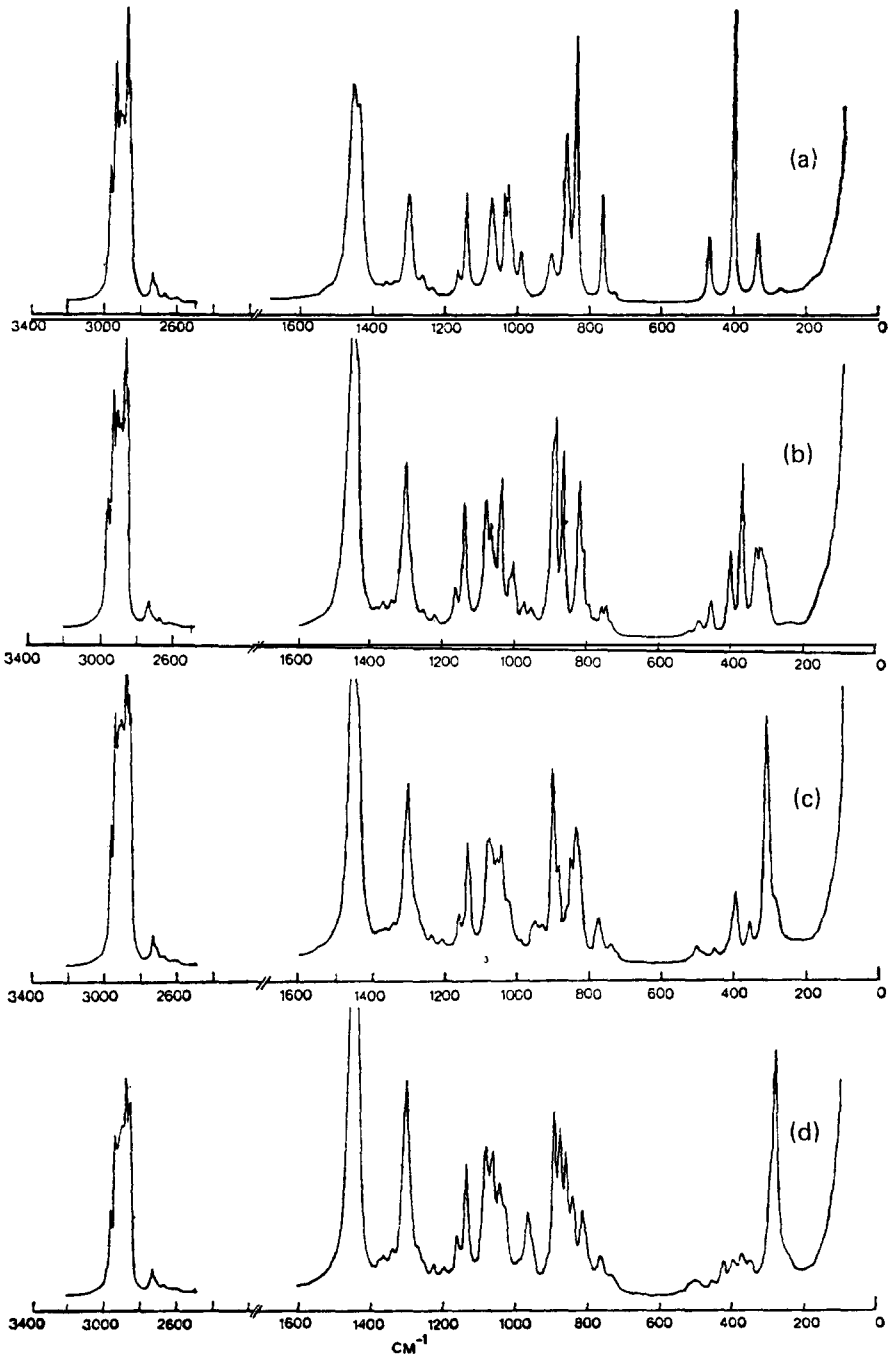

Fig. 73. Raman spectra of n-alkanes; laser 514.5 nm. (a) n-pentane; (b) n-hexane; (c) n-heptane; (d) n-octane. (From ref. [349].)

fractions. Although IR spectra of low molecular weight n-alkanes are very similar and tend to be dominated by CH stretching and bending vibrations, the Raman spectra show clearly the carbon skeleton vibrations and are, therefore, more useful for specific characterization of the molecules themselves. This is evident in fig. 73 which shows the Raman spectra of the n-alkane series C_5 to C_8 [349].

The complexity and large number of bands in the "fingerprint region" of the spectra below 1300 cm^{-1} are caused by the presence of a number of different conformers. As the number of chain carbons increases in the homologous series, the number of conformers also increases and the bands become broader and less well-resolved. In the solid state these bands are sharper, due to preferred conformations and crystallinity effects.

Chain branching also causes large differences in the Raman spectra and allows easier skeletal elucidation than in the infrared. Aromatic ring characterization has already been mentioned in section 5 on group frequencies. It was also pointed out that Raman is valuable in identifying groups such as –S–S, –C–S, and –O–O, which are found in petroleum product raw chemicals or intermediates.

In addition to the characterization of hydrocarbon types and functional groups, Raman has been applied to the examination of oil products, but there are many problems involved. For example, most oils are slightly or deeply colored. Some solid additives decompose in the beam, even at low laser power. Carbon tetrachloride dilution does not always halt these absorption effects which can sometimes cause local boiling. Fluorescence effects are frequently permanent – – i.e. they cannot be burned or quenched out – – and prolonged irradiation usually results in sample destruction.

Many oil products and formulated additives contain colloidal particles, which, in a viscous liquid, cause Tyndall scattering and the appearance of plasma lines or, in a mobile phase, cause spikes in the spectra produced by the Brownian motion of the particles as they move through the liquid. Filtration and/or centrifugation often are used to "clean up" this colloidal matter.

In spite of these problems Raman has found application to oil characterization, for example, the differentiation of synthetic and natural lube oils [349].

Raman has also been used to "fingerprint" oil spills. In order to identify pollutant sources, oil spills have been analyzed using various techniques including IR [350–352], GC, fluorescence, and low temperature luminescence. Ahmadjian and Brown [353] have shown that Raman spectra can provide confirmation or additional evidence of an oil spill source. To eliminate the major sampling problem involved – – that of the high fluorescent background – – the oil samples were diluted with pentane, shaken with coconut charcoal, filtered, and the solvent evaporated at ambient temperatures. Fig. 74 shows the large differences in the spectra of a lubricating oil, a kerosene and a No. 2 fuel oil. There obviously would be no difficulty in distinguishing among them. In the spectra of the three different No. 2 fuel oils shown in fig. 75, however, the differences are far more subtle and occur mainly in the relative peak heights. It would be much more difficult to make a specific identification unless confirmatory evidence were present. In an actual oil spill sample, shown in fig. 76 along with two suspect oils, the spectrum was a closer match with suspect A, and it was later confirmed that suspect A was from the spill source. Thus, Raman can be used as an auxiliary technique where a combination of "fingerprinting" methods are necessary to build stronger cases against suspected polluters.

In the petroleum industry, Raman can also be valuable in characterizing and identifying additives, especially polymeric or sulfur-containing ones. Obremski [354] used Raman in conjunction with IR to detect sulfur, determine how it was bonded into the system, and distinguish between three xanthates used as additives in high pressure lubricants.

Coates [349] has published the Raman spectra (as dialysis residues) of high molecular weight (MW = 1500) polyisobutene, polyalkyl methacrylate and styrene-acrylate copolymers. He has also

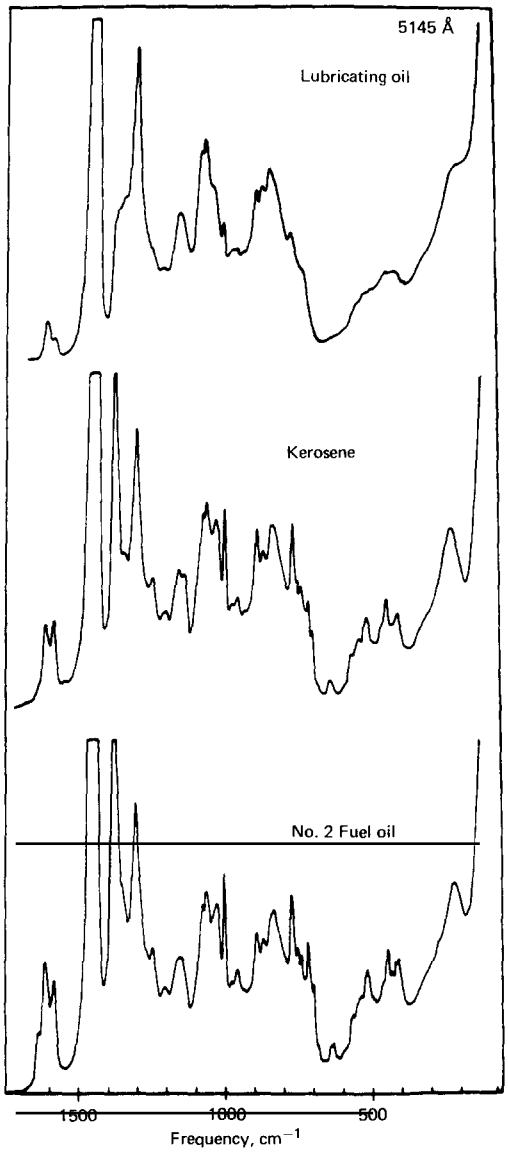

Fig. 74. Raman spectra of a lubricating oil, kerosene and No. 2 fuel oil. (From ref. [353].)

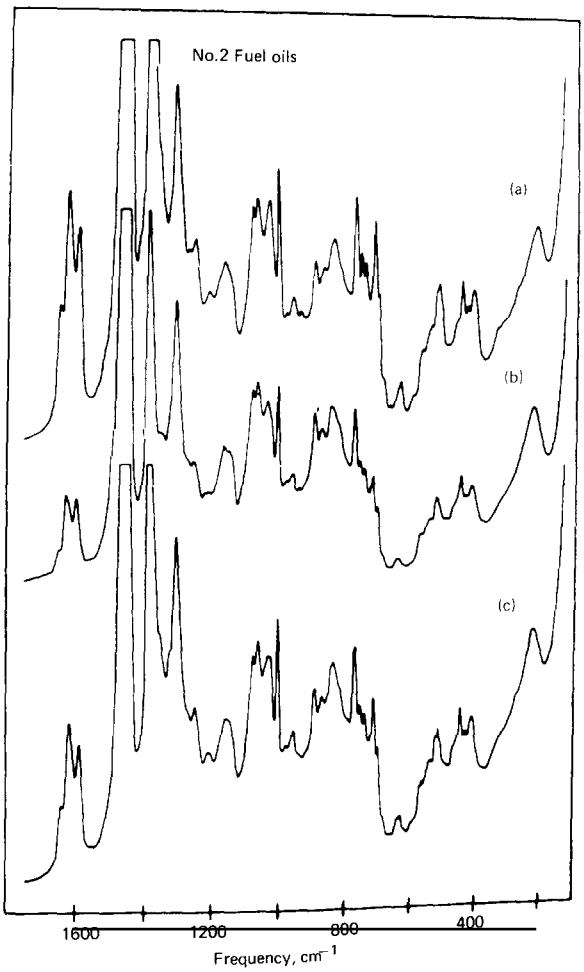

Fig. 75. Raman spectra of three different No. 2 fuel oils. (From ref. [353].)

discussed the spectrum of Amoco 150, a sulfur-containing additive used as a copper passifier in industrial oils, which is shown in fig. 77. C–S and S–S vibrations are evident at 635 cm^{-1} and ~500 cm^{-1}. The band at 731 cm^{-1} is probably associated with chain branching, i.e., an iso-octyl side chain.

Samples which are physically very small can be examined relatively easily by Raman because of the spatial resolution of the laser beam. Thus, deposits on various automotive parts can be run for identification and information as to potential source. Fig. 78 shows the spectrum reported by Grasselli et al. [41] of a white material found in a carburetor from a car in a test fleet using experimental gasolines and motor oils. The carburetor was fouled with some hydrocarbon deposit, but some tiny white crystals were also detected. They were carefully removed and examined directly with Raman

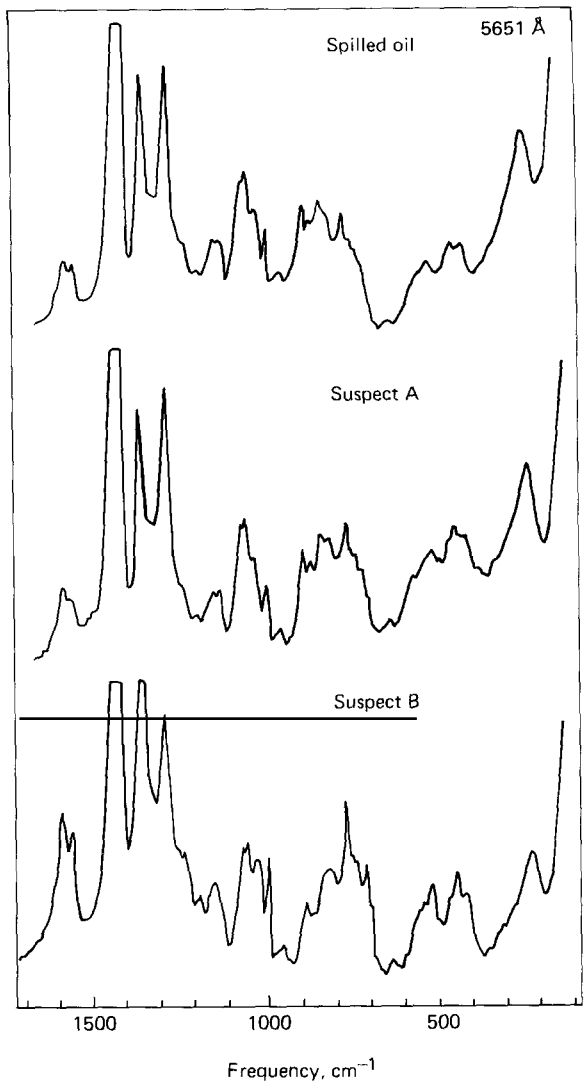

Fig. 76. Raman spectra of a spilled oil and two suspect oils. (From ref. [353].)

spectroscopy by mounting them on a glass slide on a 180° viewing platform. The intense single peak at 998 cm^{-1} is characteristic of sodium sulfate. This identification could also have been made by either IR or X-ray, but the ease and speed of the Raman analysis on this very small sample was a decided advantage.

Raman also has great potential for quantitative as well as qualitative analysis in the petroleum industry. It could be used, for example, to determine amount of sulfurization, concentrations of materials in aqueous solutions or amounts of oil additives in formulations, isomer formations, hydrocarbon type determinations or amounts of unsaturation. As instruments become less expensive and consequently more numerous within the petroleum industry, work will undoubtedly begin on these as well as other applications.

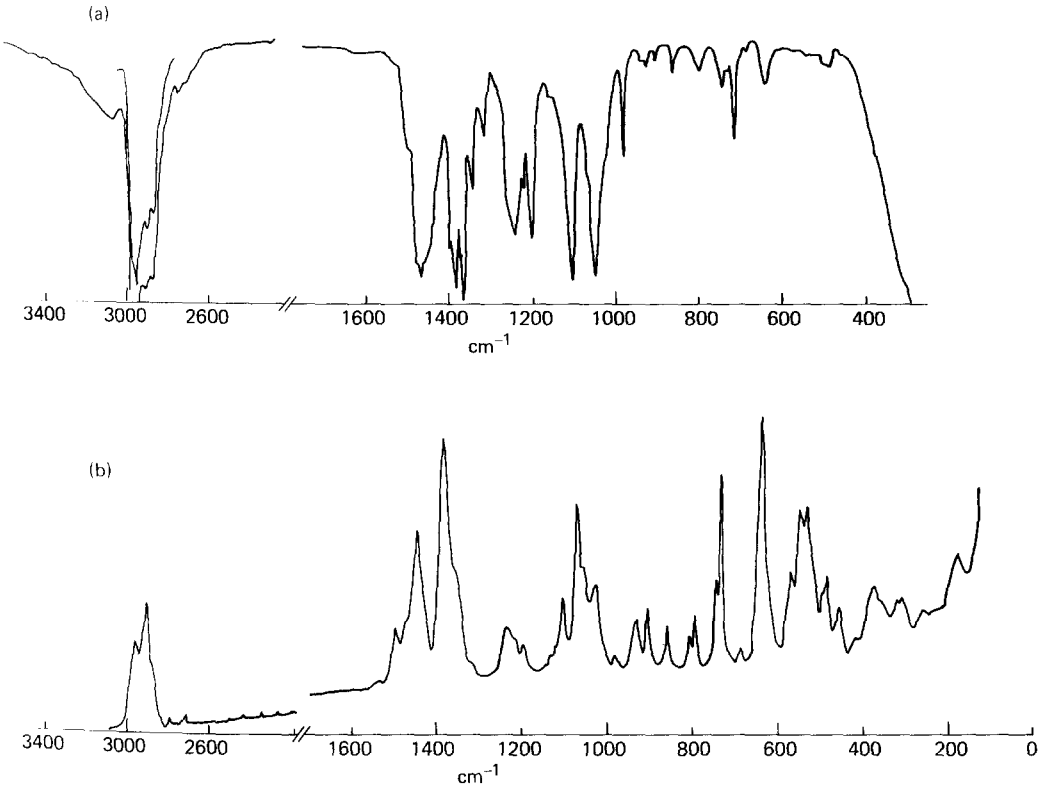

Fig. 77. (a) Infrared spectrum of Amoco 150; (b) Raman spectrum of Amoco 150, laser 647.1 nm. (From ref. [349].)

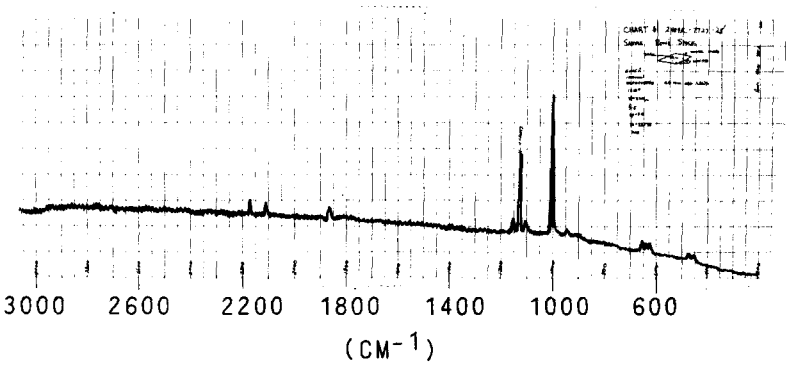

Fig. 78. Raman spectrum of carburetor deposit. (From ref. [41].)

14. Miscellaneous Raman applications

14.1. Barbiturates

Some common barbiturates have been examined by Raman to determine if they could be specifically identified. Analyses of barbiturates are important in clinical, forensic, and toxicological laboratories

and, as mentioned before, Raman has the advantage over other analytical techniques of sample handling ease and ability to work in aqueous solutions. Willis et al. [355] studied eight of the more common barbiturates including phenobarbital, barbital, secobarbital, amobarbital, pentobarbital, butabarbital, mephobarbital, and hexobarbital. All barbiturates belong to the pyrimidine class and are used as the free form or the sodium salt of the acid.

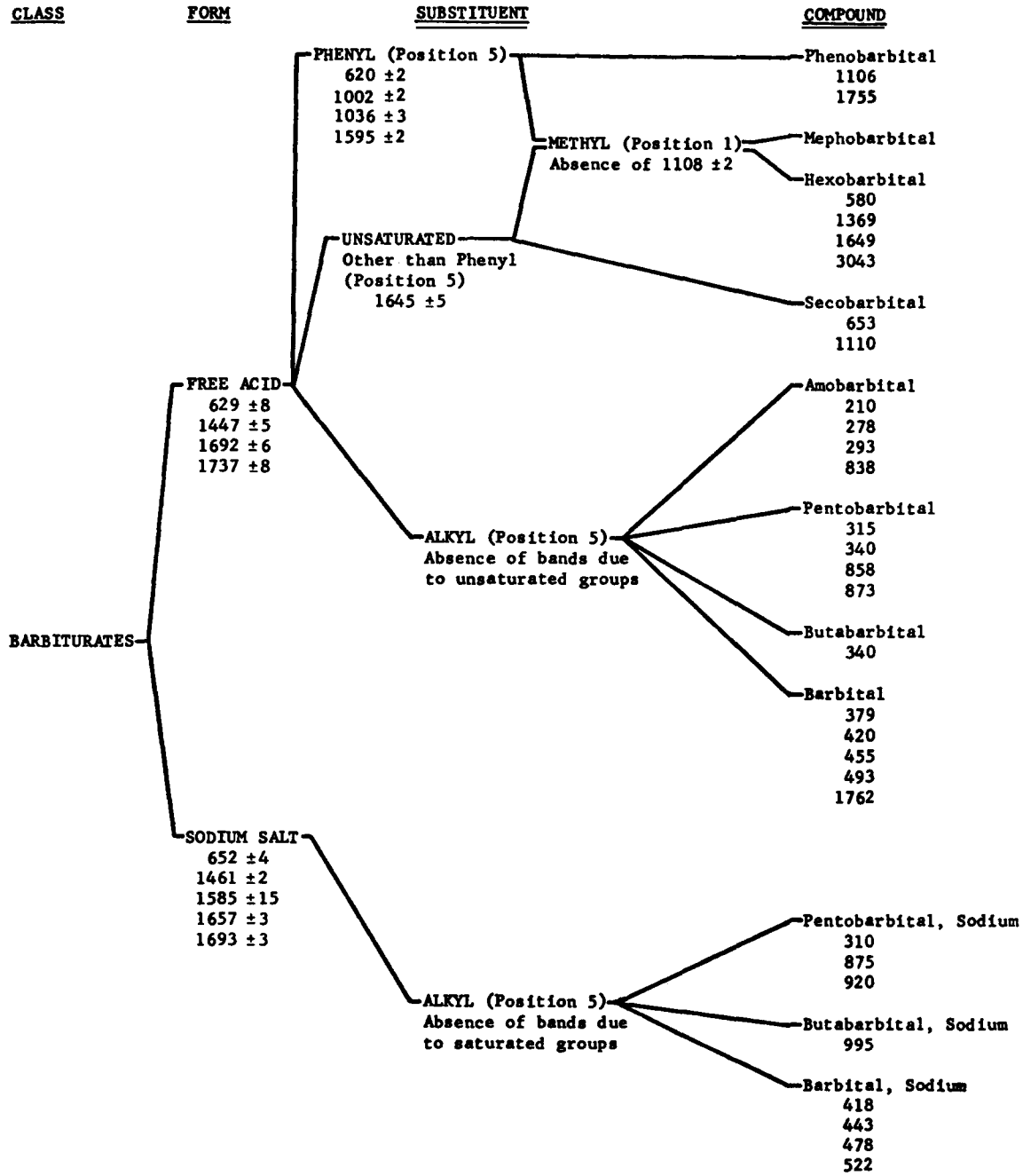

Fig. 79. Identification scheme of the common barbiturates. (From ref. [355].)

Identifying the general class of barbiturates in mixtures containing other drugs, binders, etc. is relatively easy, but distinguishing between the barbiturates is more difficult. A possible identification scheme is shown in fig. 79. Position numbers refer to positions on the pyrimidine ring.

14.2. Coals

Although Raman is not usually successful with darkly colored materials, there has been a study of coals [356]. The spectra of lignite, high volatile bituminous, low volatile bituminous, anthracite and graphite (powders and polished solids) are presented in fig. 80. The spectra are quite similar with bands at ~1585 and ~1360 cm^{-1}; the sharpness of the lines increases with increasing rank of the coals. These bands are attributed to graphitic or carbonized structures in the coal.

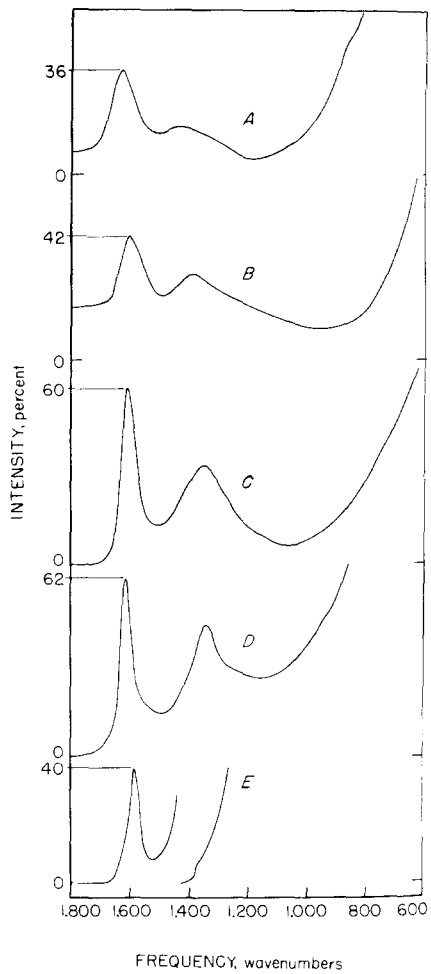

Fig. 80. Raman spectra obtained on U.S. coals. (A) lignite, 74.2 percent carbon; (B) high volatile bituminous A, 83.1 percent carbon; (C) low volatile bituminous, 90.0 percent carbon; (D) anthracite, 94.2 percent carbon; (E) graphite, highly oriented pyrolytic. (From ref. [356].)

14.3. Water pollution

There has been some activity involving Raman in the area of water pollution. In theory Raman should be able to examine water samples directly; however, in practice, fluorescence often interferes. In these cases, organic materials can be either extracted directly into carbon tetrachloride or Freon or converted into an extractable species [357]. Cunningham et al. [358] investigated detection limits for various solutes in water Solutions of nitrate, sulfate, carbonate, bicarbonate, monohydrogen phosphate, dihydrogen phosphate, acetate ion and acetic acid were measured and the influence of experimental parameters on detection sensitivity determined. Laser beam intensity and solvent background intensity are the two most influential factors. Under ideal conditions the ionic and molecular species could be detected in the 5 to 50 ppm range.

Bradley and Frenzel [359] had previously reported the detection of benzene in water at concentrations of 50 ppm and Baldwin and Brown [360] had favored detection limits of 25 to 75 ppm for various inorganic species. Using remote sensing equipment, the lower limit of detection was even higher; Akmadjian and Brown [361] could only detect 100 to 200 ppm of the inorganic species.

Ullman [362] investigated Raman for water quality assessment and detected nitrite and sulfate at 20 ppm and 8.5 ppm, respectively. Various herbicides and plant growth regulators were also investigated, but attempts to quantitate all of them were not successful.

To lower the minimal detectable concentration of pollutants, several workers took advantage of the resonance Raman effect, mentioned previously, which occurs when the exciting frequency approaches the frequency of an electronic absorption frequency. This increases the intensity of the solute spectrum

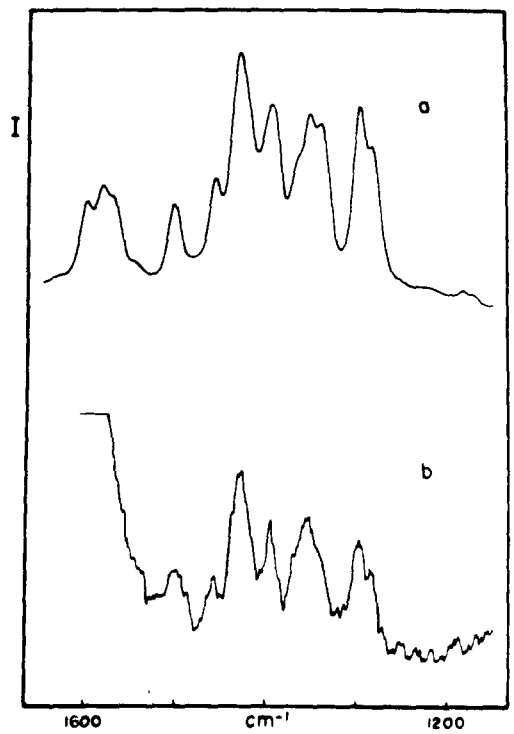

Fig. 81. Resonance Raman spectra of (a) Superlitefast Rubine in distilled water at 24.3 ppm; (b) Superlitefast Rubine in river water at 288 ppb. (From ref. [364].)

Table 19
Pesticides/fungicides, absorption band maximum, minimum detectable concentration, and observed Raman bands. (From ref. [365].)

Compound name[a]	λ_a[b] (nm)	E_a[c]	E_0[d]	Minimum detectable concentration (ppm)	Raman bands observed (cm^{-1})
2-nitrophenol	414	1.43×10^3	7.85×10^2	0.8	824, 881, 1083, 1255, 1338
2,4-dinitrophenol	357	1.02×10^4	9.81×10^2	0.7	801, 964, 1318, 1350
2-methyl-4,6-dinitrophenol (DNOC) (ditrosol)	366	7.29×10^3	1.43×10^3	0.9	1279, 1330
0,0-dimethyl-0-4-nitrophenyl phosphorothioate (methyl parathion)	278	2.86×10^3	3.74×10^1	7.0	1361
2,6-dichloro-4-nitroaniline (dichloran)	364	1.19×10^4	2.42×10^2	0.4	1338
4,6-dinitro-2-sec.butylphenol (dinoseb) (DNBP)	376	1.45×10^4	4.15×10^3	0.5	943, 1272, 1327

[a]Some trade names are given in parentheses.
[b]λ_a = position of absorption band maximum.
[c]E_a = molar absorptivity at band maximum.
[d]E_0 = molar adsorptivity at excitation wavelength, 457.9 nm.

without enhancing that of the water solvent. Brown and Lynch [363] showed the sensitivity of resonance Raman with identification of FD & C dyes in sodas and juice mixes at concentrations as low as 5 ppm. Van Haverbeke et al. [364] studied industrial fabric dyes and detected concentrations below 100 ppb and identified concentrations below 200 ppb. They simulated a "real world" situation by polluting river water with 288 ppb Superlitefast Rubine dye. Fig. 81 shows the spectrum between 1600 and 1000 cm^{-1}. For comparison, the spectrum of 24.3 ppm of the same dye in distilled water is shown in fig. 81a.

Preresonance Raman was utilized by Thibeau et al. [365] to detect pesticides and fungicides in water. Preresonance Raman differs from resonance Raman in that the exciting frequency is situated within the band envelope, but not near the center. The pesticides and fungicides studied, all based on the nitrophenol structure, are listed in table 19 along with observed Raman bands, absorption band

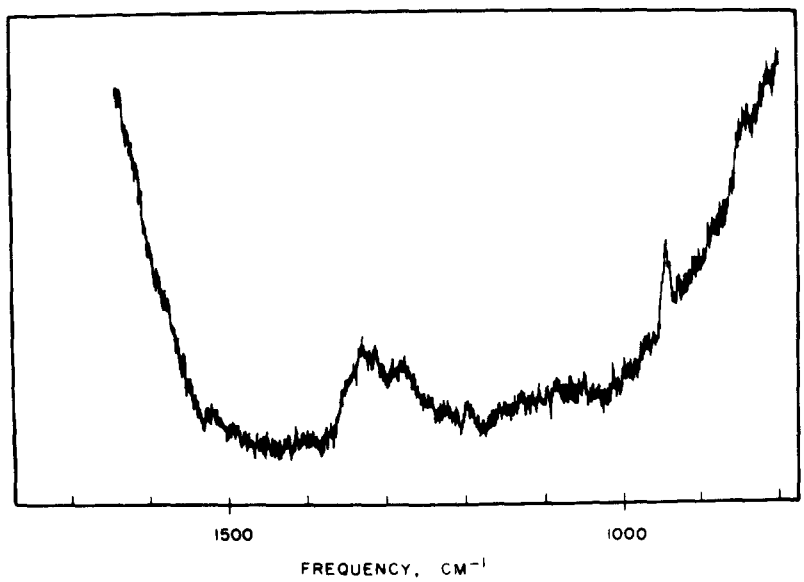

Fig. 82. Raman spectrum of a 0.5 ppm solution of 4,6-dinitro-2-sec. butylphenol in 2×10^{-4} M NaOH using 457.9 nm excitation. (From ref. [365].)

maxima, and minimum detectable concentrations. The latter were defined as the smallest concentrations which gave strong bands with a signal/noise ratio of 3 or more. A typical example is the spectrum of a 0.5 ppm solution of 4,6-dinitro–2-sec. butylphenol shown in fig. 82. The spectrum is bounded by the 1640 cm^{-1} band of water, but bands due to the compound itself are clearly evident at 943, 1272 and 1327 cm^{-1} (symmetric NO_2 stretch). Even lower concentrations of these samples could be seen by use of excitation wavelengths closer to the absorption band maxima (approaching the resonance Raman condition).

14.4. Air pollution

There has been considerable interest in the remote analysis of gaseous pollutants by Raman spectroscopy [366–367]. The current method projects the beam from a powerful laser into the atmosphere, then collects and analyzes the radiation back-scattered along the line of sight with a conventional Raman spectrometer [368]. One of the useful aspects of this Raman scattering method is that the distance of the pollutant from the detector can be related to the time delay between sending and receiving the returned pulse. This has led to the acronym for this technique – – LIDAR – – light detection and ranging. Initially equipment was very large (the unit was operated from a truck trailer) and expensive [369], but many improvements were made in second generation equipment [370]. The schematic for a field tested remote Raman system is shown in fig. 83.

Raman frequencies for some gaseous species of interest in pollution studies are shown in table 20 [58]. Detection limits vary widely among the species but, typically, 100 ppm of NO and SO_2 should be detected at a range of 300 m [368]. There is considerable interest in trying to quantitate lidar measurements [371] as well as to increase sensitivities to <1 ppm. One possibility to greatly lower detection limits is the use of resonance Raman [372] or of the rotational Raman effect, which in principle allows sensitivity to be increased by $\leq 10\,000$ over the vibrational Raman effect [373].

Lidar type systems also have great potential for smoke stack emission studies [374].

14.5. Flames and combustion

Previous to the early 1970's IR emission spectroscopy was one of the major spectroscopic tools for obtaining spectra of molecular species in flames, but it was limited by the fact that homonuclear

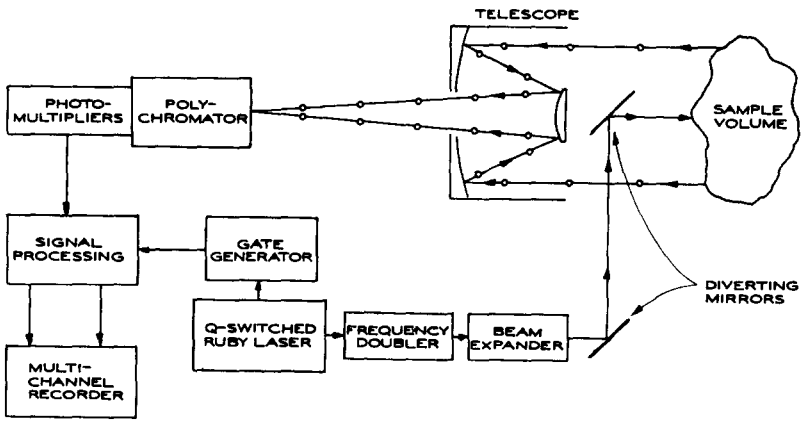

Fig. 83. Schematic of a remote Raman system. (From ref. [58].)

Table 20
Raman frequencies for some gaseous species of interest in pollution studies. (From ref. [58].)

Molecule	$\nu(cm^{-1})$	Molecule	$\nu(cm^{-1})$
CO_2	668	NO^+	2248
O_3	710	N_2	2273
SF_6	775	NO^+	2277
NH_3	950	N_2	2302
Aliphatics	987	NO^+	2305
Aromatics	992	N_2	2331
O_3	1043	CO	2349
SO_2	1151	H_2S	2611
CO_2	1242	O_3	2800
CO_2	1265	Aliphatics	2857
N_2O	1285	CH_4	2914
CO_2	1286	O_3	3050
NO_2	1320	Primary amines	3189
CO_2	1388	Primary amines	3256
CO_2	1409	NH_3	3331
CO_2	1430	Primary amines	3343
CO_2	1528	CO_2	3609
O_2	1556	H_2O	3652
O_3	1740	CO_2	3716
NO	1876	NO^+	4422
O_3	2105	N_2	4459
CO	2145	NO^+	4478
N_2^+	2175	N_2	4517
NO^+	2221	NO^+	4534
N_2O	2223	N_2	4575
N_2	2244	NO^+	4590
		N_2	4633

diatomic molecules do not give IR spectra and that the temperature in the region above the flame is too low to allow the use of any but the most sensitive of the IR instruments. Raman overcomes many of these disadvantages; it does give spectra of N_2, O_2 and H_2; lack of sample brightness is a help; and it does not have H_2O and CO_2 spectra which mask large portions of the spectra.

Arden et al. [375], using Raman and a flame isolation chamber, studied the combustion products of acetylene–oxygen, hydrogen–oxygen, methane–oxygen and propane–oxygen flames and obtained spectra of CO_2, O_2, H_2O and CO. In addition to the normal spectral lines, they found new bands appearing at higher temperature due to increased population of higher energy levels by thermal excitation. An example is the 1286 and 1388 cm^{-1} doublet of CO_2. At room temperature these two lines predominate, but as the temperature is raised there are fewer molecules in the ground state and the areas under these peaks get smaller; new bands first appear at $\Delta\nu = 1265$ and 1409 cm^{-1}, then at 1242 and 1430 cm^{-1}. For quantitative measurements all the intensities of the bands must be summed; for temperature measurements the ratio of intensities of a pair of lines can be used once their relative population in any state has been determined as a function of temperature (i.e. a plot of line intensity ratio vs. temperature).

Flame temperature calculations have also been made by Stricker [376] who developed a method of high precision over a wide temperature range. A high degree of accuracy was also claimed by Schoenung and Mitchell [377] who compared Raman and thermocouple measurements and Beardmore et al. [378] who compared four methods of calculating the temperatures in a laminar gas/air flame from the Raman spectra for N_2.

15. Raman band shapes as a source of information

Gordon [379] provided a formulation many years ago whereby information on orientational motion on the picosecond time could be obtained from the Fourier transform of Raman band shapes. An excellent summary of work up to 1974 may be found in the book edited by Lascombe [380]. In small molecules (approx. 5 atoms or fewer) reorientation provides the primary relaxation mechanism for allowed transitions. For larger molecules, vibrational relaxation mechanisms play an increasingly important role. The development of a coherent approach to such molecules has been the subject of several recent papers. The formulation most widely used is that of Nafie and Peticolas [381]. They showed that in isotropic media the overall correlation function, $C(t)$, obtained from the Raman shape, may be conveniently separated into a reorientational part $\mathrm{Tr}\langle\beta(t)\beta(0)\rangle$, where β is the anisotropic part of the polarizability, and $\langle Q(t)Q(0)\rangle$, a correlation function of all mechanisms of vibrational relaxation. This separation is achieved by computing the isotropic spectrum $I_{\mathrm{vib}} = I_{\parallel} - \frac{4}{3}I_{\perp}$, normalizing it to $\hat{I}_{\mathrm{vib}}$ whence

$$\hat{I}_{\mathrm{vib}}(\omega) = (2\pi)^{-1} \int_{-\infty}^{\infty} \langle Q(0)\, Q(t)\rangle \exp(\mathrm{i}\omega t)\, \mathrm{d}t,$$

or inversely,

$$\langle Q(0)\, Q(t)\rangle = \int_{-\infty}^{\infty} I_{\mathrm{vib}}(\omega) \exp(-\mathrm{i}\omega t)\, \mathrm{d}\omega.$$

Similarly, the Fourier transform of the normalized $I_{\perp}(\omega)$ band gives

$$\langle \mathrm{Tr}[\beta(0)\beta(t)]\rangle < Q(0)Q(t) = \int_{-\infty}^{\infty} \hat{I}_{\perp}(\omega) \exp(-\mathrm{i}\omega t)\, \mathrm{d}\omega.$$

Dividing the two results yields the reorientational correlation function, assuming that the reorientational and vibrational processes are uncorrelated.

Until recently, most workers have approached vibrational relaxation as a complication on Raman band shapes which needs to be removed if one is to study reorientational motion. Recent work, however, has shown that much valuable information about liquids might be derived from a study of vibrational relaxation processes by this method.

Before discussing specific results and interpretations it is useful to define certain additional quantities connected with the band shape and correlation function. The second moment of a band M_2 or ω^2 is obtained from

$$\int_{\mathrm{band}} (\omega - \omega_0)^2\, I(\omega)\, \mathrm{d}\omega$$

where ω_0 is the frequency at the band center. One may also define a correlation time, τ, although this

has been obtained in various ways [382]. In general, τ should be obtained from

$$\int_0^t C(t)\,\mathrm{d}t$$

where the integration is carried out to the limit of reliability of the correlation function. For pure Lorentzian or pure Gaussian bands there are other ways of obtaining τ.

Kubo [383] developed a general theory of relaxation processes which has been adapted to vibrational relaxation by several authors. In this theory, one can show that correlation functions which involve "pure dephasing" processes are given by

$$C(t) = \exp\{-\langle\omega^2\rangle\,[t\tau_c + \tau_c^2\exp(-t/\tau_c) - 1]\}.$$

This equation is often viewed in the short ($t \ll \tau_c$) and long ($t \gg \tau_c$), or, more usefully, in what are known as the slow ($\langle\omega^2\rangle^{1/2}\tau_c \gg 1$) or fast ($\langle\omega^2\rangle^{1/2}\tau_c \ll 1$) modulation regimes whence it reduces to

$$C(t) = \exp(-\tfrac{1}{2}\langle\omega^2\rangle t^2)$$

or

$$C(t) = \exp(-\langle\omega^2\rangle\tau_c t)$$

respectively.

From the viewpoint of solutions of interest to the chemist, these dephasing mechanisms appear to predominate over energy relaxation (lifetime shortening) mechanisms [382]. This is of value to the study of solution structure, as the change in environment of an excited molecule can be monitored in a rather unique way from a study of the correlation functions. As the modulation by the environment changes, both τ_c and $\langle\omega^2\rangle$ are affected. This is known as "motional narrowing". If these effects could be studied systematically they could lead to a probe of solution structures. Some examples of recent work will now be given.

Yarwood et al. [382] have been examining acetonitrile, CH_3CN, in detail. Typical vibrational relaxation correlation functions for ν_1 in carbon tetrachloride denoted as $\Phi(t)$, are shown in fig. 84. One can see the initial curvature (slow modulation) at short times followed by a linear region (fast modulation). The motional narrowing, referred to above, can be seen here, leading to a slower decaying correlation function. This is shown more directly in fig. 85, where values of τ_c and $\langle\omega^2\rangle$ are shown as a function of concentration.

From data such as these one sees that there is a substantial "core" of intermolecular dephasing mechanism which remains even after long range interactions between solute molecules have been removed. This leads to the conclusion that short range repulsive interactions control relaxation for this mode, while dipole–dipole interactions are unimportant. Yarwood et al. [382] have shown that the relaxation for other modes of CH_3CN is quite different under the same conditions. For ν_3 (1375 cm^{-1}), τ_c increases on dilution in CCl_4. This points to dipole–dipole interactions as being important as a relaxation mechanism, as is resonant energy transfer.

Schroeder et al. [384] have carried out related studies on CH_3CN and CD_3CN, examining the

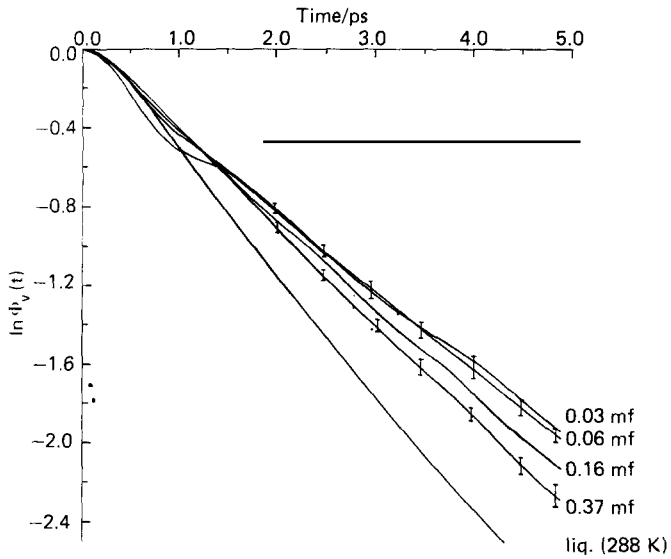

Fig. 84. Comparison of $\ln \phi_v(t)$ for ν_1 of acetonitrile at different concentrations. (From ref. [382].)

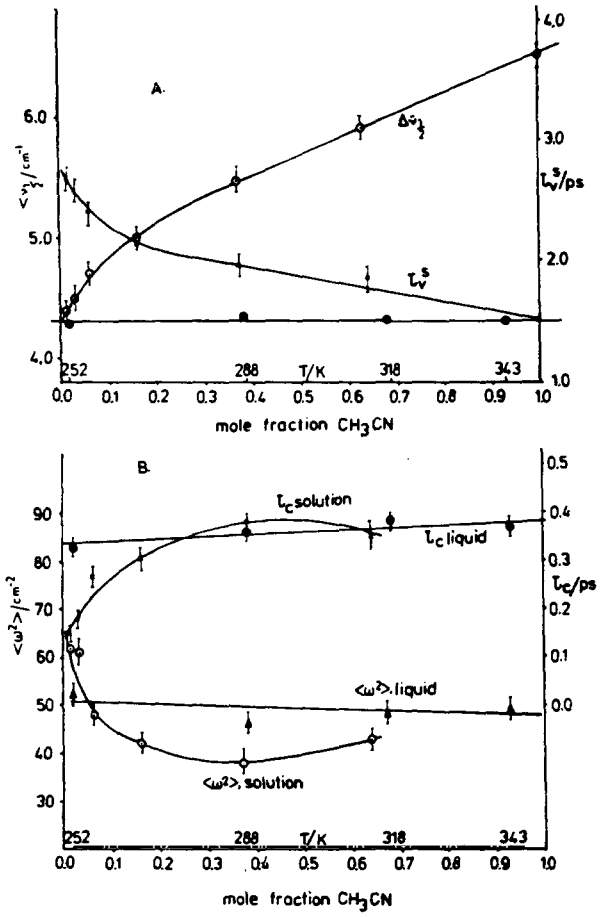

Fig. 85. (A) Changes in $\Delta\tilde{\nu}_{1/2}$ and τ_v^s for ν_1 of acetonitrile as a function of temperature and concentration in carbon tetrachloride. (Solution data are at 288°K.) (B) Changes of $\langle\omega^2\rangle$ and τ_c for ν_1 of acetonitrile (liquid and solution). (From ref. [382].)

pressure dependence of the ν_1 mode. Their results are also interpretable in a Kubo dephasing formalism. They have checked on the presence of resonance energy transfer by isotopic dilution measurements and agree that for ν_1, this is not significant.

While most work on vibrational relaxation correlation functions has been for small molecules, a few studies on larger molecules have indicated the potential for deriving information about condensed phases. Rothschild [385] has studied quinoline,

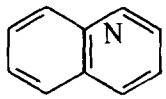

which should be large enough to have insignificant reorientation in the liquid phase during the first 5 psec. Fig. 86 shows vibrational correlation functions obtained from the 1033 cm^{-1} in phase bending in neat liquid, (both infrared and Raman) and 0.09 mole fraction in CS_2. A slight motional narrowing is seen in solution. In this case the infrared and Raman correlation functions deviate after about 2.5 psec. While Rothschild does not discuss the reasons for this, a recent paper by Yarwood et al. [386] deals with this issue for acetonitrile. It appears that there may be a fundamental theoretical problem here but more experimental work is probably needed on this point. Rothschild's work on quinoline also includes a comparison of vibrational relaxation correlation functions for crystalline and glassy quinoline. The glassy state relaxes more rapidly, consistent with the idea that it offers the greatest number of distinct

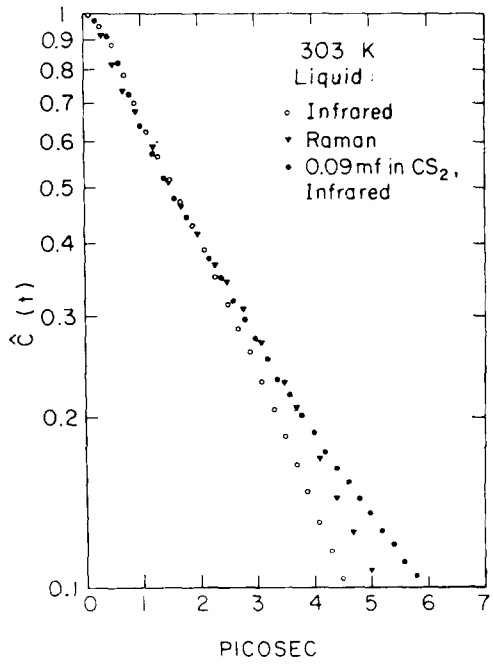

Fig. 86. Vibrational correlation functions of the 1033 cm^{-1} in-plane bending (A') of quinoline at ambient temperature. Infrared: pure liquid and 0.09 mole fraction solution in CS_2, respectively. Raman: pure liquid. (From ref. [385].)

environments. There is potential here for studying glasses and phase transitions associated with them.

Bulkin and Brenzinsky [387] have studied the CN stretching mode of 4 cyano, 4′ octyloxybiphenyl (80CB)

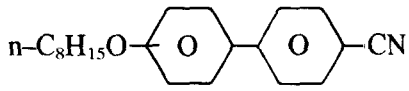

which forms two liquid crystalline phases and two solid phases, as well as an isotropic liquid phase. Fig. 87 shows that the correlation functions obtained from the liquid crystalline phases are identical with those in the isotropic phase, indicating that the short range order in all fluid phases is similar. In CCl_4 or benzene solution, there is considerable motional narrowing, as seen in fig. 88. Of further interest is the region from 0.7 to 1.5 psec, where the solution correlation functions differ from those of the pure liquid, but there is no concentration dependence. This is the slow modulation regime. In CH_3SCN or $CHCl_3$ the effect of dilution is quite different (fig. 89). No motional narrowing occurs. Clearly the solvation of the excited CN group is quite different in these solvents. These results indicate that there is a possibility for using vibrational relaxation correlation functions as a probe of solvent-solute interactions.

Band shape analysis and resolution studies have also been useful in obtaining information on

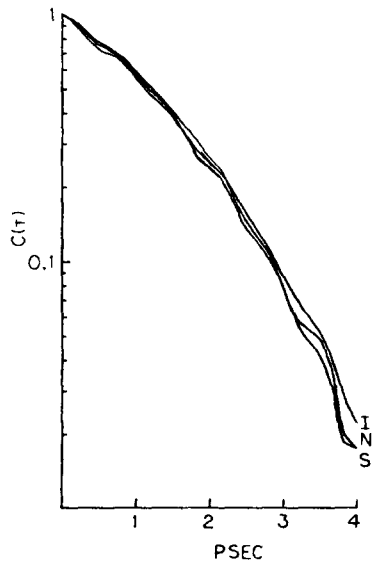

Fig. 87. Correlation functions calculated from I_{vh} of the homeotropically aligned smectic (S) and nematic (N) phase 80CB and the isotropic (I) phase 80CB. (From ref. [387].)

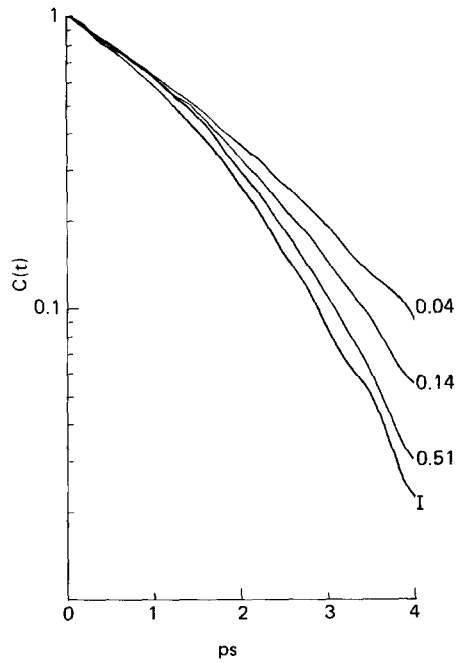

Fig. 88. C_{vh} calculated from spectra of 80CB dissolved in benzene in mole fractions of 0.51, 0.14 and 0.04. Also included is the C_{vh} from spectra of the isotropic (I) phase. (From ref. [387].)

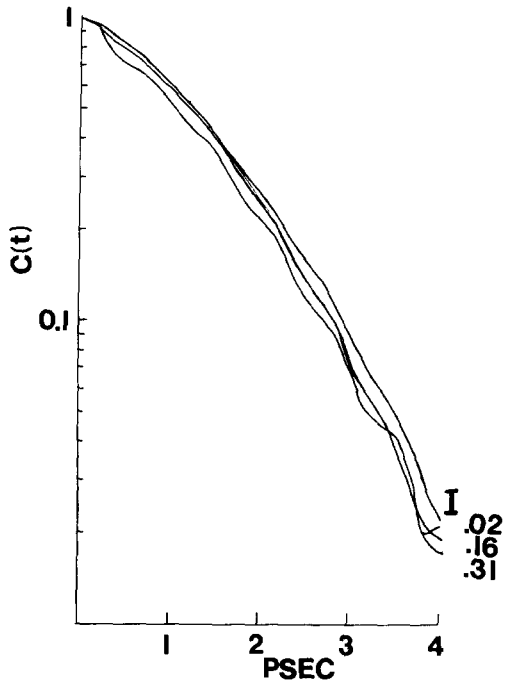

Fig. 89. C_{vh} calculated from spectra of 80CB dissolved in chloroform in mole fractions at 0.31, 0.16 and 0.02. Also included is C_{vh} from spectra of the isotropic (I) phase. (From ref. [387].)

conformational structures of polymers. Maddams et al. [388–389] applied such techniques to obtain information on the configuration and conformation of poly(vinylchloride). In a separate study [390] they also measured the profiles of eight well-defined Raman bands to establish that Raman band shapes are a reasonable approximation to the commonly assumed Lorentzian form and, therefore, that curve-fitting procedures to separate overlapping peaks are feasible.

16. Non-linear effects, particularly CARS

In the normal Raman effect, we observe a linear dependence of polarization on field strength, i.e. as the laser power is increased, the Raman signal is proportionally increased. At sufficiently high laser powers this need not be the case.

The polarization can be written as a (somewhat simplified) expansion in the field strength

$$P = \chi^{(1)}E + \chi^{(2)}E^2 + \chi^{(3)}E^3.$$

The susceptibilities χ^i fall off rapidly, typically being reduced by 10^{10} in each successive term. Normally then, only the $\chi^{(1)}$ (sometimes called α) term is important. When E exceeds ca. $10^9\ \mathrm{Vm}^{-1}$, however, the non-linear contributions can be expected to be seen. Such fields are available from many laser systems. Indeed, the non-linear effects were observed in the early days of laser-excited Raman spectroscopy. Only recently have they been applied to chemical problems.

Table 21

	Raman efficiency	Discrimination against fluorescence	Trace analysis capability	Det. of low no. densities	Comments
Normal Raman*	low	low	moderate-low	mod-low (100 mtorr)	General application.
Stimulated Raman	high	high	very low	very low (20 atm)	Limited usefulness.
Inverse Raman	high	high	low	low (? 10 torr)	Good for condensed phase. Not sens. for gas anal. at low pressure.
Hyper-Raman	very low	high	very low	very low (~1 atm)	Sens. very low, good for some structural anal.
Raman-induced Kerr effect	high	high	moderate (?)	moderate (?)	Too early for good assessment but has definite potential.
CARS*	high	very high	low (at present**)	high (<1 mtorr)	Excel. for hi resolution and anal. of gases at low pressure. Problems with trace anal. (low ppm)

*These assessments do not include improvements effected by electronic resonance enhancements.

**The limit to CARS for trace analysis is the interference from background generation of solvent or diluent gas. At this writing, there are a few ideas not yet fully tested which may markedly reduce or eliminate background generation.

A number of non-linear effects have been discovered. These are summarized in table 21. Included in the table is normal or spontaneous Raman scattering, as well as stimulated Raman scattering. Stimulated Raman has great utility in producing sources of a particular frequency [391]. It may also be an effective method to study vibrational lifetimes [392]. While conversion efficiency is high, only certain lines, usually the most intense, will emit in the stimulated mode. This is because after one reaches the threshold power for stimulated emission of one mode all further increases in power go into that mode.

The inverse Raman effect occurs as follows. If a sample is simultaneously irradiated with an intense laser beam of frequency ν_0 and a continuum from ν_0 to $\nu_0 + 4000\,\mathrm{cm}^{-1}$ (the typical range of a vibrational spectrum), absorption is observed at frequencies ν_i characteristic of the Raman active modes. Emission is also observed at ν_0. This is an inverse effect. In principle it would have an advantage over normal Raman in that fluorescence would not be important. In practice there have been few applications. This is because the absorption is weak and it is somewhat difficult to get the laser pulse and continuum to coincide spatially and temporally.

There has been some recent work on stimulated Raman spectroscopy using low power cw lasers, as well as with lower average power pulsed lasers, which does show promise for chemical applications. This is primarily the work of Owyoung [393–394] on a technique known as stimulated Raman gain spectroscopy. As will be seen below, this can also be done experimentally as inverse Raman spectroscopy.

Fig. 90 shows schematically the original Owyoung experiment using a cw He–Ne laser and a cw dye laser. The dye laser is chopped and tuned through the region of vibrational frequency differences from the He–Ne laser. The two beams are brought together by a beamsplitter in a temporal and spatial coincidence in the sample. One can measure either gain or loss as a function of frequency of the exiting beam. Because this beam is coherent, spatial filtering can be used to remove fluorescence.

Nestor [395] has done the same experiment using a pulsed nitrogen laser and two dye lasers. In that case a differential amplifier is used, with one input being the exit probe beam pulse, the other a split-off signal from the pulse before it enters the sample.

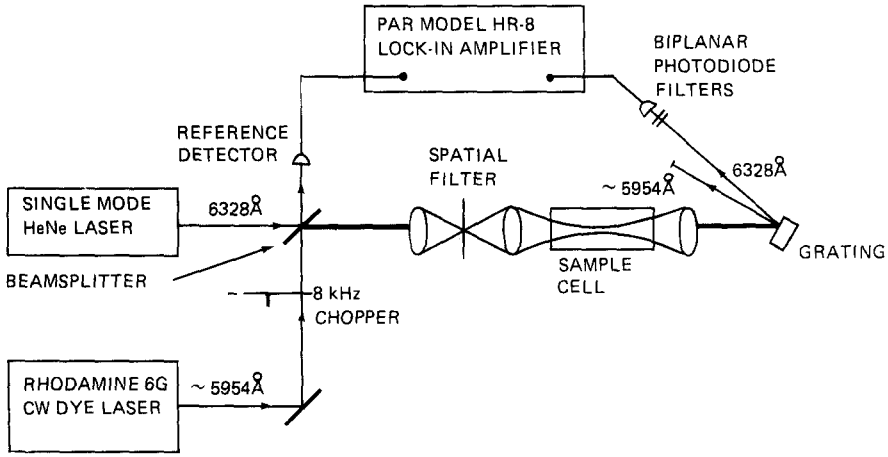

Fig. 90. Schematic diagram of the cw stimulated Raman gain spectroscopy experiment. (From ref. [394].)

These techniques have thus far only been used on test samples. However, for gas phase spectra they look very promising. In liquids there may be some cases where the significant improvement in resolution obtainable from the tunable laser vs. a monochromator is useful in solving a problem. There is interest in applying these methods to resonance Raman problems, but thus far problems of thermal blooming have not been solved.

The hyper-Raman effect (a $\chi^{(2)}$ effect) gives rise to Raman scattering at frequencies of $\nu_0 \pm \nu_i$. It is of interest because selection rules for hyper Raman scattering may be different from those of either normal Raman or infrared spectroscopy. An example is shown in table 22. The effect is extremely weak and the instrumentation complex. Hence, it is finding little application today.

The coherent anti-Stokes Raman scattering (CARS) effect is a $\chi^{(3)}$ effect. It has received more attention than any of the other non-linear effects [396]. The bulk of the work thus far has been of a very exploratory nature and the potential for solving problems is still a matter of some controversy. CARS generates coherent photons and the efficiency for the CARS process can be significantly higher than spontaneous Raman scattering.

CARS may be done with either pulsed or cw lasers, but most work to date has been done with pulsed lasers. If two beams of frequencies ω_ℓ and ω_s are focussed in a sample at sufficient power, a

Table 22
Infrared, Raman and hyper Raman activity of fundamental vibrations in sulfur hexafluoride (SF_6)

Symmetry species	x, y, z	α	Components of β	Number of distinct frequencies
A_{1g}		$\alpha_{xx} + \alpha_{yy} + \alpha_{zz}$		1
A_{2g}				0
E_g		$(\alpha_{xx} + \alpha_{yy} - 2\alpha_{zz}, \alpha_{xx} - \alpha_{yy})$		1
F_{1g}				0
F_{2g}		$(\alpha_{xy}, \alpha_{xz}, \alpha_{yz})$		1
A_{1u}				0
A_{2u}			β_{xyz}	0
E_u				0
F_{1u}	(x, y, z)		$(\beta_{xxx}, \beta_{yyy}, \beta_{zzz}), (\beta_{xyy} + \beta_{zzx}, \beta_{yzz} + \beta_{xxy}, \beta_{zxx} + \beta_{yyz})$	2
F_{2u}			$(\beta_{xyy} - \beta_{zzx}, \beta_{yzz} - \beta_{xxy}, \beta_{zxx} - \beta_{yyz})$	1

coherent beam of frequency $\omega_{as} = 2\omega_\ell - \omega_s$ may be generated in the medium. Many factors determine whether this conversion to ω_{as} takes place. These include the presence of molecular resonances at frequency $\omega_\ell - \omega_s$ and properties of these resonances.

It is possible to derive an equation for the efficiency ϵ of the CARS process and it is instructive to examine the terms in this expression. The efficiency is proportional to

$$L^2\left[\frac{\sin(\Delta k\, L/2)}{\Delta k\, L/2}\right]^2$$

where L is the length over which the beams are mixed through the sample and Δk is the mismatch between the momentum vectors such that

$$\Delta k = 2k_\ell - k_s - k_{as}.$$

Fig. 91 shows how ϵ varies with Δk at constant L, indicating that it is maximized at $\Delta k = 0$. This is known as the phase matching condition and it imposes a very strict experimental condition on CARS. To achieve $\Delta k = 0$, the beams must be crossed at angle θ (fig. 92). For gases this condition is not severe, but for liquids the angle tolerance for CARS is $<1°$.

ϵ is proportional to $|\chi^{(3)}|^2$. As mentioned above, the conversion efficiency depends on the occurrence of resonance at $\omega_\ell - \omega_s$; however, it can occur even in the absence of such resonances. One way of expressing this is to separate $\chi^{(3)}$ into a resonant and a non-resonant part

$$\chi^{(3)} = \chi^{R} + \chi^{NR}.$$

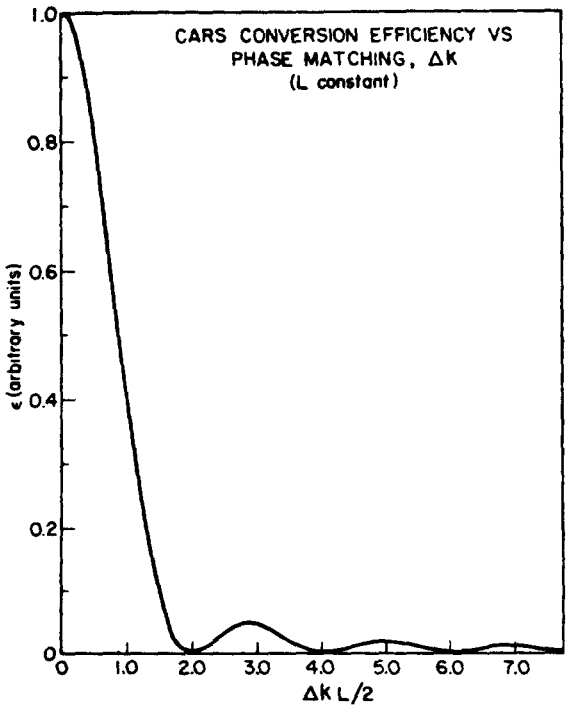

Fig. 91. CARS conversion efficiency vs. phase matching (Δk) for constant interaction length. (From ref. [397].)

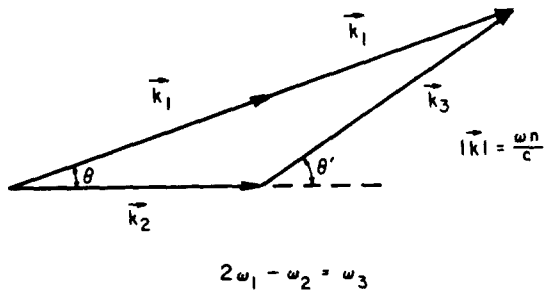

Fig. 92. Wave vector diagram for phase matching ($\Delta k = 0$). (From ref. [397].)

It is χ^R which is related to Raman spectroscopic transitions, but χ^{NR} may provide an intense background, limiting the possibility of detecting χ^R. The third order non-linear susceptibility has another important property, namely, χ^R has both real and complex parts, i.e.

$$\chi^{(3)} = \chi' + i\chi'' + \chi^{NR}.$$

The imaginary part of $\chi^{(3)}$ is associated with the normal Raman transition probability, the real part with the non-linear refractive index. These have usual forms shown in fig. 93. If these were the only factors CARS band shapes would look much like normal Raman band shapes. In the presence of a significant non-resonant background, this can change.

This is simply seen by squaring $\chi^{(3)}$

$$|\chi^{(3)}|^2 = (\chi' + \chi^{NR})^2 + (\chi'')^2 = (\chi')^2 + 2\chi'\chi^{NR} + (\chi^{NR})^2 + (\chi'')^2.$$

The mixing term $\chi'\chi^{NR}$ can distort normal band shapes leading to minima in the CARS spectra.

Tolles and Turner [397] have assessed the performance capabilities of CARS vs. spontaneous Raman and absorption spectroscopy for the analysis of gases. They find that CARS offers advantages under certain conditions of temperature and pressure, particularly for a major component of a mixture below 1 atm total pressure. The calculations they describe are quite useful to an understanding of signal/noise in a CARS experiment.

Carreira and co-workers [398] have been developing a CARS spectrometer for application to solutions. They have concentrated their efforts on situations in which resonance-enhanced CARS signals are observable. The range of solutions for which this is the case is increased by their use of ultraviolet excitation. To facilitate the operation of the spectrometer, especially in regard to the phase matching angle condition, a number of computer controlled stepping motors are utilized. These include motors to move optics as necessary for phase matching. The computer "learns" the conditions necessary for each solvent and sets these automatically.

These authors have used the micro flow cell technique in resonance enhanced CARS to good advantage. This minimizes buildup of photodecomposed products, thermal gradients, while permitting the study of excited molecules or intermediates. One possibility for application of the microflow cell in this spectrometer is as a liquid chromatograph detector. Further work in this area is needed.

Dutta, Nestor and Spiro [399] have carried out resonance CARS experiments on a biological system, flavin adenine dinucleotide, where the electronic resonance is with a flavin absorption band. This is a highly fluorescent system and the CARS data make a convincing case for the ability of CARS to obtain good Raman spectra despite this.

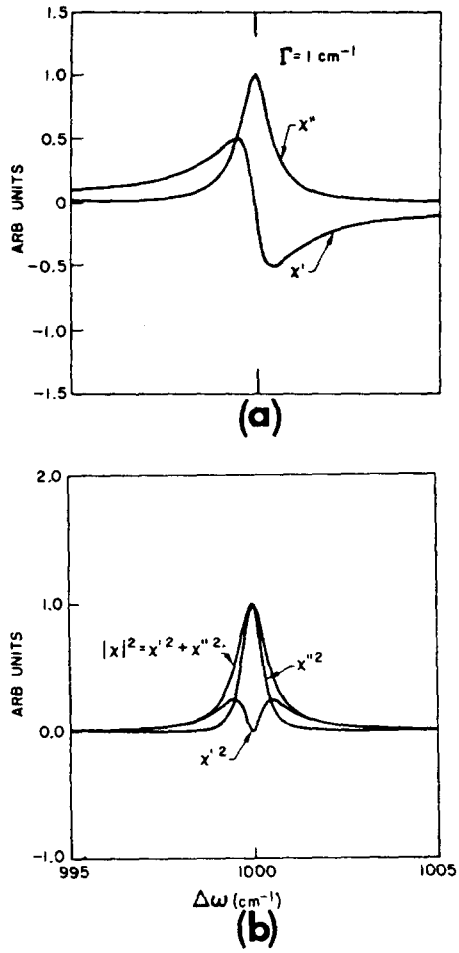

Fig. 93. (a) This trace is a plot of the real (χ') and imaginary (χ'') parts of the third-order susceptibility for a resonance centered at 1000 cm^{-1} Raman shift and a line width of 1.0 cm^{-1}. Note the fact that χ' is negative in one-half of the frequency domain. (b) Square of the quantities plotted in (a). χ^2 is directly proportional to the CARS signal. Note that at the center of the resonance the real part of the susceptibility vanishes. (From ref. [397].)

17. Recent developments in instrumentation

17.1. Image intensifiers and vidicons

Delhaye and Bridoux [400] have pioneered the use of multichannel detection systems for Raman spectroscopy. In a typical system, the scattered light, dispersed by the monochromator, is imaged on a multiple stage image intensifier tube and the resulting signal focussed on the photocathode of a vidicon television tube.

A commercial detection system – – the OMA or Optical Multi-channel analyzer – – is available based on this principle from EG & G-PAR in Princeton, N.J., U.S.A.

There are many potential applications of multi-channel techniques. With pulsed lasers, the OMA represents the best way of obtaining the Raman spectrum with a single laser pulse. Using time gating techniques, in combination with short pulses, fluorescence may be separated from Raman scattering.

Campion et al. [401] have used resonance Raman spectroscopy with the OMA to study kinetics of reactions connected with the vision process. In their work a cw laser is used. However, by interposing a rotating disk with a small slit in it, a pulse of several microseconds duration is achieved. This pulse does both photolysis and probing of the Raman spectrum. Fig. 94 shows spectra of bacteriorhodopsin obtained from this apparatus. In each succeeding spectrum (top to bottom) the slitwidth is widened to increase the pulse duration. The spectral changes observed are, of course, complex. One must consider both the increase in illumination as well as observation time, recognizing that a sum of the species present during this time is seen. Still, for production of microsecond pulses, the technique is a relatively simple one. The authors believe that 20 ns pulses can be obtained. However, one must be concerned about power/pulse, relaxation between pulses, and overall signal/noise considerations.

The most straightforward use of vidicons, obtaining Raman spectra from single laser pulses, has enabled spectra of unstable species to be obtained. When combined with resonance enhancement, this can lead to a rather sensitive molecular structure probe. Wilbrandt et al. [402] have used this to obtain spectra of a free radical in solution. Undoubtedly, there will be many such applications in chemistry.

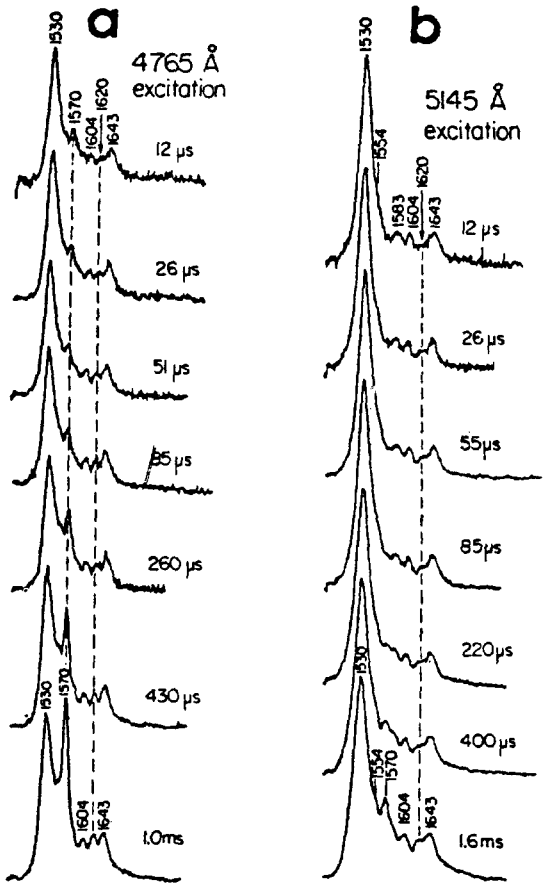

Fig. 94. Kinetic resonance Raman spectra of bacteriorhodopsin taken with two excitation wavelengths: (a) 476.5 nm; (b) 514.5 nm; at room temperature (~20°). The times are the measured laser pulse durations, determined in general by the slit width, speed, and diameter of the chopper. For this series only the slit width was varied. Peak incident laser power was ~2 W with an average power (determined by the ratio of slit width to chopper circumference) ranging from 0.5 to 60 mW. Vibrational frequencies are given in cm^{-1}.

17.2. Rapid scanning Raman spectroscopy

Slower dynamical studies via Raman spectroscopy can be carried out by rapid scanning. For some years, Spex Industries has offered a rotating quartz refractor plate as an option with their double monochromator system. The plate is placed just before the exit slit and permits a rapid scan of a small spectral range.

Beny et al. [403] and Wallart [404] have described another approach to rapid scanning. It is used on the J-Y Optical double monochromator. This instrument operates with a cosecant bar cam arrangement. By interposing a second scanning motor, cam, and variable angle quoin between the lead screw and the cosecant bar, they are able to rock the gratings through a preset angle. This angle is determined by the quoin. In this way, spectra over a range varying from 5–1500 cm^{-1} can be obtained in less than 1 sec. The system seems to be particularly useful in studying the evolution of certain phase transitions which take place slowly and yield distinct Raman bands rather close together in frequency. Few applications of rapid scanning Raman have been made to date.

18. In conclusion: Where have we come from and where are we going?

The Raman effect evolved at a propitious time in the development of chemistry. As the quantum theory of molecules developed, chemists were increasingly anxious for molecular structure information. In many cases, theory did not provide a basis for choice between alternative structures – – linear vs. bent, planar vs. non-planar, etc. Using the link between group theory, symmetry, and spectroscopy, Raman spectroscopy, often in partnership with infrared, provided many answers. Up to about 1970, such applications dominated the application of Raman spectroscopy in chemistry.

The 1970's have been a period of change. As we have seen in the foregoing sections, there have been many applications of the Raman effect to complex molecular systems. In part this has happened because other spectroscopic and diffraction techniques were providing more straightforward answers to the simpler problems. But in part it results as well from the maturity of Raman as a technique. The large volume of data and expertise on small molecules has allowed interpretable data to be obtained for biological systems, polymers, ordered condensed phases, and multicomponent systems.

The 1970's have also witnessed many developments in instrumentation, the fruits of which will be most apparent in the future. One in which the impact is already clear is in computer support for data acquisition, reduction, and interpretation. We have also been able to use the developments in molecular orbital calculations on large molecules as aids in data interpretation.

Towards the end of this decade, we are seeing the emergence of Raman as a technique for studying dynamics. This comes on many time scales. From Raman band shapes we glean information about picosecond processes. Using vidicons and pulsed lasers, nanoseconds to millisecond processes can be examined. And using rapid scanning techniques, we can probe reactions in the 0.1–10 second range. As there are relatively few good techniques for obtaining dynamical information in condensed phases with the structural detail offered by Raman spectroscopy, we can expect to see continued development along these lines.

Thus, in the 1980's, we may expect to recover the multiplex advantage in Raman spectroscopy that was given up for convenience when photographic plates were replaced by photomultiplier tubes. Some laboratories already use detector arrays, as described in section 3, but these can be expected to become more sophisticated, capable of higher resolution, and lower in price.

Computer-based analysis of data, mainly through improved library search systems algorithms, is proving to be at the transition from the 70's to the 80's in infrared spectroscopy. Such techniques will naturally come to Raman systems soon. We may also see, in the 1980's, some increased use of theory for interpretation of relative intensities of bands on a routine basis.

New sources for Raman spectroscopy will surely emerge in the next decade and impact the field. The efforts now in progress to develop a variety of improved UV and vacuum UV cw lasers will result in our ability to carry out resonance Raman experiments on virtually any material in a routine fashion. When combined with gating techniques to suppress fluorescence, this will greatly enhance the sensitivity of Raman spectroscopy at lower concentrations. It seems possible that with sophisticated computational backup, one may also be able to do intensity corrections on such resonance enhanced data to provide quantitative information on concentrations.

In addition to laser sources, we may expect to see some use of the storage ring sources in the vacuum ultraviolet, now either in operation or under construction, for resonance Raman spectroscopy in the hard vacuum UV regions. In addition to intensity, continuous tunability, and polarization, these sources have potential (not yet fully developed) for sophisticated time-resolved experiments on the nanosecond time scale. The negative side of this, however, comes in the considerable expense in carrying out such experiments. It is not clear yet whether such an expense will be justified.

We have treated the non-linear Raman effects briefly in this article. To date they have found few applications in chemistry. This will likely change in the 1980's. The simplicity of instrumentation, the high intensity and the discrimination against fluorescence offered by these techniques make it likely that they may even come to dominate spontaneous Raman spectroscopy in liquid and gas phase problems. Their application in solids is much less clear and surely warrants further work.

These developments are all experimental. What of theory? Some of the most sophisticated quantum chemistry now underway deals with condensed phase theory. We can hope that this will result in our being able to more quantitatively interpret effects seen in condensed phase spectra -- changes in band intensities, frequencies and shapes -- under varying conditions of solvent, temperature, pressure, viscosity, etc.

For some of this, we will need the results of other theoretical and experimental work now underway on the dynamics of intermode intramolecular energy transfer. Particularly in large molecules, this may be a factor in interpreting subtle effects in their Raman spectra.

There has been some access to new vibrational levels through new selection rules as the non-linear techniques have evolved and as circularly polarized radiation has been used. We may hope that theoretical work in this area of new selection rules also evolves in the future.

Finally, one may hope that the next decade will close with the result of these theoretical and experimental advances being a more complete network of links between chemistry and spectroscopy.

References

[1] H. Sloane, Appl. Spectrosc. 25 (1971) 430.
[2] D.A. Long, Raman Spectroscopy (McGraw-Hill, New York, 1977).
[3] B.J. Bulkin, J. Chem. Educ. 46 (1969) A781; ibid. A859.
[4] I.S.A. Jobin-Yvon, 16–18 rue du Canal, 91160 Longjumeau, France.
[5] B.J. Bulkin, E.H. Cole and A. Noguerola, J. Chem. Educ. 51 (1974) A273.
[6] J.G. Grasselli, M.A. Hazle and L.E. Wolfram, in: Molecular Spectroscopy, ed. A. West (Heyden, New York, 1977).
[7] J.R. Scherer, S. Kint and G.F. Bailey, J. Mol. Spectrosc. 39 (1971) 146.
[8] B.J. Bulkin, D.L. Beveridge and F.T. Prochaska, J. Chem. Phys. 55 (1971) 5828.

[9] K. Krishnan and B.J. Bulkin, Appl. Spectrosc. 32 (1978) 338.
[10] J.R. Scherer and S. Kint, Appl. Opt. 9 (1970) 1615.
[11] P.J. Hendra, in: Laboratory Methods in Infrared Spectroscopy, eds. R.E. Miller and B.C. Stace (Heyden, New York, 1972).
[12] S.K. Freeman, P.R. Reed Jr. and D.O. Landon, Mikrochim. Acta (1972) 288.
[13] R.A. Nyquist and R.O. Kagel, in: Practical Spectroscopy, Vol. 1, eds. E.G. Brame and J.G. Grasselli (Dekker, New York, 1975).
[14] G.J. Rosasco and J.H. Simmons, Am. Ceram. Soc. Bull. 53 (1974) 626.
[15] J.J. Barrett and N.I. Adams III, J. Opt. Soc. Am. 58 (1968) 3.
[16] M. Delhaye and P. Dhamelincourt, J. Raman Spectrosc. 3 (1975) 33.
[17] G.J. Rosasco and E.S. Etz, Res./Dev. 28 (1977) 20.
[18] P. Dhamelincourt, F. Wallart, M. Le Clercq, A. Nguyen and D. Landon, Anal. Chem. 51 (1979) 414A.
[19] G.J. Rosasco, E.S. Etz and W. Cassett, Appl. Spectrosc. 29 (1975) 396.
[20] B.W. Cook and J.D. Louden, J. Raman Spectrosc. in press.
[21] J.J. Blaha and G.J. Rosasco, Anal. Chem. 50 (1978) 892.
[22] E.S. Etz and G.J. Rosasco, Environmental Analysis (Academic Press, New York, 1977).
[23] W. Kiefer and H. Bernstein, Appl. Spectrosc. 25 (1971) 500.
[24] W. Kiefer and H. Bernstein, Appl. Spectrosc. 25 (1971) 609.
[25] W. Kiefer, Appl. Spectrosc. 28 (1974) 115.
[26] R.J.H. Clark, in: Advances in Infrared and Raman Spectroscopy, Vol. 1, eds. R.J.H. Clark and R. Hester (Heyden, London, 1975).
[27] W. Kiefer, in: Advances in Infrared and Raman Spectroscopy, Vol. 3, eds. R.J.H. Clark and R. Hester (Heyden, London, 1977).
[28] G.J. Sloane and R. Cook, Appl. Spectrosc. 26 (1972) 589.
[29] R. Carter and L. O'Hare, Appl. Spectrosc. 30 (1976) 187.
[30] R. Clark, O. Ellestad and P. Mitchell, Appl. Spectrosc. 28 (1974) 575.
[31] G.J. Long, L.J. Basile and J.R. Ferraro, Appl. Spectrosc. 28 (1974) 73.
[32] W. Kiefer, Appl. Spectrosc. 27 (1973) 253.
[33] J. Bodenheimer, B. Berenblut and G. Wilkinson, Chem. Phys. Lett. 14 (1972) 523.
[34] D.E. Irish and H. Chen, Appl. Spectrosc. 25 (1971) 1.
[35] T.G. Chang and D.E. Irish, J. Solution Chem. 3 (1974) 161.
[36] A.K. Covington, M.L. Hassell and D. Irish, J. Solution Chem. 3 (1974) 629.
[37] H. Baranska and A. Labudzinska, Chem. Anal. (Warsaw) 21 (1976) 93.
[38] D. Turner, J. Chem. Soc., Faraday Trans. 2 68 (1972) 643.
[39] D. Turner, J. Chem. Soc., Faraday Trans. 1 70 (1974) 1346.
[40] P.L. Wancheck and L.E. Wolfram, Appl. Spectrosc. 30 (1976) 542.
[41] J.G. Grasselli, M.A.S. Hazle, J.R. Mooney and M. Mehicic, in: Proc. Colloq. Spectrosc. Int., 21st and Int. Conf. Atomic Spectrosc., 8th. (Heyden, London, 1979).
[42] D. Long, in: The Characterization of Chemical Purity, Organic Compounds, ed. L. Stavely (Butterworths, London, 1971).
[43] B. Schrader, Angew. Chem., Int. Ed. Engl. 12 (1973) 884.
[44] D. Irish and J. Riddell, Appl. Spectrosc. 28 (1974) 481.
[45] A.K. Covington and J. Thain, Appl. Spectrosc. 29 (1975) 386.
[46] J.P. Huvenne, G. Vergoten, J. Charlier, Y. Moschetto and G. Fleury, C.R. Hebd, Seances Acad. Sci., Ser. C 286 (1978) 633.
[47] D. Adams and J. Gardner, J. Chem. Soc., Perkin Trans. 2 15 (1972) 2278.
[48] B.J. Bulkin, K. Dill and J. Dannenberg, Anal. Chem. 43 (1971) 974.
[49] R. Oertel and D. Myhre, Anal. Chem. 44 (1972) 1589.
[50] R.A. Nyquist and R.O. Kagel, in: Infrared and Raman Spectroscopy, Vol. 1, Part B, eds. E.G. Brame and J.G. Grasselli (Dekker, New York, 1977) p. 454.
[51] L. Andrews and R.C. Spiker, J. Chem. Phys. 59 (1973) 1863.
[52] L.J. Bellamy, The Infrared Spectra of Complex Molecules (2nd ed., Methuen, London, 1958).
[53] L.J. Bellamy, Advances in Infrared Group Frequencies (Methuen, London, 1968).
[54] N.B. Colthup, L.H. Daly and S.E. Wiberly, Introduction to Raman and Infrared Spectroscopy (Academic Press, New York, 1964).
[55] C.N.R. Rao, Chemical Applications of Infrared Spectroscopy (Academic Press, New York, 1963).
[56] R.N. Jones and C. Sandorfy, in: Chemical Applications of Spectroscopy, Vol. IX, ed. W. West (Wiley Interscience, New York, 1956).
[57] F.R. Dollish, W.G. Fateley and F.F. Bentley, Characteristic Raman Frequencies of Organic Compounds (Wiley Interscience, New York, 1974).
[58] S.K. Freeman, Applications of Laser Raman Spectroscopy (Wiley Interscience, New York, 1974).
[59] G. Carlson, Research and Development on the Analysis and Characterization of Experimental Materials, AFML-TR-73-33, Wright-Patterson Air Force Base, Ohio (1973).
[60] W. Meier and B. Schrader, Proc. Int. Conf. Raman Spectrosc., 5th. (1976) 48.
[61] H.A. Sloane, in: Polymer Characterization, ed. C. Craver (Plenum Press, New York, 1971).
[62] P.A. Budinger, J.R. Mooney, J.G. Grasselli, P.S. Fay and A.T. Guttman, submitted for publication in Anal. Chem.
[63] W. Washburn, Am. Lab. 10:11 (1978) 47.

[64] F. Behroozi, R.G. Priest and J.M. Schnur, J. Raman Spectrosc. 4 (1976) 379.
[65] T.S. Wang and J.J. Mannion, Appl. Spectrosc. 27 (1973) 27.
[66] J.P. Lere-Porte, J. Petrissans and S. Gromb, J. Mol. Struct. 34 (1976) 55.
[67] R.A. Nyquist, Appl. Spectrosc. 26 (1972) 81.
[68] S.K. Freeman and D. Mayo, Appl. Spectrosc. 27 (1973) 286.
[69] S.K. Freeman and D. Mayo, Appl. Spectrosc. 26 (1972) 543.
[70] C. Warren and D. Hooper, Can. J. Chem. 51 (1973) 3901.
[71] B. Schrader and W. Meier, Fresenius' Z. Anal. Chem. 260 (1972) 248.
[72] J.N. Willis, R.B. Cook and R. Jankow, Anal. Chem. 44 (1972) 1228.
[73] J.H. Van der Maas and T. Visser, J. of Raman Spectrosc. 2 (1974) 563.
[74] T. Visser and J.H. Van der Maas, J. of Raman Spectrosc. 6 (1977) 114.
[75] T. Visser and J.H. Van der Maas, J. of Raman Spectrosc. 7 (1978) 125.
[76] T. Visser and J.H. Van der Maas, J. of Raman Spectrosc. 7 (1978) 278.
[77] B. Schrader and E. Steigner, Liebigs Ann. Chem. 735 (1970) 6.
[78] E. Steigner and B. Schrader, Liebigs Ann. Chem. 735 (1970) 15.
[79] B. Schrader and E. Steigner, Fresenius' Z. Anal. Chem. 254 (1971) 177;
B. Schrader and E. Steigner, in: Modern Methods of Steroid Analysis, ed. E. Heftmann (Academic Press, New York, 1973).
[80] M.M. Sushchinskii, Raman Spectra of Molecules and Crystals (Keter Inc., New York, 1972) Chap. 9.
[81] H.G. Buge, P. Reich and E. Steger, J. Mol. Struct. 35 (1976) 175.
[82] T.R. Manley and C.G. Martin, Spectrochim. Acta, Part A 32 (1976) 357.
[83] J. Maillois, L. Bardet and L. Mavry, J. Mol. Struct. 30 (1976) 57.
[84] J.D. Lewis and J.L. Laane, Spectrochim. Acta, Part A 31 (1975) 755.
[85] W. Grossman, Anal. Chem. 46 (1974) 345R.
[86] W. Grossman, Anal. Chem. 48 (1976) 261R.
[87] D. Gardiner, Anal. Chem. 50 (1978) 131R.
[88] L.A. Carreira, J. Chem. Phys. 62 (1975) 3851.
[89] L.A. Carreira and T.G. Townes, J. Chem. Phys. 63 (1975) 5283.
[90] J.R. Durig, W.E. Bucy and A.R.H. Cole, Can. J. Phys. 53 (1975) 1832.
[91] L.A. Carreira, J. Phys. Chem. 80 (1976) 1149.
[92] J.R. Durig and Y.S. Li, J. Chem. Phys. 63 (1975) 4110.
[93] J.R. Durig and A.W. Cox Jr., J. Chem. Phys. 63 (1975) 2303.
[94] J.R. Durig, W.E. Bucy, C.J. Wurrey and L.A. Carreira, J. Chem. Phys. 79 (1975) 988.
[95] J.R. Durig, A.C. Shing, L.A. Carreira and Y.S. Li, J. Chem. Phys. 57 (1972) 4398.
[96] W. Kiefer, H.J. Bernstein, H. Wieser and M. Danyluk, J. Mol. Spectrosc. 43 (1972) 393.
[97] W. Kiefer, H.J. Bernstein, M. Danyluk and H. Wieser, Chem. Phys. Lett. 12 (1972) 605.
[98] C. Perchard and J.P. Perchard, J. Raman Spectrosc. 3 (1975) 277.
[99] N.L. Lavrik and Y. Naberulchin, Opt. Spectrosc. 37 (1974) 44.
[100] I. Pernall, U. Maier, R. Janoschek and G. Zundel, J. Chem. Soc., Faraday Trans. 2 71 (1975) 201.
[101] O.H. Ellestad and P. Klaboe, J. Mol. Struct. 26 (1975) 25.
[102] H.T. Horntvedt and P. Klaboe, Acta Chem. Scand., Ser. A 29 (1975) 427.
[103] G.S. Kastha, S.D. Roy and S.K. Nandy, Indian J. Phys. 46 (1972) 293.
[104] H. Matsuura, M. Hiraishi and T. Myazawa, Spectrochim. Acta, Part A 28 (1972) 2299.
[105] D.A. Compton, W.O. George and W. Maddams, J. Chem. Soc., Perkin Trans. 2 (1976) 1666.
[106] J.L. Koenig, Appl. Spectrosc. Rev. 4 (1971) 233.
[107] W.L. Peticolas, Adv. Poly. Sci. 9 (1972) 285.
[108] B.G. Frushour and J.L. Koenig, in: Advances in Infrared and Raman Spectroscopy, Vol. 1, eds. R.J.H. Clark and R. Hester (Heyde London, 1975).
[109] P.J. Hendra, in: Polymer Spectroscopy, ed. D.O. Hummel (Verlag Chemie, Weinheim/Bergstr., 1974).
[110] J.L. Koenig, Chem. Technol. 2 (1972) 411.
[111] M. Meeks and J.L. Koenig, J. Polym. Sci., Polym. Phys. Ed. 9 (1971) 717.
[112] J.L. Koenig, Appl. Spectrosc. Rev. 4 (1971) 233.
[113] F.J. Boerio and J.K. Yuann, J. Polym. Sci., Polymer Phys. Ed. 11 (1973) 1848.
[114] H. Sloane and R. Bramston-Cook, Appl. Spectrosc. 27 (1973) 217.
[115] S.K. Mukherjee, G.D. Guenther and A.K. Bhattacharya, Anal. Chem. 50 (1978) 1591.
[116] I.W. Shepherd, in: Advances in Infrared and Raman Spectroscopy, Vol. 3, eds. R.J.H. Clark and R. Hester (Heyden, London, 1977).
[117] I.W. Shepherd, Rep. Prog. Phys. 38 (1975) 575.
[118] T.R. Gilson and P.J. Hendra, Laser Raman Spectroscopy (Wiley Interscience, New York, 1970).
[119] B. Jasse, R.S. Chao and J.L. Koenig, J. Raman Spectrosc. in press.
[120] J.L. Koenig and A.C. Angood, J. Polym. Sci., Polym. Phys. Ed. 8 (1970) 1787;
F.J. Boerio and J.L. Koenig, J. Polym. Sci., Polym. Symp. 43 (1973) 205.

[121] R.T. Bailey, A.J. Hyde and J.J. Kim, Spectrochim. Acta, Part A 30 (1973) 91.
[122] H. Tadakoro, M. Kobayashi, M. Ukita, K. Yasufuku and S. Murahashi, J. Chem. Phys. 42 (1965) 1432.
[123] P.D. Vasko and J.L. Koenig, Macromolecules 3 (1970) 597.
[124] J.M. Chalmer 18: 7 (1977) 681.
[125] D.I. Bower, Structure and Properties of Oriented Polymers (Applied Sciences, London, 1975).
[126] J. Purvis and D.I. Bower, Polymer 15 (1974) 645.
[127] J. Purvis and D.I. Bower, J. Polym. Sci., Polym. Phys. Ed. 14 (1976) 1461.
[128] P.J. Hendra and H.A. Willis, Chem. Ind. (London) (1967) 2146.
[129] P.J. Hendra and H.A. Willis, Chem. Commun. (1968) 225.
[130] J.L. Derouault, P.J. Hendra, M. Cudby and H.A. Willis, J. Chem. Soc., Chem. Commun. (1972) 1187.
[131] M.J. Gall, P.J. Hendra, C.J. Peacock, M.E.A. Cudby and H.A. Willis, Spectrochim. Acta, Part A 28 (1972) 1485.
[132] R.J. Roe and W.R. Krigbaum, J. Appl. Phys. 35 (1964) 2215.
[133] D.Y. Yoon, C. Chang and R.S. Stein, J. Polym. Sci., Polym. Phys. Ed. 12 (1974) 2091.
[134] S.K. Satija and C.H. Wang, J. Chem. Phys. 69: 6 (1978) 2739.
[135] P.J. Hendra, in: Structural Studies of Macromolecules by Spectroscopic Methods, ed. K.J. Ivin (Wiley, London, 1976).
[136] H.A. Willis, in: Molecular Spectroscopy, ed. A. West (Heyden, New York, 1977).
[137] A series of papers by S. Krimm et al. in 5 parts:
(a) J. Polym. Sci., Polym. Lett. Ed. 14 (1976) 195.
(b) J. Appl. Phys. 47 (1976) 4265.
(c) J. Polym. Sci., Polym. Phys. Ed. 15 (1977) 1769.
(d) J. Appl. Phys. 48 (1977) 4013.
(e) J. Polym. Sci., Polym. Phys. Ed. 16 (1978) 2105.
[138] G.V. Frazer, P.J. Hendra, M.E. Cudby and H.A. Willis, J. Mater Sci. 9 (1974) 1270.
[139] M.J. Gall and P.J. Hendra, The Spex Speaker 16: 1 (1971) 1.
[140] M.M. Coleman, J.R. Shelton and J.L. Koenig, Rubber Chem. and Technol. 45: 1 (1972) 173.
[141] M.M. Coleman, J.R. Shelton and J.L. Koenig, Ind. Eng. Chem. Prod. Res. Dev. 13 (1974) 154.
[142] M.M. Coleman, P.C. Painter and J.L. Koenig, J. Raman Spectrosc. 4 (1976) 417.
[143] G. Schreier and G. Peitscher, Fresenius' Z. Anal. Chem. 258 (1972) 199.
[144] S.J. Spells and I.W. Shepherd, J. Chem. Phys. 66 (1977) 1427.
[145] L. Bardet, G. Cassanas-Fabre and M. Alain, J. Mol. Struct. 1 (1975) 153.
[146] D.L. Gerrard and W.F. Maddams, Macromolecules 8 (1975) 54.
[147] W.F. Maddams, J. Macromol. Sci., Phys. 14 (1977) 87.
[148] J.L. Koenig, Case Western Reserve Univ., Cleve., Ohio, personal communication.
[149] W.F. Maddams, The British Petroleum Co., Ltd., Chertsey Rd., Sunbury-on-Thames, Middlesex TW 16 7LN, U.K., personal communication.
[150] C.S. Lu and J.L. Koenig, Am. Chem. Soc., Div. Org. Coat. Plast. Chem., Pap. 32 (1972) 112.
[151] J.L. Koenig and P. Shih, J. Polym. Sci., Polym. Phys. Ed. 10 (1972) 721.
[152] R.A. Evans and H.E. Hallam, Polymer 17 (1976) 838.
[153] R. Shishoo and M. Lundell, J. Polym. Sci., Polym. Chem. Ed 14 (1976) 2535.
[154] F.J. Boerio and J.L. Koenig, J. Macromol. Sci. Rev. Macromol. Chem. 7: 2 (1972) 246.
[155] W.L. Peticolas, Biochimie 57 (1975) 417.
[156] R.C. Lord, Appl. Spectrosc. 31 (1977) 187.
[157] J.L. Lippert, D. Tyminski and P.J. Desmeules, J. Amer. Chem. Soc. 98 (1976) 7075.
[158] W.S. Craig and B.P. Gaber, J. Am. Chem. Soc. 99 (1977) 4130.
[159] N.T. Yu, T.S. Lin and A.T. Tu, J. Biol. Chem. 250 (1975) 1782.
[160] N.T. Yu, B.H. Jo and D.C. O'Shea, Arch. Biochem. Biophys. 156 (1973) 71.
[161] A.T. Tu, B.H. Jo and N.T. Yu, Int. J. Pept. and Protein Res. 8 (1976) 337.
[162] D.B. Boyd, Int. J. Quantum Chem., Quantum Biol. Symp. 1 (1974) 13.
[163] J.T. Edsall, J. Chem. Phys. 4 (1936) 1.
[164] G.J. Thomas, Impact Lasers Spectrosc. 49 (1975) 127.
[165] K.A. Hartman, R.C. Lord and G.J. Thomas Jr., in: Physico-Chemical Properties of Nucleic Acids, ed. J. Duchesme (Academic Press, New York, 1973).
[166] G.J. Thomas Jr., in: Structure & Conformation of Nucleic Acids and Protein – Nucleic Acid Interaction, eds. M. Sundralingam and S.T. Rao (University Park Press, Baltimore, 1975) p. 253.
[167] L. Lafleur, J. Rice and G.J. Thomas Jr., Biopolymers 11 (1972) 2423.
[168] M.C. Chan and G.J. Thomas Jr., Biopolymers 13 (1974) 615.
[169] G.J. Thomas and P. Murphy, Science 188 (1975) 1205.
[170] T.G. Spiro and T.C. Strekas, Proc. Nat. Acad. Sci. U.S.A. 69 (1972) 2622.
[171] T.G. Spiro, Acc. Chem. Res. 7 (1974) 339.
[172] P.R. Carey and H. Schneider, Acc. Chem. Res. 11 (1978) 122.

[173] J.M. Burke, J.R. Kincaid and T.G. Spiro, J. Am. Chem. Soc. 100 (1978) 6077.
[174] T.C. Strekas, D.H. Adams, A. Packer and T.G. Spiro, Appl. Spectrosc. 28 (1974) 324.
[175] J.M. Burke, J.R. Kincaid, S. Peters, R.R. Gagne, J.P. Collman and T.G. Spiro, J. Am. Chem. Soc. 100 (1978) 6083.
[176] L. Pauling, Nature (London) 203 (1964) 182.
[177] N.S. Ferris, W.H. Woodruff, D.R. Rorabacher, T.E. Jones and L.A. Ochrymowycz, J. Am. Chem. Soc. 100 (1978) 5939.
[178] K.G. Brown, E.B. Brown and W.B. Person, J. Am. Chem. Soc. 99 (1977) 3128.
[179] B.J. Bulkin and N. Krishnamachari, J. Am. Chem. Soc. 94 (1971) 1109.
[180] J.L. Lippert and W.L. Peticolas, Proc. Nat. Acad. Sci. U.S.A. 68 (1971) 1572.
[181] B.J. Bulkin and N. Yellin, unpublished data.
[182] R. Mendelsohn and J. Maisano, Biochim. Biophys. Acta 506 (1978) 192.
[183] B.J. Bulkin and N. Krishnamachari, Mol. Cryst. Liq. Cryst. 24 (1973) 53.
[184] L.J. Lis, J.W. Kauffman and D.F. Shriver, Biochim. Biophys. Acta 436 (1976) 513.
[185] B.J. Bulkin and N. Yellin, J. Phys. Chem. 82 (1978) 821.
[186] J.L. Lippert, L.E. Gorczyka and G. Meikeljohn, Biochim. Biophys. Acta 382 (1975) 51.
[187] B.J. Bulkin, Biochim. Biophys. Acta 274 (1972) 649.
[188] F.P. Milanovich, Y. Yeh, R.J. Baskin and R.C. Harney, Biochim. Biophys. Acta 419 (1976) 243.
[189] B.J. Bulkin, Adv. Liq. Cryst. 2 (1976) 199.
[190] B.J. Bulkin and K. Krishnan, J. Am. Chem. Soc. 93 (1971) 5998.
[191] J.M. Schnur, Phys. Rev. Lett. 29 (1972) 1141.
[192] J.M. Schnur, Mol. Cryst. Liq. Cryst. 23 (1973) 155.
[193] B.J. Bulkin, D. Grunbaum, T. Kennelly and W.B. Lok, Liq. Cryst., Proc. Int. Conf. 1973 (Pub. 1975) 155.
[194] F. Jahnig, Chem. Phys. Lett. 23 (1973) 262.
[195] S. Lugomer and B. Lavrencic, Solid State Commun. 15 (1974) 177.
[196] H. Gruler, Z. Naturforsch, Teil A 28 (1972) 474.
[197] B.J. Bulkin, J. Opt. Soc. Am. 59 (1969) 1387.
[198] B.J. Bulkin, J.O. Lephardt and K. Krishnan, Mol. Cryst. Liq. Cryst. 19 (1973) 295.
[199] C.H. Wang, J. Am. Chem. Soc. 94 (1972) 8605.
[200] E.B. Priestly, P.S. Pershan, R.B. Meyer and P.H. Dolphin, Vijnana Parishad Anusandhan Patrika 14 (1971) 93.
[201] E.B. Priestly and P.S. Pershan, Mol. Cryst. Liq. Cryst. 23 (1973) 369.
[202] R.L. Humphries, P.G. James and G.R. Luckhurst, J. Chem. Soc., Faraday Trans. 2 68 (1972) 1031.
[203] W. Maier and A. Saupe, Z. Naturforsch, Teil A 15 (1960) 287.
[204] J.D. Boyd and C.H. Wang, J. Chem. Phys. 60 (1974) 1185.
[205] B.J. Bulkin and D. Grunbaum, in: Liquid Crystals and Ordered Fluids, Vol. 1, eds. R. Porter and J. Johnson (Plenum Press, New York, 1970).
[206] B.J. Bulkin and F.T. Prochaska, J. Chem. Phys. 54 (1971) 635.
[207] N.M. Amer and Y.R. Shen, J. Chem. Phys. 56 (1972) 2654.
[208] A. Sakamoto, K. Yoshino, U. Kubo and Y. Inuishi, J. Appl. Phys. 13 (1974) 1691.
[209] T. Riste and R. Pynn, Solid State Commun. 12 (1973) 407.
[210] K.K. Kobayashi, Mol. Cryst. Liq. Cryst. 13 (1971) 137.
[211] W.G.F. Ford, J. Chem. Phys. 56 (1972) 6270.
[212] B.J. Bulkin and D. Grunbaum, J. Phys. Chem. 79 (1975) 821.
[213] B.J. Bulkin and W.B. Lok, J. Phys. Chem. 77 (1973) 326.
[214] B.J. Bulkin, D. Grunbaum and A. Santoro, J. Chem. Phys. 51 (1969) 1602.
[215] J. Billard, M. Delhaye, J.C. Merlin and G. Vergoten, C.R. Acad. Sci., Ser B 273 (1971) 1105.
[216] W.J. Borer, S.S. Mitra and C.W. Brown, Phys. Rev. Lett. 27 (1971) 379.
[217] G. Vergoten, R. Demal and G. Fleury, Trav. Soc. Pharm. Montpellier 33 (1973) 321.
[218] N.M. Amer and Y.R. Shen, Solid State Commun. 12 (1972) 263.
[219] A.S. Zhdanova, L.F. Morozova, G. Peregudov and M. Sushchinskii, Opt. Spektrosk. 26 (1969) 209.
[220] J.M. Schnur and M. Fontana, J. Phys. (Paris) Lett. 35 (1974) 53.
[221] D. Dvorjetski, V. Volterra and E. Wiener-Avnear, Phys. Rev. A 12 (1975) 681.
[222] K. Nakamoto, Infrared and Raman Spectra of Inorganic and Coordination Compounds (3rd ed., Wiley, New York, 1978).
[223] D.M. Adams, Metal-Ligand and Related Vibrations (St. Martin's Press, New York, 1968).
[224] R.J.H. Clark, The Spex Speaker 18: 1 (1973) 1.
[225] R.L. Carter, in: Infrared and Raman Spectroscopy, Vol. 1, Part A, eds. E.G. Brame and J.G. Grasselli (Dekker, New York, 1977).
[226] W.P. Griffith, in: The Infra-Red Spectra of Minerals, ed. V.C. Farmer (Mineralogical Society, London, 1974).
[227] G. Turrell, Infrared and Raman Spectra of Crystals (Academic Press, New York, 1972).
[228] W.G. Fateley, F.R. Dollish, N.T. McDevitt and F.F. Bentley, Infrared and Raman Selection Rules for Molecular and Lattice Vibrations; The Correlation Method (Wiley, New York, 1972).
[229] P.P. Shorygin, Russ. Chem. Rev. 40 (1974) 367.
[230] R.J.H. Clark and B. Stewart, in: Structure and Bonding, Vol. 36, eds. J.D. Dunitz et al. (Springer-Verlag, New York, 1979).

[231] E.J. Baran, Z. Anorg. Allg. Chem. 442 (1978) 112.
[232] E.J. Baran, Monatsh. Chem. 106: 1 (1975) 1.
[233] Y.S. Jain, V.K. Kapoor and H.D. Bist, Appl. Spectrosc. 30: 4 (1976) 440.
[234] R.L. Carter and C.E. Bricker, Spectrochim. Acta, Part A 30 (1974) 1793.
[235] J.S. Filippo Jr. and H.J. Sniadoch, Inorg. Chem. 12: 10 (1973) 2326.
[236] C. Angell, paper at Eastern Analytical Symposium, Atlantic City, N.J., November, 1972.
[237] M.A. Py, P.E. Schmid and J.T. Vallin, Nuovo Cimento Soc. Ital. Fis. B 38: 2 (1977) 271.
[238] P.J. Miller, Spectrochim. Acta, Part A 27 (1971) 957.
[239] M. Liegeois-Duyckaerts, Spectrochim. Acta, Part A 31 (1975) 1585.
[240] M. Liegeois-Duyckaerts and P. Tarte, Spectrochim. Acta, Part A 30 (1974) 1771.
[241] M.T. Paques-Ledent, Spectrochim. Acta, Part A 32 (1976) 1339.
[242] J.R. Allkins and P.J. Hendra, J. Chem. Soc. A (1967) 1325.
[243] R.J.H. Clark, G. Natile, U. Belluco, L. Cattalini and C. Filipin, J. Chem. Soc. A (1970) 659.
[244] J. Wong and C.A. Angell, Appl. Spectrosc. Rev. 4 (1971) 155.
[245] V. Fawcett, D.A. Long and L. Taylor, Proc. Int. Conf. Raman Spectrosc., 5th (1976) 112.
[246] G.B. Rouse, P.J. Miller and W.M. Risen Jr., J. Non-Cryst. Solids 28: 2 (1978) 193.
[247] W.L. Komjnendijk, Phys. Chem. Glasses 17: 6 (1976) 205.
[248] H. Verweij, H. Van den Boom and R. Breemer, J. Am. Ceram. Soc. 61: 3 (1978) 118.
[249] T. Furukawa, Diss, Abstr. Int. B 38 (12, Ptl) (1978) 6091. Avail. Univ. Microfilms Int. Order No. 7808361.
[250] G. Lucovsky, F.L. Galeener, R.H. Geils and R.C. Keezer, Struct. Non-Cryst. Mater., Proc. Symp. 1976 (Pub. 1977) 127.
[251] S.A. Brawer and W.B. White, J. Mater. Sci. 13: 9 (1978) 1907.
[252] G.E. Walrafen and J.P. Luongo, The Spex Speaker 20: 3 (1975) 1.
[253] T. Okeshoji, Y. Ono and T. Mizuno, Appl. Opt. 12 (1973) 2236.
[254] V.V. Baptizmanskii, I.I. Novak and A.E. Chmel, Opt. Spectrosc. (USSR) 43: 1 (1977) 106.
[255] R. Vidano and D.B. Fischbach, Raman Spectroscopy of Carbon Materials: I. New Spectral Lines; II. Characterization of Materials, American Ceramic Society Pacific Coast Regional Meeting, San Francisco, Oct. 31–Nov. 3, 1976.
[256] T.G. Miller, D.B. Fischbach and J.M. Macklin, Ext. Abstr. Program-Bienn. Conf. Carbon 12 (1975) 105.
[257] R. Vidano and D.B. Fischbach, Ext. Abstr. Program-Bienn. Conf. Carbon 13 (1977) 272.
[258] R. Vidano and D.B. Fischbach, J. Am. Ceram. Soc. 61: 1 (1978) 13.
[259] G. Gautier and M. Debeau, Spectrochim. Acta, Part A 32 (1976) 1007.
[260] G.J. Janz, E. Roduner, J.W. Coutts and J.R. Downey Jr., Inorg. Chem. 15: 8 (1976) 1751.
[261] G.J. Janz, J.W. Coutts, J.R. Downey Jr. and E. Roduner, Inorg. Chem. 15: 8 (1976) 1755.
[262] G.J. Janz, J.R. Downey Jr., E. Roduner, G.J. Wasilczyk, J.W. Coutts and A. Eluard, Inorg. Chem. 15: 8 (1976) 1759.
[263] F.P. Daly and C.W. Brown, J. Phys. Chem. 77: 15 (1973) 1859.
[264] F.P. Daly and C.W. Brown, J. Phys. Chem. 80: 5 (1976) 480.
[265] B. Meyer and W.E. Johns, Holzforschung 32: 3 (1978) 102.
[266] G.J. Rosasco and J.H. Simmons, Am. Ceram. Soc. Bull. 54: 6 (1975) 590.
[267] A.T. Ward, J. Phys. Chem. 72: 12 (1968) 4133.
[268] G.A. Ozin, Prog. Inorg. Chem. 14 (1971) 173;
I.R. Beattie, Chem. Br. 3 (1967) 347.
[269] D.A. Long, ref. [2] p. 169.
[270] D.A. Long, Colloq. Spectrosc. Int., Plenary Lect. Rep., 16th, 1971 (Adam Hilger, Ltd., London, 1972).
[271] A.D. Prasad Rao, R.S. Katiyar and S.P.S. Porto, in: Advances in Raman Spectroscopy, ed. J.P. Mathieu (Heyden, London, 1973).
[272] C. Caville, V. Fawcett and D.A. Long, Proc. Int. Conf. Raman Spectrosc., 5th (1976) 626.
[273] B.I. Swanson, B.C. Lucas and R.R. Ryan, J. Chem. Phys. 69: 10 (1978) 4328.
[274] G.E. Walrafen, J. Chem. Phys. 43 (1965) 479.
[275] L.A. Woodward, G. Garton and H.L. Roberts, J. Chem. Soc. (1956) 3723.
[276] G.J. Janz and D.W. James, J. Chem. Phys. 38 (1963) 905.
[277] R.J.H. Clark and P.D. Mitchell, J. Chem. Soc., Dalton Trans. (1972) 2432.
[278] J.E.D. Davies and D.A. Long, J. Chem. Soc. A (1968) 2564.
[279] J.E.D. Davies and D.A. Long, J. Chem. Soc. A (1968) 2054.
[280] J.E.D. Davies and D.A. Long, J. Chem. Soc. A (1968) 2050.
[281] J.E.D. Davies and D.A. Long, J. Chem. Soc. A (1968) 1761.
[282] K.H. Tytko and B. Schonfeld, Z. Naturforsch, Teil B 30 (1975) 471.
[283] V.E. Steger, K. Herzog and J. Klosowski, Z. Anorg. Allg. Chem. 432 (1977) 42.
[284] R.J.H. Clark and M.L. Franks, J. Chem. Soc., Chem. Commun. 9 (1974) 316.
[285] F.A. Cotton and C.B. Harris, Inorg. Chem. 6 (1967) 924.
[286] C.D. Cowman and H.B. Gray, J. Am. Chem. Soc. 95 (1973) 8177.
[287] R.J.H. Clark and P.D. Mitchell, J. Am. Chem. Soc. 95 (1973) 8300.

[288] R.J.H. Clark and M.L. Franks, Chem. Phys. Lett. 34 (1975) 69.
[289] J.F. Hesse, S.C. Abbi and A. Compaan, J. Appl. Phys. 47: 12 (1976) 5467.
[290] W.P. Griffith, J. Chem. Soc. A (1970) 286.
[291] N. Sheppard and T.T. Ngurjen, in: Advances in Infrared and Raman Spectroscopy, Vol. 5, eds. R.J.H. Clark and R. Hester (Heyden, London, 1978) p. 67.
[292] R.L. Paul and P.J. Hendra, Miner. Sci. Eng. 8 (1976) 171.
[293] R.P. Cooney, G. Curthoys and N.T. Tam, Adv. Catal. 24 (1975) 293.
[294] E. Buechler and J. Turkevich, J. Phys. Chem. 76 (1972) 2325.
[295] J.M. Stencel and E.B. Bradley, Spectrosc. Lett. 11: 8 (1978) 563.
[296] J.M. Stencel, D.M. Noland, E.B. Bradley and C.A. Frenzel, Rev. Sci. Instrum. 49: 8 (1978) 1163.
[297] R.O. Kagel, R.A. Koster and W.T. Allen, Appl. Spectrosc. 30: 3 (1976) 350.
[298] B.A. Morrow, J. Phys. Chem. 81 (1977) 2663.
[299] Y. Yamamoto and H. Yamada, Bull. Chem. Soc. Jpn. 51: 10 (1978) 3063.
[300] N. Tam, R.P. Cooney and G. Curthoys, J. Chem. Soc., Faraday Trans. 1 72 (1976) 2591.
[301] N. Tam, R.P. Cooney and G. Curthoys, J. Chem. Soc., Faraday Trans. 1 72 (1976) 2592.
[302] N. Tam and R.P. Cooney, J. Chem. Soc., Faraday Trans. 1 72 (1976) 2598.
[303] N. Tam, P. Tsai and R.P. Cooney, Aust. J. Chem. 31: 2 (1978) 255.
[304] P.J. Trotter, J. Phys. Chem. 82 (1978) 2396.
[305] W. Krasser and A.J. Renouprez, J. Raman Spectrosc. 8: 2 (1979) 92.
[306] M. Moskovits, J. Chem. Phys. 69 (1978) 4159.
[307] R.M. Hexter and M.G. Albrecht, Spectrochim. Acta, Part A 35 (1979) 233.
[308] M. Fleishmann, P.J. Hendra and A.J. McQuillan, Chem. Phys. Lett. 26 (1974) 163.
[309] P.J. Hendra, I.D.M. Turner, E.J. Loader and M. Stacey, J. Phys. Chem. 78 (1974) 300.
[310] T.A. Egerton, A.H. Hardin, Y. Koziovovski and N. Sheppard, J. Catal. 32 (1974) 343.
[311] T.A. Egerton, A.H. Hardin and N. Sheppard, Can. J. Chem. 54 (1976) 586.
[312] R.P. Van Duyne, J. Phys. (Paris) Colloq. 52 (1977) 239.
[313] M. Fleischmann, P.J. Hendra and A.J. McQuillian, J. Chem. Soc. D (1973) 80.
[314] M.G. Albrecht and J.A. Creighton, J. Am. Chem. Soc. 99 (1977) 5215.
[315] G. Hagen, B.S. Glaueski and E. Yeager, Abstract No. 535, Extended Abstracts, Electrochem Soc., Spring Meeting, Seattle, Washington, May 21–26, 1978.
[316] B. Pettinger and U. Wenning, Chem. Phys. Lett. 56 (1978) 253.
[317] T.E. Furtak, Solid State Commun. 28 (1978) 903.
[318] R.L. Paul, A.J. McQuillan, P.J. Hendra and M. Fleischmann, J. Electroanal. Chem. Interfacial Electrochem. 66 (1975) 248.
[319] N. Fleischmann, P.J. Hendra, A.J. McQuillan, R.L. Paul and E.S. Reid, J. Raman Spectrosc. 4 (1976) 269.
[320] R.P. Cooney, P.J. Hendra and M. Fleischmann, J. Raman Spectrosc. 6 (1977) 264.
[321] H. Yamada and H. Naono, Hyomen 15 (1977) 470.
[322] H. Yamada, Indian J. Pure Appl. Phys. 16 (1978) 159.
[323] S. Efrima and H. Metiu, J. Chem. Phys. 70 (1979) 1939.
[324] Y. Yamamoto and H. Yamada, J. Chem. Soc., Faraday Trans. 1 74 (1978) 1562.
[325] T. Takenaka and T. Nakanaga, J. Phys. Chem. 80 (1976) 475.
[326] D.L. Jeanmaire, M.R. Suchanski and R.P. Van Duyne, J. Am. Chem. Soc. 97 (1975) 1699.
[327] M.R. Suchanski and R.P. Van Duyne, J. Am. Chem. Soc. 98 (1976) 250.
[328] D.L. Jeanmaire and R.P. Van Duyne, J. Am. Chem. Soc. 98 (1976) 4029.
[329] D.L. Jeanmaire and R.P. Van Duyne, J. Am. Chem. Soc. 98 (1976) 4034.
[330] R. Dupeyrat, in: Proc. Int. Conf. Raman Spectrosc., 6th (Heyden, London, 1978).
[331] P.J. Hendra, The Spex Speaker 19:1 (1974) 1.
[332] T. Takenaka and H. Fukuzaki, J. Raman Spectrosc. 8 (1979) 51.
[333] R.J. Thibeau, C.W. Brown and R.H. Heidersbach, Appl. Spectrosc. 32 (1978) 532.
[334] W.L. Peticolas, E.W. Small and B. Fanconi, in: Polymer Characterization Interdisciplinary Approaches, ed. C.D. Smith-Craver (Plenum Press, New York, 1971) p. 47.
[335] J.L. Callahan, R.K. Grasselli, E.C. Milberger and H.A. Strecker, Ind. Eng. Chem. Prod. Res. Dev. 9 (1970) 134.
[336] B.C. Gates, J.R. Katzer and G.C.A. Schuit, Chemistry of Catalytic Processes (McGraw-Hill, New York, 1979).
[337] R.K. Grasselli and D.D. Suresh, J. Catal. 25 (1972) 273.
[338] A.W. Sleight, W.J. Linn and K. Aykan, Chem. Technol. 8: 4 (1978) 235.
[339] P.L. Villa, A. Szabo, F. Trifiro and M. Carbucicchio, J. Catal. 47 (1977) 122.
[340] E.V. Hoefs, J.R. Monnier and G.W. Keulks, J. Catal. 57 (1979) 331.
[341] E. Payen, J. Barbillat, J. Grimblot and J.P. Bonnelle, Spectrosc. Lett. 11 (1978) 997.
[342] J. Medema, C. VanStam, V.H.J. DeBeer, A.J.A. Konings and D.C. Koningsberger, J. Catal. 53 (1978) 386.

[343] F.R. Brown and L.E. Makovsky, Appl. Spectrosc. 31 (1977) 44;
F.R. Brown, L.E. Makovsky and K.H. Rhee, J. Catal. 50 (1977) 162; 385;
F.R. Brown, L.E. Makovsky and K.H. Rhee, Appl. Spectrosc. 31 (1977) 563.
[344] H. Knözinger and H. Jeziorowski, J. Phys. Chem. 82 (1978) 2002.
[345] F.P.J.M. Kerkhof, J.A. Moulÿn and R.Thomas, J. Catal. 56 (1979) 279.
[346] K. Aykan, J. Catal. 12 (1968) 281;
L.Y. Erman and E.L. Galperin, Russ. J. Inorg. Chem. (Engl. Transl.) 13 (1968) 487.
[347] V. Boudeville, F. Figueras, M. Forissier, J.L. Portefaix and J.C. Vedrine, J. Catal. 58 (1979) 52.
[348] P.B. Tooke, in: Infrared and Raman Spectroscopy, Vol. 1, Part B, eds. E.G. Brame and J.G. Grasselli (Dekker, New York, 1977).
[349] J.P. Coates in: Recent Analytical Developmentals in the Petroleum Industry, ed. D.R. Hodges (Applied Science Publishers, Ltd., Essex, 1974).
[350] C.W. Brown, P.F. Lynch and M. Ahmadjian, Appl. Spectrosc. Rev. 9 (1975) 223.
[351] C.W. Brown, P.F. Lynch, M. Ahmadjian and C.D. Baer, Am. Lab. 7 (1975) 59.
[352] C.W. Brown and P.F. Lynch, Anal. Chem. 48 (1976) 191.
[353] M. Ahmadjian and C.W. Brown, Anal. Chem. 48 (1976) 1257.
[354] R.J. Obremski, Spectra-Physics Raman Technical Bulletin (Spectra-Physics, Mountain View, CA, 1970).
[355] J.N. Willis, R.B. Cook and R. Jankow, Anal. Chem. 44 (1972) 1228.
[356] R.A. Friedel and G.L. Carlson, Chem. Ind. (London) (1971) 1128.
[357] D.S. Lavery, in: Infrared and Raman Spectroscopy, Vol. 1, Part B, eds. E.G. Brame and J.G. Grasselli (Dekker, New York, 1977).
[358] K.M. Cunningham, M.C. Goldberg and E.R. Weiner, Anal. Chem. 49 (1977) 75.
[359] F.B. Bradley and C.A. Frenzel, Water Res. 4 (1970) 125.
[360] S.F. Baldwin and C.W. Brown, Water Res. 6 (1972) 1601.
[361] M. Akmadjian and C.W. Brown, Environ. Sci. Technol. 7 (1973) 452.
[362] F.G. Ullman, U.S. Natl. Techn. Inform. Serv. PB Rep., No. 261238 (1976).
[363] C.W. Brown and P.F. Lynch, J. Food Sci. 41 (1976) 1231.
[364] L. Van Haverbeke, P.F. Lynch and C.W. Brown, Anal. Chem. 50 (1978) 315.
[365] R.J. Thibeau, L. Van Haverbeke and C.W. Brown, Appl. Spectrosc. 32 (1978) 98.
[366] C.K.N. Patel, Science 4364 (1978) 157.
[367] T. Haaka, Denshi Gyutsu Sogo Kenkyusho Iho 42 (1978) 376.
[368] H.A. Willis, in: Advances in Infrared and Raman Spectroscopy, Vol. 2, eds. R.J.H. Clark and R. Hester (Heyden, London, 1976) p. 132.
[369] E.R. Schildkraut, Am. Lab. 4 (1972) 23.
[370] T. Hirschfeld, E.R. Schildkraut, H. Tannenbaum and D. Tannenbaum, Appl. Phys. Lett. 22 (1973) 38.
[371] S.K. Poultney, M.L. Brumfeld and J.H. Siviter Jr., Appl. Opt. 16 (1977) 3180.
[372] O. Chamberlain, P. Robrish and H. Rosen, U.S. Natl. Techn. Inform. Serv. PB Rep., No. 262336 (1976).
[373] W.H. Smith and R.A. King, U.S. Natl. Techn. Inform. Serv. PB Rep., No. 273101 (1977).
[374] K. Fredriksson, I. Lindgren and S. Svanberg, Jt. Conf. Sens. Environ. Pollut. (Conf. Proc.), 4th, 1977 (Pub. 1978) p. 446.
[375] W.M. Arden, T.B. Hirschfeld, S.M. Klainer and W.A. Mueller, Appl. Spectrosc. 28 (1974) 554.
[376] W. Stricker, Laser 77 (Seventy-Seven) Opto-Electron., Conf. Proc. (1977) 174.
[377] S.M. Schoenung and B.E. Mitchell, U.S. Natl. Techn. Inform. Serv. SAND Rep., No. 77-8722 (1977).
[378] L. Beardmore, H.G.M. Edwards, D.A. Long and T.K. Tan, Lasers Chem., Proc. Conf. (1977) 79.
[379] R.G. Gordon, J. Chem. Phys. 43 (1965) 1307.
[380] J. Lascombe, ed., Molecular Motions in Liquids (Reidel, Dordrecht, Netherlands, 1974).
[381] L.A. Nafie and W. Peticolas, J. Chem. Phys. 57 (1972) 3145.
[382] J. Yarwood, R. Arndt and G. Döge, Chem. Phys. 25 (1977) 387.
[383] R. Kubo, in: Fluctuations, Relaxation, and Resonance in Magnetic Systems, ed. D. Ter Haar (Oliver and Boyd, Edinburgh, 1962).
[384] J. Schroeder, D.H. Schiemann, P.T. Sharko and J. Jones, J. Chem. Phys. 68 (1977) 3215.
[385] W.G. Rothschild, J. Chem. Phys. 65 (1976) 455.
[386] J. Yarwood, P.L. James, G. Döge and R. Arndt, Faraday Discuss. Chem. Soc. 66 (1979) in press.
[387] B.J. Bulkin and K. Brezinsky, J. Chem. Phys. 69 (1978) 15.
[388] A. Baruya, A.D. Booth, W.F. Maddams, J.G. Grasselli and M.A.S. Hazle, J. Polym. Sci., Polym. Lett. Ed. 14 (1976) 329.
[389] M.E.R. Robinson, D.I. Bower and W.F. Maddams, Polymer 17 (1976) 355.
[390] C. Baker, W.F. Maddams, J.G. Grasselli and M.A.S. Hazle, Spectrochim. Acta, Part A 34 (1978) 761.
[391] M.J. Colles and G.E. Walrafen, Appl. Spectrosc. 30 (1976) 463.
[392] A. Laubereau, D. Vander Linde and W. Kaiser, Phys. Rev. Lett. 28 (1972) 1162.
[393] A. Owyoung, IEEE J. Quantum Electron. 14 (1978) 192.
[394] A. Owyoung and E.D. Jones, Opt. Lett. 1 (1977) 152.
[395] J.R. Nestor, J. Chem. Phys. 69 (1978) 1778.
[396] W.M. Tolles, J.W. Nibler, J.R. McDonald and A.B. Harvey, Appl. Spectrosc. 31 (1977) 253.

[397] W.M. Tolles and R.D. Turner, Appl. Spectrosc. 31 (1977) 96.
[398] L.B. Rogers, J.D. Stuart, L.P. Goss, T.B. Malloy Jr. and L.A. Carreira, Anal. Chem. 49 (1977) 960.
[399] P.K. Dutta, J.R. Nestor and T.G. Spiro, Proc. Nat. Acad. Sci. U.S.A. 74 (1977) 4146.
[400] M. Bridoux and M. Delhaye, Nouv. Rev. Opt. Appl. 1 (1970) 23.
[401] A. Campion, M.A. El-Sayed and J. Terner, Biophys. J. 20 (1977) 369.
[402] R. Wilbrandt, P. Pagsberg, K.B. Hansen and C.V. Weisberg, Chem. Phys. Lett. 36 (1975) 76.
[403] J.M. Beny, B. Sombret, F. Wallart and M. Leclercq, J. Mol. Struct. 45 (1978) 349.
[404] F. Wallart, Ph.D. Thesis, Univ. of Lille, France (1970).